CRANFIELD UNIVERSITY

POONEH AREF

Development of a Framework for Thermoeconomic Optimization of Simple and Combined Gas-Turbine Cycles

School of Engineering

PhD THESIS

CRANFIELD UNIVERSITY

SCHOOL OF ENGINEERING

PhD THESIS

Academic Year 2008-2012

Pooneh Aref

Development of a Framework for Thermoeconomic Optimization of Simple and Combined Gas-Turbine Cycles

Supervisor: Prof. Pericles Pilidis

November 2012

This thesis is submitted in partial fulfilment of the requirements for the degree of Doctor of Philosophy (PhD).

Abstract

The problem consists of selecting simple and combined gas-turbine cycles with high thermal efficiency and low capital cost is the subject of this study. In order to solve this problem, the so-called thermoeconomic optimization approach was used by selecting an appropriate objective function that combines the expenditures of financial resources (economic) and thermodynamic equations. Recently, a new definition of objective function has been proposed to take into account environmental considerations as well. Thermoeconomic optimization is still an open research problem and currently under investigation. The present study is a part of ongoing research aimed at development of Techno-economical Environmental Risk Analysis (TERA) methodology at Cranfield University for the evaluation of advanced power plant concepts in order to meet challenging environmental goals. The object of this work is to apply "design" and "operation" types of thermoeconomic optimization method to a simple and a combined gas-turbine cycle with pollution reduction. The optimization process adapts updated models for power demand patterns, legislation, capital cost, and inflation. The outcome of study is the design of cost efficient systems with reduced environmental impact.

The study case is a single-shaft engine inspired by the Alstom GT13-E2 gas turbine with 184.5 MW output power. The study began with creating design-point and operating performance models of this engine in the VariFlow code. The design-point

model consists of blocks that correspond to engine components (compressor, combustor, turbine, etc.), where the performance parameters in each block can be determined from given data and using the aero-thermodynamic equations. Unfortunately, not all the engine performance parameters are available (such as component efficiencies). What was suggested is to use the so-called engine's performance adaptation that allows us to match the engine's model with the performance data obtained from experiment. The adaptation results showed a good agreement between simulation model and measured values. With the fixed engine geometry from the design-point, the engine must operate effectively over a range of ambient temperature changes. The prediction results showed that the high ambient temperatures decrease the air density and hence the inlet mass flow rate and output power. The higher the ambient temperature, more heat is exhausted to the atmosphere, therefore, the hotter temperatures lead to a decrease in the thermal efficiency as well. Next, the design-point diagrams of the engine were created for the changes in compressor pressure ratio and turbine entry temperature. The results showed that for a given turbine entry temperature value, there is a corresponding compressor pressure ratio value that maximizes the gas turbine efficiency, such that, the optimum pressure ratio increases with increasing turbine entry temperature. The effects of extracting air from compressor for turbine cooling on the engine's performance were also investigated. The cooling air usually is extracted from the exit stage of high-pressure compressor and carried by ducts to the guide vanes and rotor of hight-pressure turbine. The performance prediction results showed that both thermal efficiency and specific power fall with an increase in the amount of bled air from the compressor of engine. The required amount of bled air depends on the allowable metal temperature and turbine entry temperature such that more amount of air needs to be extracted for cooling if the turbine entry temperature increases. The amount of cooling air increases for a metal with smaller allowable temperature as well.

This study presents the correlation functions existing between actual engine parameters of pressure ratio, turbine inlet temperature, and air mass flow of commercial gas turbines regardless of the manufacturer. According to these trends, the real gas turbine data can be separated to low and high power engines. The simulation results were updated with taking into account these correlation functions and then simulation trends were compared with the engine data. A good agreement again was found. An updated capital cost model was proposed as well that takes into account these correlation functions. The cost predictions were compared with available engine prices and again a good agreement was found. The cost predictions showed that the gas turbine unit capital cost (defined as capital cost per kw) is large for small engines and relatively unchanged for medium and large engines.

The performance prediction and integration of a gas turbine with a heat recovery steam generator (HRSG) was studied next. The gas turbine used again is based on 184.5 MW power engine. The configurations that have been considered include single-, dual-, and triple-pressure HRSG. It is desirable that selected HRSG extracts maximum useful work for given exhaust gas conditions. However, the selected system needs to minimize number of heat exchanger units and reduce the construction cost as well. The results showed that all combined cycles have much higher overall efficiency than simple gas turbine. The finding showed that the best HRSG type selection to combine the 184.5MW gas turbine with steam turbine is a dual-pressure HRSG. Also, the design-point diagrams showed that the optimum pressure ratio that maximizes combined cycle efficiency is relatively smaller than of a simple gas turbine cycle.

Different methods of optimization were used to solve the problems of constrained or unconstrained and single-variable or multiple-variable types. Also, a new optimization method was proposed to find the global minimum. This method is based on the expected improvement function predicted from a Kriging interpolation. The objective

function is the cost of producing electivity that needs to be minimized. The optimization problem began with a simple single-variable optimization and then continued for multiple-variable optimization including some design constraints. All optimization variables were limited to an upper and lower bound defined from a reasonable range of variables. The results of optimization methods were compared with each other. It was shown that expected improvement function has the least computational effort among used methods. The optimization results suggested that engine designs with high turbine entry temperature have less cost of producing electricity, although this temperature becomes limited if compressor air is used to cool turbine.

The study tools included VariFlow code and Tera code which was developed by the author. This code features a hands-off update of input files that is very useful for the optimization study. Also, the code predicts the performance of combined gas-steam cycles for single-, dual- and triple-pressure-level HRSG. The code models the cost of producing electricity for simple and combined gas-turbine cycles as well. This cost includes capital costs, costs of resources, and pollution. Different optimization solvers were utilized in the code to find the optimal design of each cycle as well.

Acknowledgments

My PhD study was supported by the EPSRC grant under funding from E.ON company. I wish to express my gratitude and thanks for this financial support.

The completion of this dissertation would not have been possible without the support of many people in many different ways. First of all, I am deeply grateful to my supervisor Prof. Pericles Pilidis for his guidance, support and encouragement. I consider myself very fortune for being conduct this research under his supervision. My sincerest thanks to his warm support and patience for going through and revising all my results, reports, presentations, dissertation and many others. I also like to thank my industrial mentor, Mr. Martyn Adams at E.ON for his great suggestions and comments during this study.

My thanks to all other members of TERA project at Cranfield. The group has been a source of friendships as well as good collaboration and members have been providing me helpful comments and made my PhD enjoyable. Special thanks to Dr. Stephen Ogaji, the project director. Also, it was my great pleasure to work with a number of Master students and I would like to thank them for their contributions to this research. I am also grateful to Nicola Datt and Gill Hargreaves who took care of my registration, meetings with my supervisor, etc while I was living in the United States.

An especial thank from bottom of my heart to Prof. Russ Cummings at US Air Force Academy and his lovely wife Dr Signe Blach for the support and encouragements

they have given me. They also have been helping me to improve the English and grammar of this dissertation.

My heartiest endless thanks to my beloved husband and son for being by my side all these years. My husband finished his PhD at Cranfield University under supervision of Professor Pilidis as well. Therefore, I had been so fortunate as to learn, and ask him many questions when I do not understand something. It was not possible for me to remain focused and finish my studies without his inspiration and motivation. Thank you.

Contents

List of Tables

List of Figures

Nomenclature

Symbols

A_{noz}	Nozzle surface area, m^2
A_{phtr}	Preheater surface area, m^2
B	Interest payment coefficient
C_0	The plant purchased equipment cost, US$
C_{cmp}	The compressor purchased equipment cost, US$
C_{cmb}	The combustor purchased equipment cost, US$
C_{CO}	The annual tax on CO emission, US$
C_E	The annual electricity cost, US$
$\dot{C}_E$	The unit price of producing electricity, $\frac{C_E}{\dot{W}_g\ N}$, US$/kwh
$C_{eco/eva}$	The economizer/evaporator purchased equipment cost, US$
C_{fuel}	The annual cost of fuel consumed, US$
$C_{\text{fuel}_{\text{des}}}$	The annual cost of fuel consumed at design-point conditions, US$
C_{gtu}	The turbine purchased equipment cost, US$
C_{NO_x}	The annual tax on NO_x emission, US$
C_{OM}	The annual cost of operation and maintenance, US$
C_p	The specific heat at constant pressure, J/kg.K
C_{phtr}	The pre-heater purchased equipment cost, US$
C_{water}	The annual cost of water consumed, US$
$\dot{C}_z$	The annualized capital cost, $\frac{\beta C_0 + C_{OM}}{N}$, US$/hr

c_{ij}	Combined cycle economic parameters
c_{fuel}	Fuel cost per unit of energy
c_{water}	Water unit cost per liter
D	Discount rate
$\dot{G}_c$	Compressor normalized mass flow rate
$\dot{G}_t$	Turbine normalized mass flow rate
H	Life of the plant in years; also influence coefficient matrix
h	Enthalpy
L	Load factor, $\dfrac{\dot{W}_{gi}}{\dot{W}_{g\text{des}}}$
$\dot{m}$	Mass flow rate, kg/s
$\dot{m}_a$	Compressor entering air mass flow rate, kg/s
$\dot{m}_{\text{bleed}}$	Compressor bleeding air mass flow rate, kg/s
$\dot{m}_{\text{cd}}$	The amount of air that enters combustor, kg/s
$\dot{m}_{\text{cool}}$	Cooling air mass flow rate, kg/s
$\dot{m}_{\text{exh}}$	Gas turbine exhaust mass flow rate, kg/s
$\dot{m}_{\text{fuel}}$	Fuel mass flow rate, kg/s
$\dot{m}_s$	Steam cycle water mass flow rate, kg/s
$\dot{m}_g$	Turbine entering air mass flow rate, kg/s
$\dot{m}_{HP}$	HP steam mass flow rate, kg/s
$\dot{m}_{LP}$	LP steam mass flow rate, kg/s
$\dot{m}_{\text{w}}$	water mass flow rate, kg/s
$\dot{N}_c$	Compressor normalized rotating speed, $N\sqrt{\text{T}_{\text{std}}/\text{T}_{\text{air}}}$
$\dot{N}_t$	Turbine normalized rotating speed
N	Operating hours in year, hr; also rotating speed, rpm
N_{des}	Operating hours in year at design-point conditions, hr
P_1	Compressor inlet pressure, pa

P_2	Compressor outlet pressure, pa
P_3	Turbine inlet pressure, pa
P_4	Turbine outlet pressure, pa
P_{air}	Air pressure, pa
P_{std}	Standard air pressure, pa
$\dot{Q}$	Heat transfer
$\dot{Q}_{ec}$	Heat transfer in the economizer
$\dot{Q}_{eva}$	Heat transfer in the evaporator
$\dot{Q}_{boiler}$	Heat transfer in the boiler
r_c	compressor pressure ratio, P_2/P_1
s	entropy
t	Primary zone residence time , sec
t_{ev}	Fuel evaporation time, sec
T_1	Compressor inlet temperature, K
T_2	Compressor outlet temperature, K
T_3	Turbine inlet temperature, K
T_4	Turbine outlet temperature, K
T_{air}	Air temperature, K
$\mathtt{T}_{\text{bleed}}$	Bleeding air temperature, K
$\mathtt{T}_{\text{cool}}$	Cooling air temperature, K
T_{exh}	Exhaust air temperature, K
T_{pz}	Primary zone combustion temperature, K
$\mathrm{T}_s(p)$	Saturation temperature at given pressure, 4^oC
T_{st}	Standard ambient temperature, K
T_{air}	Air temperature, K
$\dot{W}_{cmp}$	Compressor work, kw
$\dot{W}_{\text{pump}}$	Feed-water pump work, kw

$\dot{W}_g$	The plant gross power, kw
$\dot{W}_{g\text{des}}$	The plant gross power at design-point, kw
$\dot{W}_{gi}$	The plant gross power at off-design conditions, kw
$\dot{W}_{gtu}$	Turbine work, kw
$\dot{W}_{st}$	Steam-turbine work

Greek

α	Combustor pressure ratioP_3/P_2
β	Capital charge factor
$\Delta \mathrm{T}_a$	Approach temperature difference, ^{o}C
ΔP_{cc}	Combustion chamber pressure loss
$\Delta \mathrm{T}_p$	Pinch point temperature, ^{o}C
δ_{bleed}	Bleeding air temperature ratio
δ_{cool}	Cooling air temperature ratio
$\Delta \mathrm{T}_{sh}$	Superheat pinch temperature, ^{o}C
η_{cc}	Combined cycle efficiency
η_{cmb}	Combustor efficiency
η_{des}	Thermal efficiency at design point
η_{gt}	Gas turbine efficiency
η_{HRSG}	HRSG efficiency
η_{th}	Thermal efficiency
η_{R}	Rankine cycle efficiency
η_{scp}	Compressor isentropic efficiency
η_{sgt}	Turbine isentropic efficiency
η_{st}	Steam-turbine thermal efficiency
λ_{bleed}	Bleeding air mass flow ratio

λ_{cool}	Cooling air mass flow ratio
Φ_r	Maintenance factor
$\dot{\Gamma}$	Annualized cost per output power, US$/kwh
γ	Specific heat ratio

Abbreviations

CCGT	Combined cycle gas turbine
EIF	Expected improvement function
FCI	Fixed capital investment
FCR	Annual fixed change rate percent
HP	High pressure
HRSG	Heat recovery steam generator
IP	Intermediate pressure
ISA	International standard atmosphere
LHV	Lower heating value
LP	Low pressure
PEC	Purchased equipment cost
PR	Compressor pressure ratio
SCGT	Simple cycle gas turbine
TCI	Total capital investment
TERA	Technoeconomical environmental risk analysis
TET	Turbine entry temperature

Chapter 1

INTRODUCTION

1.1 Application Requirements

The power-generation sector is the major anthropogenic (man-made) source of greenhouse gas emissions, which is believed to cause changes to our global climate and health in many ways [1]. The gas is a mixture of mainly carbon-dioxide (CO_2) and methan (CH_4), where, currently in the UK, power generation accounts for a third of total carbon-dioxide emissions [2]. To restrict future emissions, the UK government has introduced carbon-dioxide taxes in the hope of prompting investment in low-carbon power-generation technologies. Due to these policies, we are seeing a shift towards new single and combined gas-turbine designs, which aim to reduce the emitted pollutants. In this context, Cranfield University began to develop a Techno-economical Environmental Risk Analysis (TERA) methodology for the evaluation of advanced power plant concepts in order to meet challenging environmental goals.

The present study is a part of TERA program, and in particular considers the thermoeconomic optimization of single and combined gas-turbine cycles. The optimization includes both "design" and "operation" conditions. The optimization process adapts updated models for power demand patterns, legislation, capital cost, and inflation. This work contributes to the understanding of the current and future design

of cost efficient systems with reduced environmental impacts. It follows the previous works in this field but employs an updated model of capital cost, a surrogate-based optimization method, and extends previous work for different HRSGs at design and operating conditions.

1.2 Objectives of Work

In summary, the present study contributes to the design of future power plants by achieving five main objectives:

- Establishing a framework for optimal design of simple and combined gas-turbine cycles
- Capital cost modeling
- Integration of gas turbine with a heat recovery steam generator
- Multiple-variable thermoeconomic optimization of single and combined gas turbine cycles.
- Surrogate-based thermoeconomic optimization

The application of multiple variable optimization methods to such complex cycles can be a challenging task. In order to better understand the optimization results and for the purpose of code development, following scenarios were also defined and investigated:

- Single-variable thermodynamic optimization of gas turbine
- Single-variable thermoeconomic optimization of gas turbine
- Single-variable thermodynamic optimization of combined cycle

- Single-variable thermoeconomic optimization of combined cycle
- Multiple-variable thermoeconomic optimization of combined cycle
- Single-variable thermoeconomic optimization of gas turbine at off-design conditions

1.3 Study Tools

Multidisciplinary tools are required for modeling a gas turbine's performance, in conjunction with steam cycle and combined cycle power plant and quantifying emissions, environmental impacts and cost analysis of power plant and resources. For the gas turbine's performance, the Cranfield University code of VariFlow was used, however for optimization purposes, a call function is required in order to automatically generate an input file, launch the calculations and return the engine performance data for objective function quantifications. For the models of steam cycle and combined cycle there are various available TERA approaches developed by the author and former Cranfield University researchers [3], [4] and [5]. These codes were stand-alone and needed to be integrated with performance simulation codes within optimization framework. Also, different algorithms are available for the optimization problem. The MATLAB platform was used in order to integrate all simulation model tools with the optimization methods. A new optimization method based on expected improvement function was also proposed and used.

1.4 Thesis Outline

This thesis is divided into seven chapters:

- **Chapter 1**: This presents the main objectives and approaches considered to reach the targeted objectives

- **Chapter 2**: The review of the relevant literature provides a comprehensive understanding of the subject and identifies what research is needed.

- **Chapter 3**: The third chapter presents discussions in detail to the used meth odologies and techniques for modeling gas turbine performance. The performance prediction of gas turbine from VarilFlow is described for design point, off-design and bleeding air scenario.

- **Chapter 4**: This chapter provides some equations to estimate the capital cost of gas turbine. The cost predictions are compared with the available engine data.

- **Chapter 5**: This chapter reviews the performance equation of combined cycles with 1,2, and 3 pressure level HRSG. The combined cycle performance is compared against gas turbine and then effects of design parameters into thermal efficiency are evaluated.

- **Chapter 6**: The results of single-variable and multiple variable optimization of simple and combined cycles are described. The optimization approach is extended to include the constraints, e.g. metal temperature and steam quality. Also, the optimization results at different operating conditions are discussed.

- **Chapter 7**: This chapter summarizes the findings from the present investigation and presents general recommendations for future studies.

1.5 Summary of Authors Contributions

This investigation makes a contribution to knowledge in the following ways:

1. The research undertaken led to a performance methodology which specially adapted for an industrial gas-turbine. The accuracy of the resulting predictions

has been compared with available engine data from manufacturer and experimental measurements. The simulation model was run for different ambient temperatures to assess the engine's capability to satisfy the operating conditions. In addition, the feasibility of bleeding air was studied.

2. Selection of a HRSG configuration to combine the gas and steam power plants

3. This study presents the trends of single and combined engine design parameters for different scenarios.

4. Updated equations were proposed for capital cost estimation. The predictions were compared with available engine data.

5. A new optimization method based on surrogate modeling was used. This approach helps to find the global minima but at a reduced cost compared with Genetic Algorithm approach.

Chapter 2

BACKGROUND AND RELATED WORK

The thermoeconomic analysis of thermal systems is a scientific discipline that has drawn extensive attention in recent years due to increased competitions in the energy market. The main objective of thermoeconomics is to find a trade-off between high thermal efficiency and low capital cost. In this context, a distinction should be made between thermoeconomics and thermodynamics in which is the science of energy and its transformation [6]. The thermodynamic performance of a system is determined using energy and mass conservation equations for each component and their integration into whole system for given input parameters [7]. Although thermodynamic analysis can be used to improve the system performance, such an approach has no assessment of the feasibility of design in terms of cost estimation and economic analysis. On the contrary, a thermoeconomic method combines expenditures of financial resources (economic) with thermodynamic equations of an energy system [8] and provides a compromise between maximum thermodynamic performance and cost minimization [9]. The thermoeconomic methods can be formulated using the second law of thermodynamics (exergy) with economic principles and these methods

therefore are named exergoeconomic [10].

The scope of thermoeconomics is very extensive. It ranges from cost analysis, improvement, and technical comparisons to the feasibility and optimization of energy systems. The thermoeconomic optimization of simple and combined cycle gas turbine power plants is considered in this work with the objective function of minimum cost under the given constraints. The cost function is the unit price of producing electricity and is defined as the ratio of total system cost to the installed killowatt of electrical energy capacity. The total cost consists of fuel, capital, maintenance, and operating costs. Also, many new government regulations face the energy industry to reduce the amount of emitted pollutants [11]. In 1991, Frangopoulos [12] introduced environmental considerations in the cost function as well. His approach was accepted as a new definition for application of recent thermoeconomic methods. The outcome of thermoeconomic analysis, as it is termed today, is the design of cost efficient systems with reduced environmental impact [13].

Thermoeconomic methods might be classified into "synthesis", "design", and "operation" types [14]. Sometimes the definition terms of "design" and "synthesis" can overlap each other. In synthesis optimization, designer concerns flow diagrams of energy in the system by choosing components and interconnections, while in the design type optimization, the design parameters of each component are considered at "design-point" conditions. As energy flow diagrams and parameters are fixed, operating optimization is employed in order to find optimal operating point under "off-design" conditions. This term applies to engine operation parameters such as speed of evolution, power output, mass flow rates, pressures, and other parameters that deviate from the design point.

The methods presented in this thesis are intended to address these issues.

2.1 Gas Turbine Technology

The gas turbines were originally introduced in jet engines for aircraft and eventually found subsequent applications in the power-plants (so-called heavy-duty gas turbines). Between 1910 and 1980, the power generation development was mainly dominated by the steam turbine power plants [15]. However, steam turbines suffer from large scale production, long construction time, long term investment, and high capital intensity. The unit capital cost of steam plants is also strongly scale-dependent [16]. In recent years, the heavy-duty gas turbines have taken a dominant role in the power generation development [17]. The gas turbines are economically attractive due to low capital cost, high power ratio to size, high reliability, and flexibility of using wide range of fuels [18]. In contrast to the jet engines that must be light weight and very reliable, the heavy-duty gas turbines must be inexpensive to operate. The thrust/weight ratio is an important design parameter of aircraft gas turbines but the power/weight ratio does not play an important role in the design of heavy-duty gas turbines [19], therefore the design paths for aviation and industrial gas turbines have diverged. For example, the aeroderivative engines tend to have a lower exhaust temperature which could limit their application for use in power generation development [20].

The industrial gas turbines used in power plants can be classified into two major types: a) an open (simple) cycle b) and a combined cycle configuration. The open cycle gas turbines can be started and stopped so easily compared with other power plants and therefore are used for peak load power and tertiary reserve and operate for limited number of hours per year, typically between 2,000 and 5,000 hours [21]. The gas turbines used for electric power generation can produce electric power ranging from 20 to 250 megawatts with efficiencies around 40% [21]. These gas turbines typically have a single-shaft configuration, operate at Brayton cycle [22] and consist of a compressor, a combustion chamber, and a turbine as shown in Fig. 2.1. Today's

modern heavy-duty gas turbine generally have an axial compressor with pressure ratios between 15 to 19 and isentropic efficiencies of around 87% [23]. In the combustion chamber, fuel is added to the compressed air and ignited to increase the gas temperature as much as 1400^{o}C or higher. This temperature has significant effects on the plant thermal efficiency: the gas turbine efficiency is enhanced by increasing the turbine inlet temperature. Higher turbine inlet temperature possibly adds to the purchased equipment cost due to using cooling designs and new expensive materials. The materials used in modern turbines could typically cope with an inlet temperature of 1425^{o}C [23]. The hot air is then expanded in the turbine and produces work. The common shaft drives both the air compressor and the electric generator at a fixed rotational speed. The combustion products are exhausted to the atmosphere with relatively high temperatures.

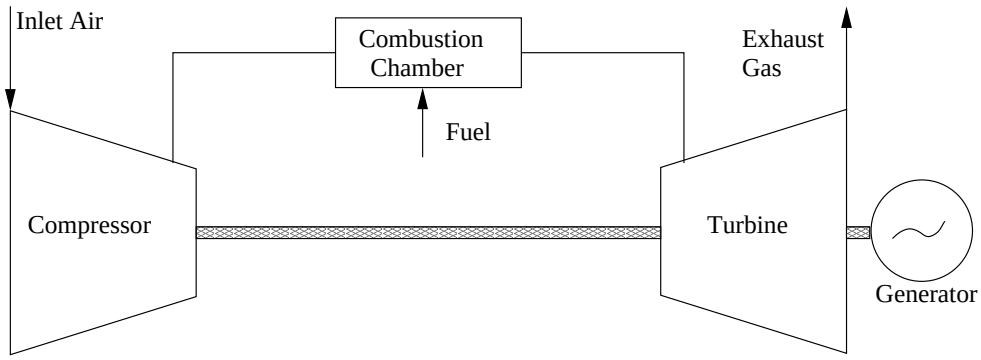

Figure 2.1: A single-shaft simple cycle power plant.

One way to use a gas turbine exhaust heat is to generate steam in a combined cycle power plant. The combined cycle power plant usually consists of a gas turbine plant, a Heat Recovery Steam Generator (HRSG), and a steam turbine plant as shown in Fig. 2.2. The gas turbine and steam plants are often called topping and bottoming cycles, respectively. The high-temperature exhaust gases leaving the gas turbine enter the HRSG, where the energy is transferred from the exhaust gases to the water

in the steam power plant [24]. The HRSG consists of three heat exchanger sections: 1) the economizer, 2) the evaporator, 3) and the superheater [25]. In the economizer, the liquid water from the pump is heated up to a temperature close to its saturation point. In the evaporator, the water is evaporated at constant temperature and pressure. A drum is used to separate the water from steam in which is then heated in the superheater until it reaches to the desired live-steam temperature. The HRSG models are classified with respect to steam pressure levels; typical configurations are single-pressure, dual-pressure, and triple-pressure HRSG. The single-pressure HRSG is relatively simple but the stack temperature (final gas temperature) is relatively high. Dual- and triple-pressure level configurations aid in to extract more heat from the gas turbine exhaust gas and therefore the stack gas has lower temperatures leaving HRSG. Figure 2.3 shows the temperature-heat diagram of a single-pressure level combined cycle, where the water in the steam plant enters the HRSG economizer as a subcooler liquid (state a). The water temperature is increased in the economizer till it becomes saturated liquid (state b). This is the point where the minimum temperature difference between the water in the steam cycle and the exhaust gases occurs and is called the pinch point [24]. Pinch point values are typically in the range of 8^oc to 15^oc; the small pinch point difference results in larger heat-transfer surface area. In the b-v process, water is changed from a saturated liquid to a saturated vapor in the evaporator, and then is super heated in the v-d process till it reaches the steam cycle maximum temperature. The gas turbine exhaust gas enters the HRSG at state 4 and leave the HRSG at state 5. It is desirable to reduce the exit gas temperature (state 5) as much as possible to have a higher combine cycle thermal efficiency. A combined cycle could have an overall efficiency as high as 58%.

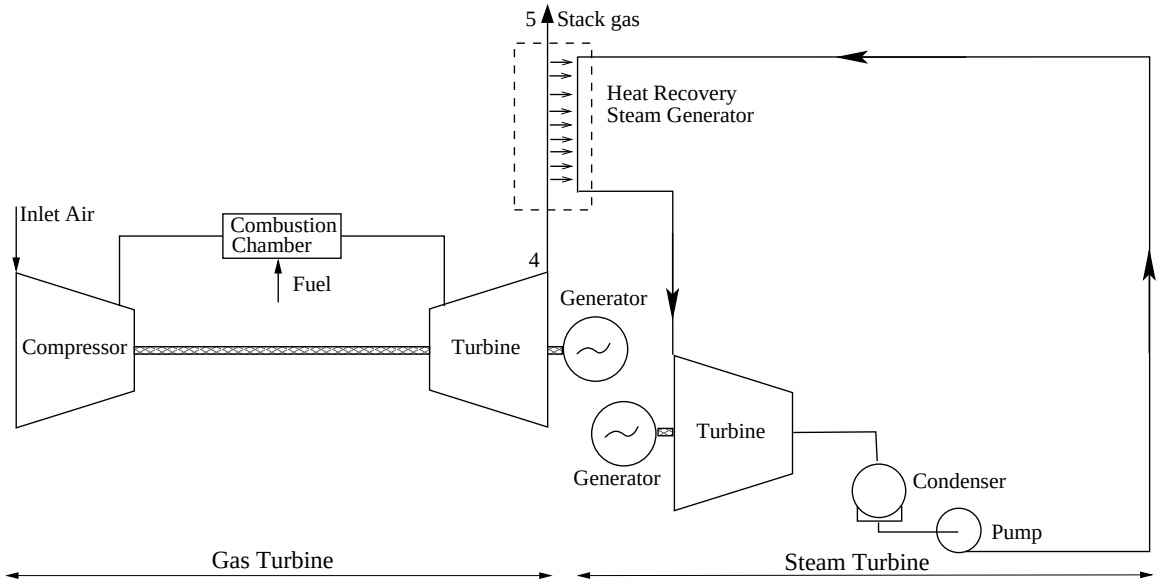

Figure 2.2: Combined gas and steam cycle power plant.

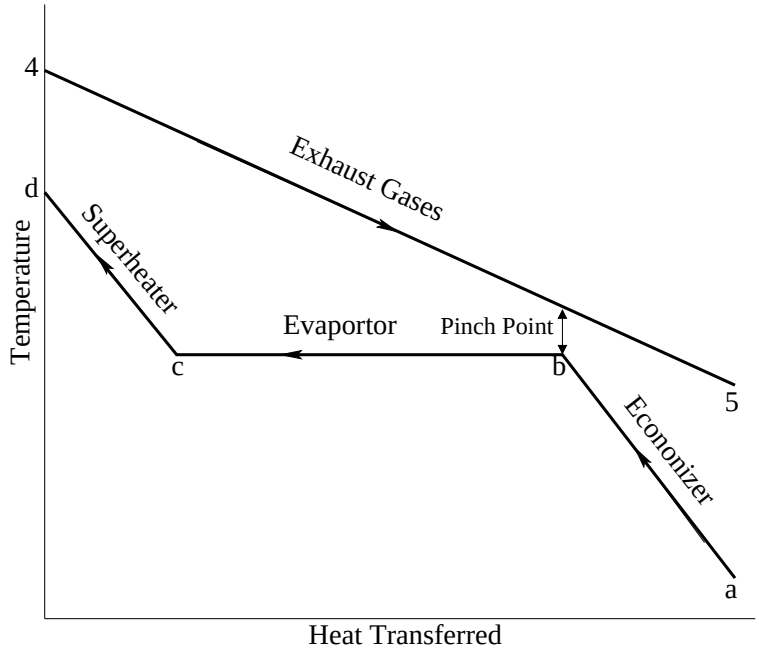

Figure 2.3: Temperature-heat diagram of a single-pressure combined cycle.

2.2 Economics of Power Plants

In thermodynamics, the performance of a system is measured by thermal efficiency. It should be noted that in a comparison between two competitive plants, high efficiency plant does not always offer lower cost. A thermodynamically optimal design is generally more different from a cost-optimal design: the total cost of a thermodynamically optimal design is always higher than cost-optimal design. An economic performance indicator is therefore needed to compare the economy of different power plants. The concept of unit price of producing electricity by the plant (e.g. US$/kwh) is a simple and convenient definition to examine and compare the economic of power plants [26]. Traditionally, these costs are assigned to the capital cost and the cost of consuming resources (fuel). Recently, this term has included any pollution and degradation of the environment as well [27]. The annual cost of the electricity produced, as it is termed today, includes the purchased equipment cost, resources consumption cost (fuel), the annual cost of operation and maintenance, and the pollution cost (mainly NO_x and CO). This cost is expressed as [26]

$$C_E = \beta C_0 + C_{\text{fuel}} + C_{\text{OM}} + C_{\text{NO}_x} + C_{\text{CO}} \tag{2.1}$$

where C_E is the annual electricity cost (e.g. US$); C_0 is the purchased equipment cost of power plant; β is a capital charge factor that relates to the discount rate on capital and the life of the plant; C_{fuel} is the annual cost of fuel consumed; C_{OM} is the annual cost of operation and maintenance; C_{NO_x} and C_{CO} are pollution taxes. The unit price of producing electricity is then defined as

$$\dot{C_E} = \frac{C_E}{\dot{W}_g\ N} = \frac{\beta C_0}{\dot{W}_g\ N} + \frac{C_{\text{fuel}}}{\dot{W}_g\ N} + \frac{C_{\text{OM}}}{\dot{W}_g\ N} + \frac{C_{\text{NO}_x}}{\dot{W}_g\ N} + \frac{C_{\text{CO}}}{\dot{W}_g\ N} \tag{2.2}$$

where $\dot{W}_g$ is the plant gross power (kw) and N is number of operating hours per year.

The unit of $\dot{C}_E$ is commonly expressed in US$/kwh. Note that the second term in above equation is related to thermal efficiency of plant. The annual cost of fuel is written as:

$$C_{\text{fuel}} = c_{\text{fuel}} \times (\dot{m}_{\text{fuel}} \times \text{LHV}) \times N \tag{2.3}$$

where c_{fuel} is the fuel cost per unit of energy; LHV is the lower heating value and $\dot{m}_{\text{fuel}}$ is the fuel mass flow rate. Equation 2.2 then changes to:

$$\dot{C}_E = \frac{\beta C_0}{\dot{W}_g\ N} + \frac{c_{\text{fuel}}}{\eta_{th}} + \frac{C_{\text{OM}}}{\dot{W}_g\ N} + \frac{C_{\text{NO}_\text{x}}}{\dot{W}_g\ N} + \frac{C_{\text{CO}}}{\dot{W}_g\ N} \tag{2.4}$$

where $\eta_{th} = \dot{W}_g/(\dot{m}_{\text{fuel}} \times \text{LHV})$ is the thermal efficiency. Equation 2.4 shows that the larger gross power (plant size), the smaller the cost function of $\dot{C}_E$. Equation 2.4 has both the effects of efficiency and cost, where the typical trends of cost and efficiency with the plant size are shown in Fig 2.4. This figure shows that efficiency increases with increasing the plant size and then nearly remains unchanged. Figure 2.4 also shows that the larger plant size the smaller initial cost per kilowatt [28]. The initial cost per kilowatt sharply rises for small power plant as shown in Fig 2.4.

The capital charge factor (β) is used to take into account the cost recovery of the plant purchased equipment cost during plant lifetime. Note that the money has a time value and the money earned in the plant lifetime is not the same as money invested initially. Assuming that initial plant capital cost is C_0 and the plant has a life of H years, the annual cost is then $D \times C_0 + B$, where the first term is the simple interest payment and the second term is related to cost repayment after H years, where D is the discount rate. The interest added to the accumulated cost at the end of each year is then found as:

$$B\left[1 + (1+D) + (1+D)^2 + ... + (1+D)^{H-1}\right] = C_0 \tag{2.5}$$

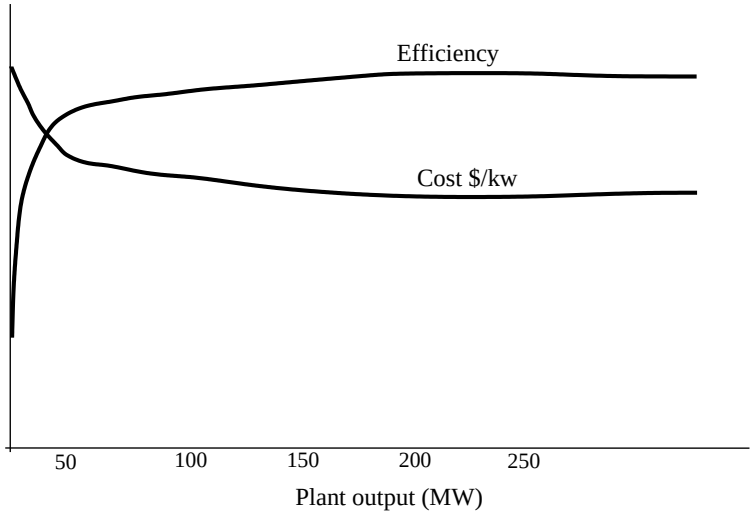

Figure 2.4: Typical trends of plant cost and efficiency.

and therefore

$$B = \frac{D\ C_0}{(1+D)^H - 1} \tag{2.6}$$

where the total annual payment is:

$$D.C_0 + B = C_0 \left[D + \frac{D}{(1+D)^H - 1} \right] = D.C_0 \left[D + \frac{(1+D)^H}{(1+D)^H - 1} \right] = \beta C_0 \tag{2.7}$$

and then the capital charge factor (β) is calculated as:

$$\beta = \left[\frac{D(1+D)^H}{(1+D)^H - 1} \right] \tag{2.8}$$

where in above, the capital charge factor depends on the discount rate (D) and the life of the plant (H years).

In design-type economic study, the power ($\dot{W}_g$), fuel cost (C_{fuel}), and pollution

costs ($C_{\mathrm{NO_x}}$ and C_{CO}) are obtained from design point conditions and nearly unchanged during the power plant lifetime. However, the power plant performance will change because of ambient air changes and operating at different loads [29]. Assuming, the power plant hours of $[N_1, N_2, ..., N_n]$ corresponding to different operation conditions (see Fig. 2.5), the gross powers, fuel cost, and pollution costs corresponding to these hours are denoted as $[\dot{W}_{g1}, \dot{W}_{g2}, ..., \dot{W}_{gn}]$ and $[C_{\mathrm{fuel}1}, C_{\mathrm{fuel}2}, ..., C_{\mathrm{fuel}n}]$, $[C_{\mathrm{NOx}1}, C_{\mathrm{NOx}2}, ..., C_{\mathrm{NOx}n}]$, $[C_{\mathrm{CO}1}, C_{\mathrm{CO}2}, ..., C_{\mathrm{CO}n}]$ respectively. Equation 2.2 then changes to

$$\dot{C_E} = \frac{\beta C_0}{\sum_{i=1}^{n} \dot{W}_{gi}\ N_i} + \frac{\sum_{i=1}^{n} C_{\mathrm{fuel}i}}{\sum_{i=1}^{n} \dot{W}_{gi}\ N_i} + \frac{C_{\mathrm{OM}}}{\sum_{i=1}^{n} \dot{W}_{gi}\ N_i} + \frac{\sum_{i=1}^{n} C_{\mathrm{NOx}i}}{\sum_{i=1}^{n} \dot{W}_{gi}\ N_i} + \frac{\sum_{i=1}^{n} C_{\mathrm{CO}i}}{\sum_{i=1}^{n} \dot{W}_{gi}\ N_i} \tag{2.9}$$

where index i corresponds to each part load conditions. The part load powers of $\dot{W}_{gi}$ could be written as the product of the design-point power and a load factor L_i, i.e

$$\dot{W}_{gi} = \dot{W}_{g\mathrm{des}} \times \frac{\dot{W}_{gi}}{\dot{W}_{g\mathrm{des}}} = \dot{W}_{g\mathrm{des}} \times L_i \tag{2.10}$$

Likewise the part load fuel cost can be written in the form of design point conditions, i.e.

$$C_{\mathrm{fuel}i} = C_{\mathrm{fuel}\mathrm{des}} \times L_i \times \frac{\eta_{\mathrm{des}}}{\eta_i} \times \frac{N_i}{N_{\mathrm{des}}} \tag{2.11}$$

2.3 Capital Cost Modeling

Capital cost is regarded as the sum of capital investment, operating (excluding fuel) and the maintenance costs [30]. Though capital investment cost is a "one-time" cost but operating and maintenance cost are continuing during the life of system [8], hence,

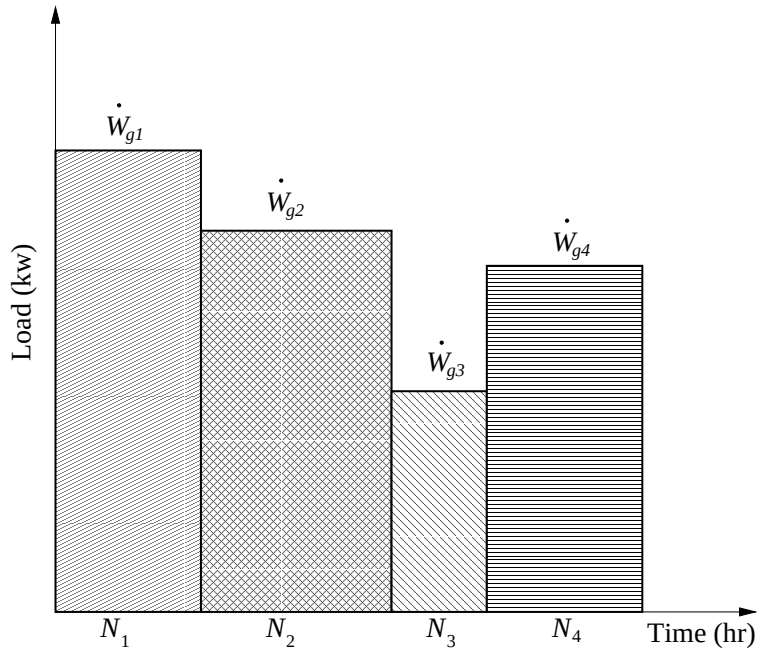

Figure 2.5: Part-load operation of a power plant.

"annualized capital cost" is defined and used here:

$$\dot{C}_z = \frac{\beta C_0 + C_{\mathrm{OM}}}{N} = \frac{C_0 \times FCR \times \Phi_r}{N} \tag{2.12}$$

where, FCR is the annual fixed change rate percent with standard value of 18.2 percent, Φ_r is maintenance factor with standard value of 1.06, N is number of operating hours per year and C_0 shows the capital investment in US$. Annualized capital cost is denoted by $\dot{C}_z$ and expressed in US$/h.

According to Eq. 2.12, the cost of capital investment (C_0) is required for estimation of capital cost. Two approaches can be considered in order to estimate the capital investment. Agazzani *et al.* [31] and von Spakovsky and Frangopoulos [27] have presented a number of empirical functions in order to estimate the "Purchased Equipment Cost" (PEC) of gas turbine's parts. In the first consideration, the sum of the PECs of all units (called component capital cost) are solely used as the cost of

capital investment, while in the second approach additional costs for purchasing the land, installation, piping, and etc. are also considered. This approach is often called Total Capital Investment (TCI).

Massardo and Scialo [32] and Bejan *et al.* [8] split TCI into fixed capital investment (FCI) and costs during actual design and construction period such as start-up cost, research and development cost. FCI itself consists of "direct" and "indirect" expenditures, where the former is the cost of equipment, materials, and labor that are used for all life-time of a system, while the latter includes the expenditures that are not permanent part of system such as engineering and supervision costs. Finally, direct costs include "on-site" and "off-site" costs. All installed equipment costs lie in the category of on-site costs and all costs associated with the production and distribution in a system (Land, civil and etc) are examples of the "off-site" type. Bejan *et al.* [8] correlated TCI to PEC for two different scenarios of new system and expansion (see Fig. 2.6):

$$C_0 = \begin{cases} 4.30 & \text{PEC (new system)} \\ 2.83 & \text{PEC (expansion)} \end{cases} \tag{2.13}$$

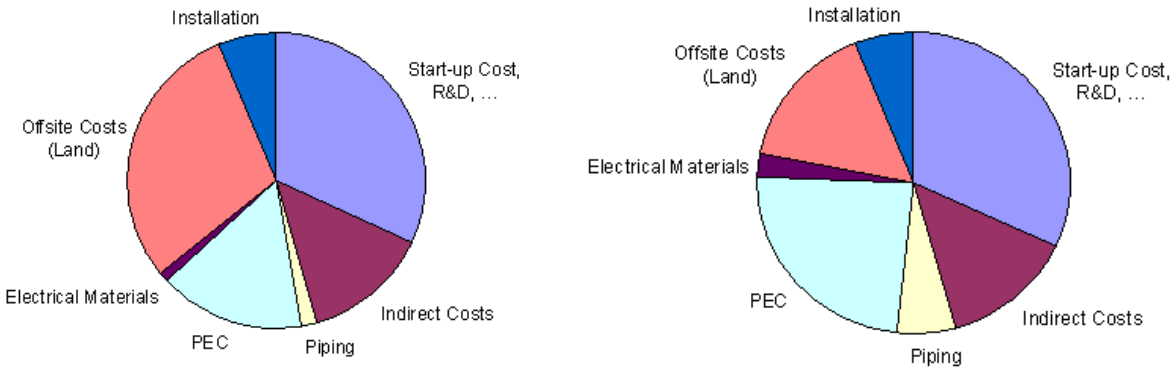

New Design Expansion

Figure 2.6: Breakdown of total capital investment.

However, PEC values are still required for capital investment estimation (both component and total type). Questions concerning the type of capital cost income can be answered by taking into account the design requirements and designer's preferences. Agazzani et al. [31] and von Spakovsky and Frangopoulos [27], for example, have used component cost, while Massardo and Scialo's threomeconomic analysis [32] has considered both component and total capital investments.

Furthermore, for effective implementation of capital cost (or PEC) in the optimization problem, correlations between capital cost and the size and performance of system are required. To draw these conclusions, the functions proposed by El-sayed and Tribus [33] and modified by von Spakovski and Frangopolous [27] and used by Agazzani *et al.* [31] and Massardo and Scialo [32] were implemented. These functions are as follows:

$$C^{\$}_{cmp} = \frac{c_{11}}{c_{12} - \eta_{scp}} \frac{P_2}{P_1} \dot{m}_a \tag{2.14a}$$

$$C^{\$}_{cmb} = \frac{c_{21}}{c_{22} - \dfrac{P_3}{P_2}} [1 + \exp(c_{23} \mathrm{T}_3 - c_{24})] \dot{m}_a \tag{2.14b}$$

$$C^{\$}_{gtu} = \frac{c_{31}}{c_{32} - \eta_{sgt}} \ln(\frac{P_3}{P_4}) [1 + \exp(c_{33} \mathrm{T}_3 - c_{34}] \dot{m}_g \tag{2.14c}$$

$$C^{\$}_{phtr} = c_{41} (A_{phtr})^{0.6} \tag{2.14d}$$

$$\begin{aligned} C^{\$}_{eco/eva} = {} & c_{51} [(\frac{\dot{Q}_{eco}}{\Delta T_{LM_{eco}}})^{0.8} + (\frac{\dot{Q}_{eva}}{\Delta T_{LM_{eva}}})^{0.8}] \\ & + c_{52} \dot{m}_{st} + c_{53} \dot{m}_g^{1.2} \end{aligned} \tag{2.14e}$$

where c_{ij} coefficients are given in Appendix A. In Eqs. 2.14, η_{scp} and η_{sgt} denote the compressor and turbine isentropic efficiencies, respectively. Also, P_1, P_2, P_3 and P_4 present the air and gas pressure at the inlet and outlet of compressor and turbine, respectively. T_3 is the maximum gas turbine temperature in Kelvin, while $\dot{m}_a$ and

$\dot{m}_g$ are compressor entering air and gas mass flow rates in kg/s, respectively. ΔT_{LM} denotes a log mean temperature difference; $\dot{Q}_{ec}$ and $\dot{Q}_{eva}$ represents the rates of heat transfer in the economizer and evaporator, respectively. The purchased equipment cost is then calculated as the sum of all component costs, i.e.:

$$\text{PEC} = C_{cmp} + C_{cmb} + C_{gtu} + C_{phtr} + C_{eco/eva} \tag{2.15}$$

2.4 The Cost Of Resources

For a combined cycle problem, the consumed resources are fuel and water. These costs are named running cost [34]. The following equations are used in order to quantify corresponding costs:

$$C_{\text{fuel}} = c_{\text{fuel}} \times (\dot{m}_{\text{fuel}} \times \text{LHV}) \times N \tag{2.16}$$

$$C_{\text{water}} = c_{\text{water}} \times \dot{m}_{\text{w}} \times N \tag{2.17}$$

where C_{fuel} is the annual fuel cost, c_{fuel} is the fuel unit cost per unit energy; LHV is the lower heating value; $\dot{m}_{\text{fuel}}$ is the fuel mass flow; C_{water} is the annual water cost; c_{water} is the water unit cost per liter; $\dot{m}_{\text{w}}$ is the water mass flow; and N is the operating hours per year. The coefficients of c_{fuel} and c_{water} are given in Appendix A.

2.5 The Cost Of Pollution

Typical exhaust emissions from a stationary gas turbine are listed in Table 2.5. In general, emissions of NOx and CO are the main sources of changing air quality and need to be controlled [35]. The gas turbine combustion chamber is specially designed to produce the minimum quantity of NOx. This NOx is produced at high temperature

by a reaction between oxygen and nitrogen in the air, but this can be controlled by controlling the combustion process so that all the oxygen is used during combustion, leaving none to react with nitrogen. Figure 2.7 shows the reduction in Nox of gas turbine combustors over the past 30 years by the change in fuels, steam or water injection, and the development of advanced combustor technologies. The New Source Performance Standards (NSPS) regulations for gas turbines on September 1979 required that gas turbine with powers ranging from 1,000 to 10,000 hp to reduce the Nox emission below 75 ppm (part per million) [36]. The steam or water injection has been used successfully to reduce Nox levels [37]. The amount of water required for this purpose approximately ranges from 0.5% to 0.75% of the fule flow [28]. The steam or water injection changes the engine performance such that the output power increases but the efficiency falls [38]. The steam or water injection used in the single-nozzle combustors can only reduce the NOx level below 42 ppm. Since 1987, using multi-nozzle combustors with steam water injection has helped to reduce Nox emissions below 25 ppm; this was further lowered by the use of the dry low emission/Nox combustors in the 1990s [28]. Catalytic combustors can now reduce NOx formation below single digit ppm [39].

Table 2.1: Gas turbine emissions burning conventional fuels.

Pollutants	Typical Concentration	Source
Nitric Oxide(NO)	20 - 220	Oxidation of Atmosphere Nitrogen
Nitric Dioxide (NO_2)	2 - 20	Oxidation of Fuel-Bound Organic Nitrogen
Carbon Monoxide (CO)	5 - 330	Incomplete Oxidation of Fuel Carbon
Sulfur Dioxide (SO_2)	Trace - 100	Oxidation of Fuel-Bound Organic Sulfur
Sulfur Trioxide (SO_3)	Trace - 4	Oxidation of Fuel-Bound Organic Sulfur
Unburned Hydrocarbons (UHC)	5 - 300	Incomplete Oxidation of Fuel or Intermediates
Particulate Matter Smoke	Trace - 25	Inlet Ingestion, Fuel Ash, Hot-Gas-Path, Attrition, Incomplete Oxidation of Fuel or Intermediates

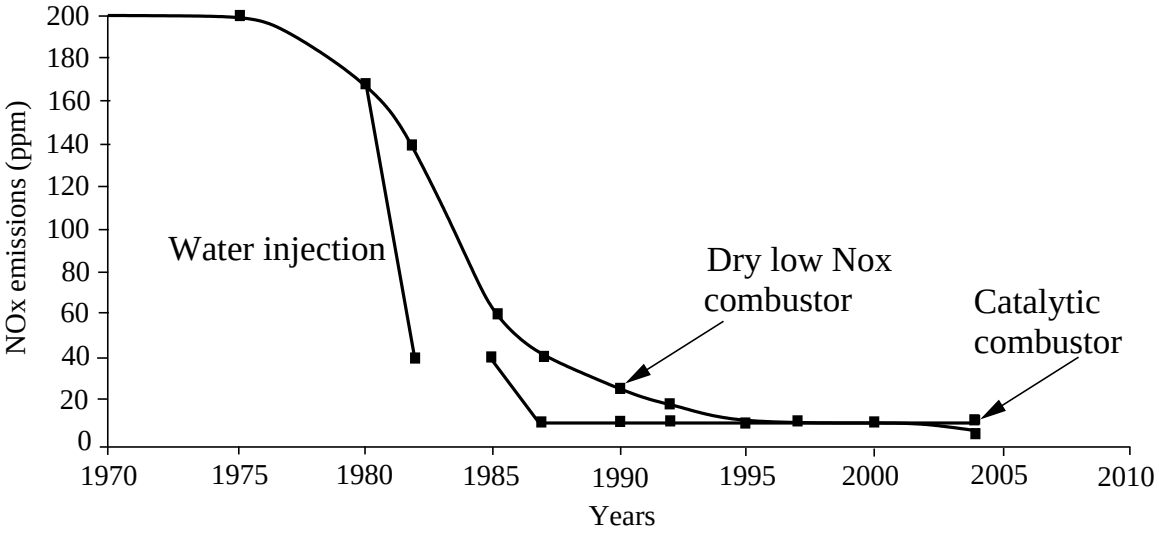

Figure 2.7: Control of gas turbine NO_x emissions over the years.

This study concerns only the costs of NO_x and CO in the optimization problem. The cost of emission approximates a monetary quantification of environmental damages originating from pollutants of energy system and commonly, named external costs [13]. The basic equations for estimating the emission cost are derived from emission taxes forced by authorities to the energy sector, thus the validity and utility of these equations depend largely on the region where power plant is being used. The first step towards the cost estimation is an estimation of amount of pollutant emissions. Again, for this optimization only CO and NO_x emissions were considered. Estimation of these pollutants is a complex and challenging task. Ideally these estimations should be provided by a high-fidelity computational method that receives optimized independent parameters and generates an estimation amount. Unfortunately, the employed gas turbine's performance simulation code does not include any emission analysis. In order to overcome this deficit, correlations initially proposed by Lefebvre [40] and later elaborated by Rizk and Mongia [41] were employed. These correlations give the emissions in g/kg fuel as:

$$\dot{m}_{\mathrm{NO_x}} = 0.15\mathrm{e}16\ (t - 0.5t_{ev})^{0.5}.\exp(\frac{-71100}{T_{st}})/(P^{0.05}(\frac{\Delta P}{P})^{0.5}) \quad (2.18)$$

$$\dot{m}_{\mathrm{CO_x}} = 0.179\mathrm{e}9\exp\ (\frac{7800}{T_{pz}})/(P^2(t - 0.4t_{ev})(\frac{\Delta P}{P})^{0.5})) \quad (2.19)$$

$$(2.20)$$

where, t_{ev} denotes the fuel evaporation time in seconds. T_{st} and T_{pz} are stoichiometric temperature of combustor flame and the primary zone combustion temperature in ^{o}K, P denotes the combustion pressure in Pa and t is the primary-zone residence time in seconds.

For optimization purposes, these correlations need more elaborations. Whether the compressor pressure ratio (PR) is part of the independent variables for the optimization, the amount of NO_x and CO must be related to the variation of PR. The PR changes are considered through the changes in kg fuel (predicted from engine's performance simulation program assuming fuel flow is a variable) and the changes in term P in above equations. The former effect also applies to changes in a framework such that turbine entry temperature (TET) is used for optimization, but additional equations are needed to correlate TET with T_{pz} and T_{st} in above equations.

The cost of pollutant are quantified from the mass flow rate calculations:

$$C_{\mathrm{NOx}} = c_{\mathrm{Nox}} \times \dot{m}_{\mathrm{NO_x}} \times N \quad (2.21)$$

$$C_{\mathrm{CO}} = c_{\mathrm{CO}} \times \dot{m}_{\mathrm{CO_x}} \times N \quad (2.22)$$

where c_{NOx} and c_{CO} are given in Appendix A.

2.6 Thermodynamics Modeling of Combined Cycles

There is an increasing interest to apply thermoeconomic optimization methods to large and complex combined cycle power plants [13, 42, 43, 44]. Pelster *et al.* [13] have detailed an environmic/thermoeconomic optimization method of the synthesis, design, and operation of an advanced combined cycle power plant. Valdes *et al.* [42] presented a genetic algorithm optimization method of a single- and a triple-pressure HRSG. Attala *et al.* [43] described a definition of production cost objective function for combined cycles as well. A thermoeconomic study needs a thermodynamic model of combined cycle. This model is detailed below:

2.6.1 Gas Turbine Performance

A prediction and understanding of engine's performance is desirable prior to a thermoeconomic analysis and optimization study. The engine's performance could be determined by experiment or predicted by simulation codes. Engine experiments must take into account human safety, the flexibility of test repeats, reliability and uncertainty issues [45]. All these difficulties, plus the associated high costs of experiments, have resulted in only a few number of test beds being developed around the world [46]. As a result, an analytical performance model of the engine, based upon component characteristics and aero-thermo relationships, was developed.

With the advantages and capabilities of computers, several different engine-simulation codes have been developed. In order to make these performance models easily employed by a non-specialist they must be reliable, repeatable and possess generic features e.g. off-design and deteriorated engine's performance. Furthermore, they must predict with reasonable accuracy over the entire operating condition and flight envelope. For such a performance model, the understanding of the behavior of the gas

turbine is very important. References of [47], [48] and [49] described the key factors governing the gas turbine's performance.

Engine's performance is usually represented by thrust (aviation use) or power (industrial applications), fuel consumption, SFC or thermal efficiency (industrial) and specific power (industrial) or thrust. Predicting the engine's performance is achieved by solving thermodynamical equations obtained for the behavior of each component based on the physical laws of conservation of energy and mass flow ratio.

From the preceding arguments, an accurate model can be established to predict the engine's behavior. For an arbitrary gas-turbine, the following relationship between the dependent variables, y, and the component variables (independent) vector x and the input vector, u is usually employed.

$$y = h(u, x) \tag{2.23}$$

The x vector contains the component characteristics (i.e. mainly efficiencies and flow capacities) whereas the vector u defines the engine's operating conditions. The function h is based on a set of theoretical or empirical equations.

The solution of Eq. 2.23 for the given component and input variables calculates the engine's performance conditions. Depending on the operating conditions, these equations can be linear or non-linear. The assumption of linearity is appropriate for the simulation of models with small perturbations about a single operating point.

The conventional gas turbine cycle is the Brayton cycle as shown in Fig 2.8. The relation of thermodynamic models of such a cycle are briefly described.

- Air Compressor: The compressor output temperature is calculated as:

$$\mathrm{T}_2 = \mathrm{T}_1 + \left[1 + \frac{1}{\eta_{scp}} \left[r_c \frac{\gamma_a - 1}{\gamma_a} - 1\right]\right] \tag{2.24}$$

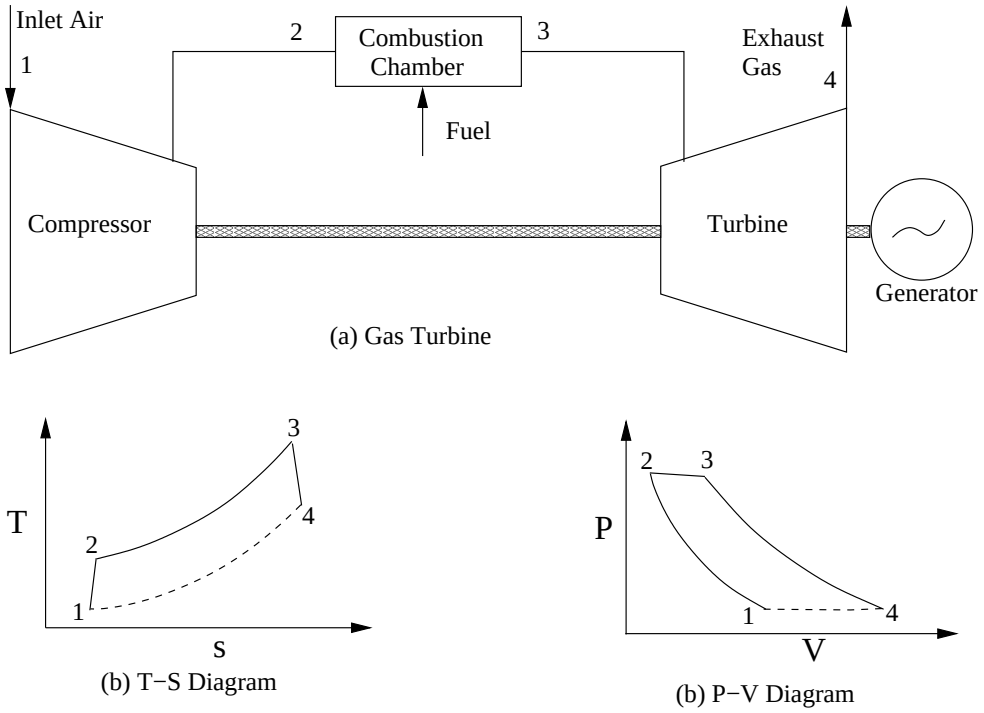

Figure 2.8: Gas turbine thermodynamic model.

where T_1 is the compressor inlet temperature; η_{scp} denote the compressor isentropic efficiency; γ_a is the air specific ratio; and $r_c = P_2/P_1$ is the compressor pressure ratio. The work needed to derive compressor is:

$$\dot{W}_{cmp} = \dot{m}_a \; C_{pa} \; (T_2 - T_1) \tag{2.25}$$

where, $\dot{m}_a$ is the inlet mass flow rate and C_{pa} is the air specific heat at constant pressure.

- Combustion Chamber: The heat balance equation in the combustion chamber is:

$$\dot{m}_a \; h_2 + \dot{m}_{\text{fuel}}\text{LHV} = \dot{m}_g \; h_3 + (1 - \eta_{cmb})\dot{m}_{\text{fuel}}\text{LHV} \tag{2.26}$$

where h_2 and h_3 are the enthalpy at the combustion chamber inlet and outlet,

respectively; $\dot{m}_g = \dot{m}_a + \dot{m}_{\text{fuel}}$; and η_{cmb} is the combustion efficiency. The outlet pressure is also found as:

$$\frac{P_3}{P_2} = (1 - \Delta P_{cc}) \tag{2.27}$$

where ΔP_{cc} is the combustion chamber pressure loss.

- Turbine: The turbine outlet temperature is calculated as:

$$\mathrm{T}_4 = \mathrm{T}_3 + \left[1 - \eta_{sgt}\left[1 - \frac{P_3}{P_4}^{(1-\gamma_g)/\gamma_g}\right]\right] \tag{2.28}$$

where η_{sgt} is turbine isentropic efficiency; and P_3 and P_4 are turbine inlet and outlet temperature, respectively. The turbine work is:

$$\dot{W}_{gtu} = \dot{m}_g \; C_{pg} \; (\mathrm{T}_3 - \mathrm{T}_4) \tag{2.29}$$

The output power is then $\dot{W}_{gt} = \dot{W}_{gtu} - \dot{W}_{cmp}$ and the thermal efficiency is:

$$\eta_{th} = \frac{\dot{W}_g}{\dot{m}_{\text{fuel}} \; \text{LHV}} \tag{2.30}$$

2.6.2 Steam Cycle Performance

The steam turbine operates on the Rankine Cycle as shown in Fig. 2.9. In Fig. 2.9 (b) the process $1-2$ corresponds to the feeding pump; process $2-3$ shows heat addition in the boiler; in process $3-4$ the steam is expanded in the turbine; and the process $4-1$ corresponds to heat release in the condenser. The relation of thermodynamic models of each component are briefly described.

- Feed Pump: The water as saturated liquid is pumped in the feed pump before it sent to boiler. The pump work per unit mass of water is:

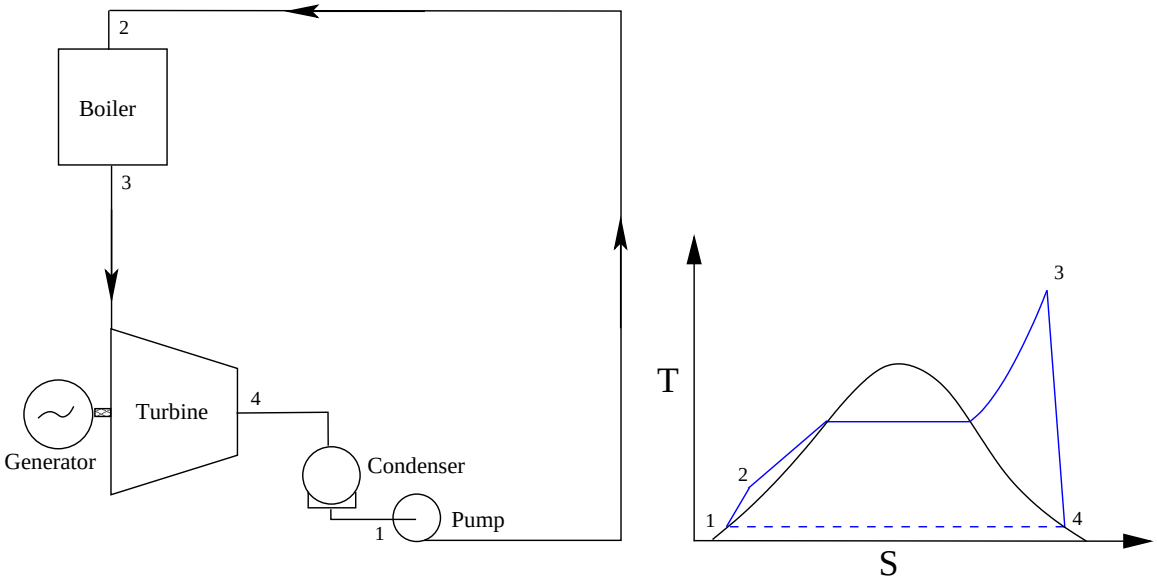

(a) Steam Turbine (b) T−S Diagram

Figure 2.9: Steam turbine thermodynamic model.

$$\dot{W}_{\text{pump}} = (h_2 - h_1) \tag{2.31}$$

where, h_1 and h_2 are the enthalpy at the pump inlet and outlet stations, respectively. From first and second law combined together:

$$dh = h_2 - h_1 = \mathrm{T}.ds + v.dP \tag{2.32}$$

where v is the water volume; T is the temperature; ds is entropy changes; and dP shows the pressure changes. For an adiabatic process, $ds = 0$ and therefore

$$dh = h_2 - h_1 = v.dP = v_1 \left(P_2 - P_1\right) \tag{2.33}$$

and the work is:

$$\dot{W}_{\text{pump}} = v_4 \left(P_2 - P_1\right) \tag{2.34}$$

- Boiler: In the boiler, the high pressure water from the pump is heated until it changes into steam. The heat added equals to:

$$\dot{Q}_{\text{add}} = (h_3 - h_2) \tag{2.35}$$

- Turbine: The steam from boiler is sent to steam turbine where the work is produced. The steam generally changes to steam/liquid mixture, where the steam quality should be above 85% to avoid condensation of steam on turbine blades and the material corrosion. Turbine work per unit water mass is:

$$\dot{W}_{st} = (h_3 - h_4) \tag{2.36}$$

- Condenser: The heat rejection occurs in the condenser at nearly constant pressure causing steam transformed to saturated liquid. The heat rejected is:

$$\dot{Q}_{\text{rejected}} = (h_4 - h_1) \tag{2.37}$$

and the cycle efficiency is:

$$\eta_{st} = \frac{\dot{W}_{\text{turbine}} - \dot{W}_{\text{pump}}}{\dot{Q}_{\text{add}}} \tag{2.38}$$

or in terms of enthalpy

$$\eta_{st} = \frac{(h_3 - h_4) - (h_2 - h_1)}{(h_3 - h_2)} \tag{2.39}$$

where, the enthalpy values at each point might be found using the Mollier Diagram.

2.6.3 Combined Cycle Performance

The thermodynamic models of single-, dual-, and triple-pressure HRSG are considered in this work. The single pressure model is only described here. This model is shown in Fig. 2.10.

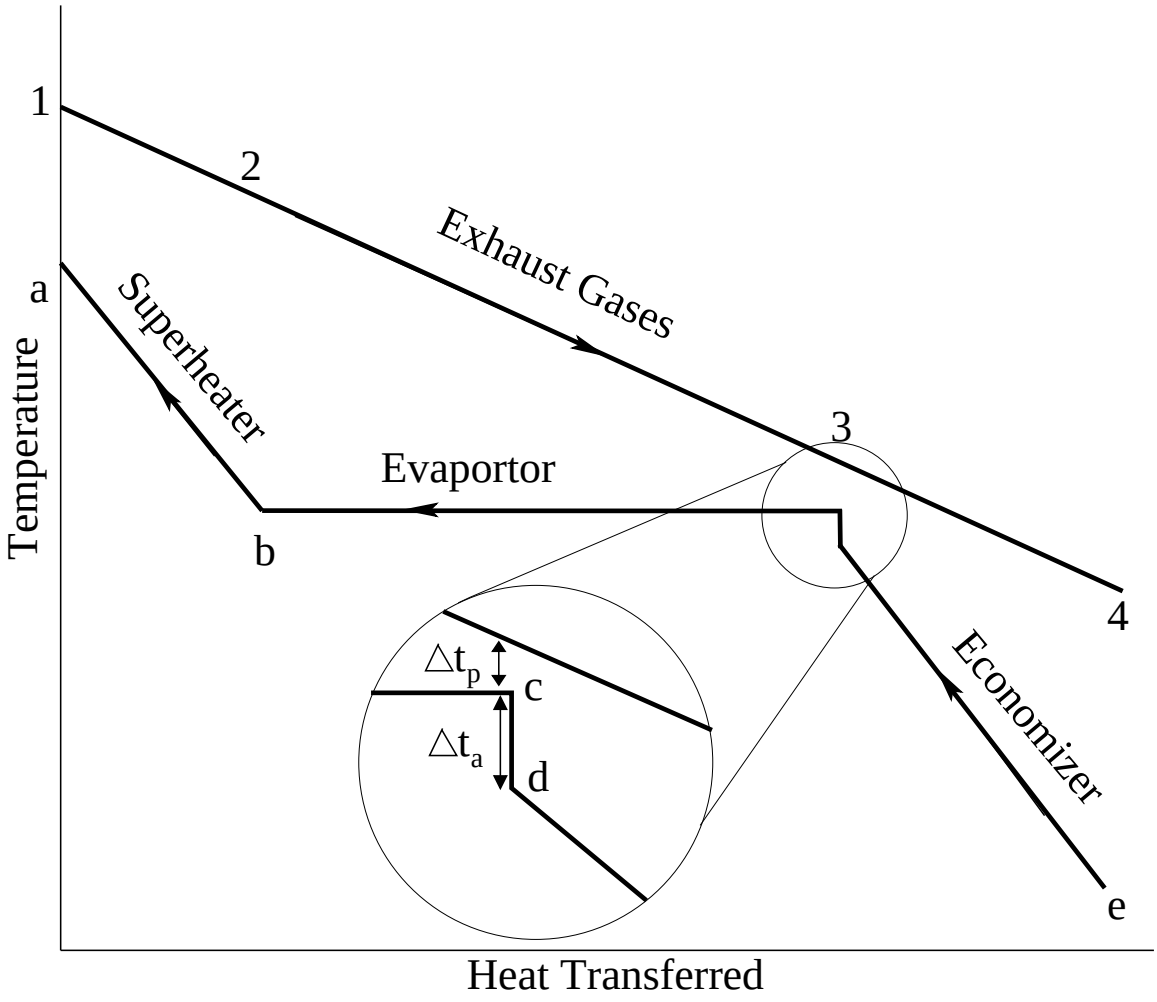

Figure 2.10: Single-pressure HRSG thermodynamic model.

The two important design parameters of a HRSG are approach temperature difference and pinch-point temperature difference. The approach temperature difference (denoted by Δt_a in Fig. 2.10) is the temperature difference between economizer outlet and the boiler circuit that the economizer serves [50]. Typical approach temperature

difference ranges from 5^o to 12^oC. The pinch-point temperature (denoted by Δt_p in Fig. 2.10) is the difference between evaporator steam outlet temperature and the exhaust gas temperature at that physical location in the HRSG [50]. Typical pinch temperature difference ranges from 8^o to 15^oC. From Fig. 2.10, the temperature of the pinch point in the water side (T_c) can be determined as:

$$\mathrm{T}_c = \mathrm{T}_b = \mathrm{T}_s(p) \tag{2.40}$$

where $\mathrm{T}_s(p)$ is the saturation temperature at given feed-water pump pressure of P and can be found from the Mollier Diagram. Assuming the pinch point temperature difference ($\Delta\mathrm{T}_p$) is given, then the pinch point on the gas side is:

$$\mathrm{T}_3 = \mathrm{T}_c + \Delta\mathrm{T}_p \tag{2.41}$$

Likewise the economizer outlet temperature can be determined from given approach temperature difference ($\Delta\mathrm{T}_a$), i.e.:

$$\mathrm{T}_d = \mathrm{T}_c + \Delta\mathrm{T}_a \tag{2.42}$$

The heat exchange above the pinch is:

$$\dot{Q}_{1-3} = (\mathrm{T}_1 - \mathrm{T}_3) \times C_p \times \dot{m}_g \tag{2.43}$$

where C_p is the gas specific heat at constant pressure and $\dot{m}_g$ is the gas mass flow rate. C_p is a function of gas temperature and can be estimated following equations [51]: For gas temperatures between 250-599^{o}K:

$$C_p = 1.023204 - 1.76021 \times 10^{-4}.\mathrm{T} + 4.0205 \times 10^{-7}.\mathrm{T}^2 - 4.87272 \times 10^{-11}.\mathrm{T}^3 \tag{2.44}$$

For gas temperatures between 600-1500^{o}K:

$$C_p = 0.874334 - 3.22814 \times 10^{-4}.\mathrm{T} + 3.58694 \times 10^{-8}.\mathrm{T}^2 - 1.99196 \times 10^{-11}.\mathrm{T}^3 \quad (2.45)$$

This amount of heat is captured by the water/steam circuit in the evaporator and superheater sections. The water mass flow $\dot{m}_s$ is determined as:

$$\dot{m}_s = \frac{\dot{Q}_{1-3}}{h_a - h_d} \quad (2.46)$$

where h denotes water enthalpy value. The heat exchange below the pinch is given by the water side energy balance as:

$$\dot{Q}_{3-4} = \dot{Q}_{e-d} = \dot{m}_s \times (h_d - h_e) \quad (2.47)$$

this can give the stack temperature of T_4 as

$$\mathrm{T}_4 = \mathrm{T}_3 - \frac{\dot{Q}_{3-4}}{C_p \times \dot{m}_g} \quad (2.48)$$

Given the superheat temperature and pressure, h_a and s_a can be found from the Mollier Diagram. For the condenser pressure of P_c and an isentropic expansion, the isentropic steam quality $x_{0(is)}$ and the isentropic outlet enthalpy $h_{0(is)}$ can be found. The isentropic turbine work is then:

$$\Delta h_{st(is)} = h_a - h_{0(is)} \quad (2.49)$$

Assuming an isentropic efficiency of η_{ST}, the actual steam turbine work is:

$$\dot{W}_{st} = \Delta h_{st(is)} \times \dot{m}_s \times \eta_{st} \quad (2.50)$$

the combined cycle efficiency is then:

$$\eta_{cc} = \eta_{gt} \times (\dot{W}_{gt} + \dot{W}_{st})/\dot{W}_{gt} \tag{2.51}$$

where η_{gt} is the gas turbine thermal efficiency and $\dot{W}_{gt}$ is gas turbine output power. The HRSG efficiency is also defined as:

$$\eta_{\mathrm{HRSG}} = \frac{\mathrm{T}_1 - \mathrm{T}_4}{\mathrm{T}_1 - \mathrm{T}_{air}} \tag{2.52}$$

also the Rankine cycle efficiency is:

$$\eta_{\mathrm{R}} = \frac{\dot{W}_{st}}{(\mathrm{T}_1 - \mathrm{T}_4) \times C_p \times \dot{m}_g} \tag{2.53}$$

The combined cycle performance is also influenced by ambient temperature changes. Figure 2.11(a) shows the effects of ambient temperature changes into relative efficiency of gas turbine, steam turbine, and combined cycle power plants. The relative efficiency is defined as the operating-to-design efficiency ratio. The ambient temperature changes have a slight increase in the combined cycle efficiency as shown in Fig. 2.11(a). This is because the increased temperature gives a rise into gas turbine exhaust temperature, that will improve the steam cycle efficiency. This increased efficiency compensates the reduced efficiency of gas turbine, and hence slightly improves the combined cycle efficiency [25].

Figure 2.11(b) also shows the relative power changes of gas turbine, steam turbine, and combined cycle with ambient temperature changes. The increased temperature results in the reduced power in the gas turbine, as the mass flow rate falls with increasing temperature. The steam cycle power increases with increasing ambient temperature. This is again due to increased exhaust temperature that increases the steam maximum temperature as well. Figure 2.11(b) shows that the combined cycle power falls with increasing temperature, however, the rate of power decrease is smaller than the rates in the gas turbine.

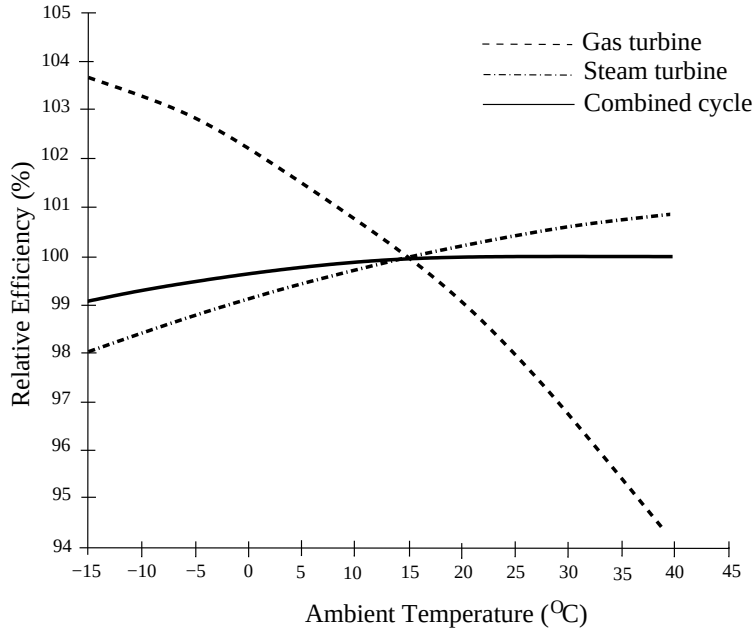

(a) Relative efficiency

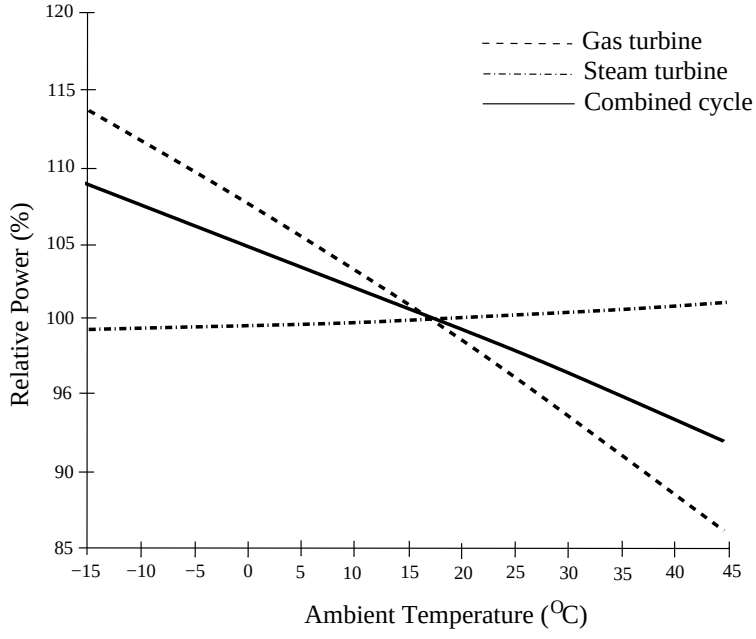

(b) Relative Power

Figure 2.11: Effect of ambient temperature changes into gas turbine, steam turbine, and combined cycle.

2.7 Thermoeconomic Cost Function

The goal of thermoeconomic optimization is to minimize a cost objective function that couples thermodynamic and economic models with environmental considerations. The mathematical model of thermoeconomic optimization used in the present study is unit price of producing electricity by the plant, denoted by $\dot{C}_E$ expressed in US$/kwh. For a design-type optimization, this function remains unchanged within time and is defined as:

$$\dot{C_E} = \frac{\beta C_0}{\dot{W}_g\ N} + \frac{C_{\text{fuel}}}{\dot{W}_g\ N} + \frac{C_{\text{OM}}}{\dot{W}_g\ N} + \frac{C_{\text{NO}_\text{x}}}{\dot{W}_g\ N} + \frac{C_{\text{CO}}}{\dot{W}_g\ N} \tag{2.54}$$

Each annualized cost per output power is denoted as $\dot{\Gamma}$, therefore:

$$\dot{C_E} = \dot{\Gamma}_z + \dot{\Gamma}_{\text{fuel}} + \dot{\Gamma}_{\text{NO}_\text{x}} + \dot{\Gamma}_{\text{CO}} \tag{2.55}$$

where, $\dot{\Gamma}_z = (\beta C_0 + C_{\text{OM}})/(\dot{W}_g\ N)$. The objective of design-type thermoeconomic optimization is to find design variables that minimize $\dot{C}_E$ such that:

$$\begin{aligned} \text{minimize: } \dot{C}_E &= \dot{C}_E(x,y) \\ \text{subject to: } h_j(x,y) &= 0 \quad \text{j=1,...J (equality constraints)} \\ g_k(x,y) &\geq 0 \quad \text{k=1,...K (inequality constraints)} \\ \text{where, } x &= \{x_i\} \ \text{i=1,...I (independent variables)} \\ y &= \{y_j\} \ \text{j=1,...J (dependent variables)} \end{aligned} \tag{2.56}$$

where, x denote the independent variables, (often called decision, design and operating variables) and y represents dependent variables. For operating-type optimization, the power plants performance will change because of ambient air changes and operating

at different loads. Assuming n different values of $\dot{C}_E$ in a year, then optimization is defined as:

$$\begin{aligned} \text{minimize: } \sum_{i=1}^{n} \dot{C}_E &= \sum_{i=1}^{n} \dot{C}_E(x,y) \\ \text{subject to: } h_j(x,y) &= 0 \quad \text{j=1,...J (equality constraints)} \\ g_k(x,y) &\geq 0 \quad \text{k=1,...K (inequality constraints)} \\ \text{where, } x &= \{x_i\} \text{ i=1,...I (independent variables)} \\ y &= \{y_j\} \text{ j=1,...J (dependent variables)} \end{aligned} \tag{2.57}$$

Optimization method is iterative, starting with an initial guess. Initial independent variables (guessed values) of x are input to Eqs. 2.56 and 2.57. The set of dependent variables y can be estimated through the equality constraints. They include thermodynamic, economics and environment components. The corresponding cost function $\dot{\Gamma}^{\$}_{tot}$ is then evaluated. A new set of independent values is then guessed and the process is repeated while the method finds a minimum point. The results of optimization are finally interpreted, using the inequality constraints. Any design and operation limits, state regulations, safety requirements are examples of inequality constraint functions .

2.8 Solution of The Optimization Problems

2.8.1 Optimization Methods

There is a variety of methods for solving different types of optimization problems. Optimization problems are categorized as linear or nonlinear, constrained or unconstrained and single-variable or multiple variable types. *Golden section search*

(sometime named Fibonacci search) [52] , *Newton-Raphson* method [53] and *Regula Falsi method* [54] are a few examples of solver methods of unconstrained single variable problem. *Generalized Reduced Gradient* (GRG) method [55], and *Sequential Quadratic Programming* (SQP)[56] are also two common methods for solving multiple optimization problems. Furthermore, *LP Simplex*, *Sequential Linear Method* (SLM) and *Sequential Quadratic Method* (SQM) are commonly applied to constrained optimization problems. The classical methods require differentiable objective functions for effectiveness. Also, since the methods use differential calculus, for *multimodal* (an example function is shown in Fig.2.12) functions, the optimum search algorithm risk finding a local minimum instead of global minimum.

2.8.2 Genetic Algorithm Optimization

Genetic Algorithms(GA) [57] and *Simulated Annealing* [58] have also being used for thermo-economic optimizations. In contrast to classical methods, these algorithms might find the global minimum but incur greater costs in terms of computational time. In general, the complexity and problem size, convergence of solver, number of iterations, quality of solution and integrity are several factors that can be used in order to select an optimization solver.

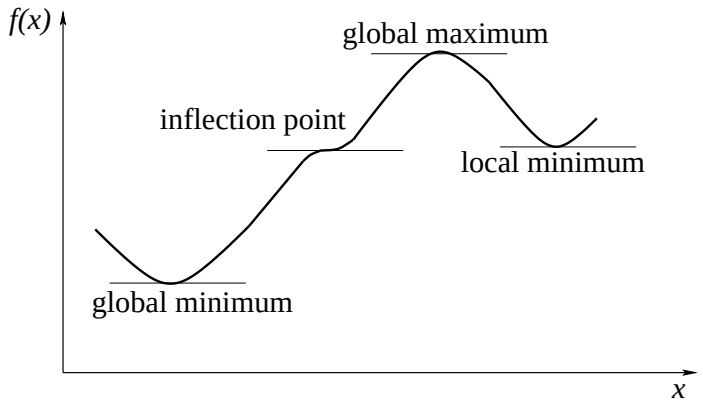

Figure 2.12: An example of multi-modal functions.

The genetic algorithm optimization method is based on mimicking the natural genetics by using evolutionary principles and chromosomal processing [59]. The genetic algorithm search typically starts with a random set of samples, where a fitness value is assigned with each sample. The population of solutions at each generation is updated using the fitness values and three operation of reproduction, crossover, and mutation. The reproduction operation consists of increasing or decreasing the number of offspring of each sample according to the estimated fitness value to ensure the good solutions have a higher chance to being passed to the next generation; the chromosomes of some selected samples are swaped in the crossover operation; and then some bits of each chromosome are altered in the mutation process [60]. The optimization continues until a termination criteria is satisfied. The algorithm can be described as follows:

```
Begin:
   Initialize (old-population)
   Evaluate (old-population)
   Do (until generation = maximum number of generations)
      Reproduction (old-population);
      Cross-over (new-population);
      Mutation (new-population);
      Old-population = new-population;
   End;
End;
```

In GA, the search is done from a population of points instead of single-point, therefore the genetic algorithm typically takes a longer time to terminate compared with classical optimization methods. The solution time significantly increases with increasing number of independent variables.

2.8.3 Surrogate-Based Optimization

A new approach for the global optimization is the "Expected Improvement Function" (EIF) which is defined to generate dense samples at the global minimum or maximum. This method is based on Kriging modeling that more details will follow. Assume that n initial samples are available for a function of k independent variables. Each sample is denoted as $x^{(i)} = (x_1^{(i)}, ..., x_k^{(i)})$ with corresponding observations (responses) $y^{(i)} = y(x^{(i)})$, for $i = 1, ..., n$. A Kriging function is used to approximate the target function as

$$\hat{y}(x^*) = \mu + \epsilon \tag{2.58}$$

where μ is the mean value and ϵ is the normally distributed error term with zero mean and variance σ^2. Universal Kriging, which is used in this study, assumes that the mean value μ is a linear combination of known functions $f_0(x), ...f_k(x)$. In this study the linear functions are used where $f_0(x) = 1$ and $f_j(x) = x_j$ for $j = 1, ...k$. Thus, a universal Kriging model with linear regression functions is written as

$$\hat{y}(x^*) = \sum_{h=0}^{k} \beta_h f_h(x^*) + \epsilon \tag{2.59}$$

In order to estimate the correlation for the error term, define a spatially weighted distance formula between samples $x^{(i)}$ and $x^{(j)}$ as

$$d(x^{(i)}, x^{(j)}) = \sum_{q=1}^{k} \theta_q |x_q^{(i)} - x_q^{(j)}|^{p_q} \ \ (\theta_q \geq 0, p_q \epsilon [1, 2]) \tag{2.60}$$

where the parameter θ_q expresses the importance of the qth component and the exponent p_q is related to the smoothness of the function in coordinate direction q. A

correlation matrix R is then defined by

$$R = \begin{bmatrix} exp[-d(x^1, x^1)] & exp[-d(x^1, x^2)] & ... & exp[-d(x^1, x^n)] \\ exp[-d(x^2, x^1)] & exp[-d(x^2, x^2)] & ... & exp[-d(x^2, x^n)] \\ \vdots & \vdots & & \vdots \\ exp[-d(x^n, x^1)] & exp[-d(x^n, x^2)] & ... & exp[-d(x^n, x^n)] \end{bmatrix}$$

To compute the Kriging model, values must be estimated for the $\beta' s$ and σ in conjunction with $\theta_1, ..., \theta_k$ and $p_1, ..., p_k$. This results in $3k + 2$ parameters to be calculated for a linear regression model. The parameters can be quantified using the Maximum Likelihood Estimator (MLE), as described by Jones et al [61]. The predictions at an unsampled location x^* can then be obtained from Eq. 2.58. Let $\mathbf{r}$ denote the n-vector of correlations between the new point x^* and the previous n sample points, based on the distance formula, giving

$$\mathbf{r} = \begin{bmatrix} exp[-d(x^*, x^1)] \\ exp[-d(x^*, x^2)] \\ \vdots \\ exp[-d(x^*, x^n)] \end{bmatrix}.$$

then the Kriging estimate is given by

$$\hat{y}(x^*) = \sum_{h=0}^{k} \beta_h f_h(x^*) + \mathbf{r}^T R^{-1}(y - F\beta) \tag{2.61}$$

where $\beta = (\beta_0, \beta_1, ..., \beta_k)$ is the $k + 1$ dimensional vector of regression coefficients and

$$F = \begin{bmatrix} f_0(x_1^{(i)}) & f_1(x_1^{(i)}) & ... & f_k(x_1^{(i)}) \\ f_0(x_2^{(i)}) & f_1(x_2^{(i)}) & ... & f_k(x_2^{(i)}) \\ \vdots & \vdots & & \vdots \\ f_0(x_n^{(i)}) & f_1(x_n^{(i)}) & ... & f_k(x_n^{(i)}) \end{bmatrix}$$

A confidence interval can be calculated for this prediction. If x^* is close to sample points, there is a high level of confidence in the prediction. This is reflected by the expression for the Mean Squared Error (MSE) of the predictor [62]

$$s^2(x^*) = \sigma^2 - \mathbf{r}^T R^{-1}\mathbf{r} + (f(x^*) - \mathbf{r}^T R^{-1}F)(F^T R^{-1}F)^{-1}(f(x^*) - \mathbf{r}^T R^{-1}F)^T \quad (2.62)$$

with $f(x^*) = (f_0(x^*), f_1(x^*), ..., f_k(x^*))$ is the vector of regression coefficients corresponding to x^*. The MSE is zero at observed points and increases as the distance between samples increases. Assuming that f_{min}^n be the minimum sampled value of the objective function $y = f(x)$ after n evaluations, where x is a array of input values. The function y might be treated as a realization of a random variable $Y(x)$ assumed to be Gaussian with variance $s^2(x)$. Using Kriging [61] to predict $\hat{y}$ and $\hat{s}$, the expected improvement function is defined as [63]:

$$E[I(x)] = (f_{min} - \hat{y})\Phi(\frac{f_{min} - \hat{y}}{\hat{s}}) + \hat{s}\phi.(\frac{f_{min} - \hat{y}}{\hat{s}}) \quad (2.63)$$

In the above, f_{min} is the minimum value of the sample points and ϕ and Φ are the standard normal density and distribution function. The first term in Equation 2.63 represents the difference between the current minimum and the predicted value multiplied by the probability that $Y(x)$ is smaller than f_{min}^n . The second term is the standard deviation of $y(x)$ multiplied by the probability that $y(x)$ is equal to f_{min}^n . Therefore, the expected improvement function balances local and global search of

minimum point. A sample is generated at maximum EIF value and then this iterates until EIF values fall below a preset threshold.

2.9 TERA Optimization Framework

2.9.1 Introduction

The present study is a part of on-going research into the development of TERA methodology [5] at Cranfield University for the evaluation of advanced engine concepts in order to meet challenging environmental goals. In preceding sections, the correlation of capital cost and gas turbine independent variables were described. These correlation functions are subset of equality functions in Eqs. 2.56 and 2.57. However, for a gas turbine power system, estimation of fuel mass flow rate is challenging, in particular for bleeding air scenario, off-design performance and degraded engine conditions. The task is getting more sophisticated for the integration of a gas turbine with a steam turbine cycle. In the past studies, gas turbines have been modeled with simple thermodynamic laws in design point conditions. However, the engine's performance might deviate from actual one, if engine configuration becomes more complex. The approach of this work is to integrate a code of gas turbine performance and combined cycle inside the optimization code. Cranfield Gas Turbine engine's performance simulation program (VariFlow) is used in the present study. VariFlow [1] is an adaptive engine-configuration code and has been widely used for design point and off-design conditions. Also, a MATLAB [2] code is used for performance calculations of steam turbine cycle and combined cycle. Fig 2.13 presents an overview of optimization code, showing aspects of its functionality, process and dataflow.

Two core modules are:

[1] VariFlow user guide, http://www.cranfield.ac.uk
[2] MATLAB V2008a, The MathWorks, Inc. http://www.mathworks.com

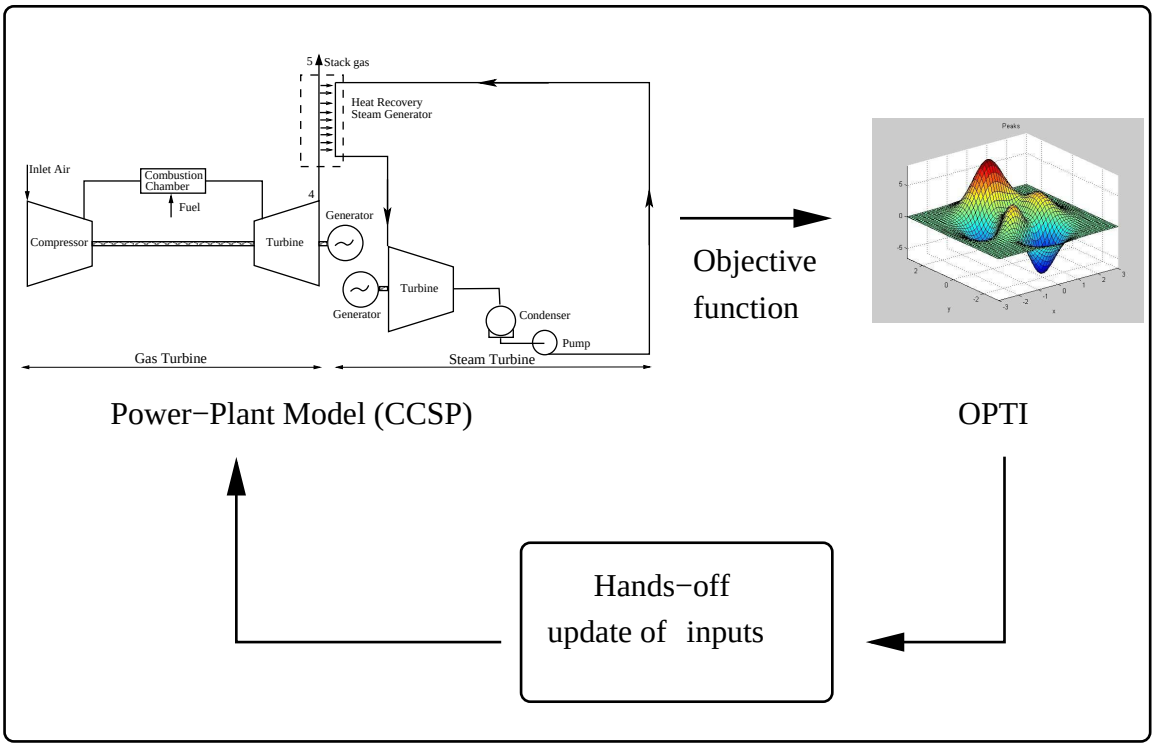

Figure 2.13: TERA-optimization architecture.

1. Combined Cycle Simulation Program (CCSP): This module includes a gas turbine simulation code (VariFlow) in addition to all the thermodynamic equations needed to calculate a steam cycle operational variables (steam mass flow rate, efficiency, power, etc.) that is combined with the gas turbine model.

2. Optimization Module (OPTI): This is the module in which objective function is quantified and MATLAB optimization techniques are employed.

The VariFlow source code is Fortran that predicts engine's performance at design and off-design conditions. The code was integrated into MATLAB environment for optimization purposes. A MATLAB interference was written by the author in order to allow "hands-off" calculations. This call fills the input file, launches calculations and processes the output file for optimization code.

Chapter 3

GAS TURBINE PERFORMANCE PREDICTION

3.1 Introduction

The performance simulation of an industrial gas turbine is described in this chapter. The gas turbine configuration and performance data are inspired by the Alstom GT13-E2 with 184.5 MW output power. The performance analysis can be categorized into design-point and off-design modeling and the simulation must predict accurately the engine's behavior for design as well as off-design conditions. The starting point for predicting engine's performance is to create a design-point model under steady-state and standard-ambient conditions. The design point model consists of blocks that correspond to engine components (compressor, combustor, turbine, etc.), where the performance parameters in each block can be determined from given data and using the aero-thermodynamic equations. Unfortunately, not all the engine performance parameters are available (such as component efficiencies) and hence these parameters may be guessed. In order to assess the performance model, the prediction values could be compared with available engine test-bed data, but it is high probability

that the engine's performance based on assumed values vary from the actual data. A trial and error approach could be used to improve the initial assumptions but this approach becomes tedious and cumbersome as the number of parameters increases. Thus, an approach is required that allows a more accurate evaluation of these parameters. The approach used here is to match the engine's model with the performance data obtained from experiment; this approach is so-called the engine's performance adaptation. With the fixed engine geometry from the design-point, the engine must operate effectively over a range of ambient temperature changes. The engine at different ambient conditions produce different exhaust gas conditions. These conditions that geometry is fixed and operating conditions are changing called off-design conditions.

The computer programs for predicting the engine's performance involve solving the aero-thermodynamic equations which are derived from the physical laws of conservations of energy as well as mass flow ratios. Advances in computer technology have led to the development of several computer simulation techniques, which are capable of simulating an engine's behavior under steady-state as well as transient conditions. The simulation technique has benefits with respect to the cost and time reductions along with the elimination of operational as well as hazards involved with engine testing [46]. The simulation code used in this work is the Cranfield gas turbine performance simulation code of VariFlow [64] that allows performance prediction of single-shaft industrial gas turbines. The code solves the aero-thermodynamic equations to find the design-point performance model from given data. The off-design modeling in the code is based on successive guesses for the off-design operating point on pre-defined component maps: these guesses will be updated by iteration procedure until specified constraints (sometimes called handles) are satisfied. Once the successive iteration is complete, overall cycle parameters such as power and fuel consumption can easily be derived.

In this chapter the aero-thermodynamic equations for modeling gas turbine performance are presented followed by description of the simulation code of VariFlow. The baseline gas turbine, GT13-E2 engine, is described and the design point refers to the maximum shaft speed under standard-ambient conditions. The adapted simulation model at these conditions is validated against experimental data. The validated model then is used to investigate the off-design performance. Finally, the effects of turbine blade cooling and different engine-configurations into engine's performance are studied.

3.2 Formulation

3.2.1 Design-Point Performance Modeling

The first stage of the engine simulation is the design-point performance analysis. The design point, sometimes called on deisgn [65], is referred to the conditions that engine has designed for. The engine's behavioral equations are solved using components characteristics for the design-point in association with ambient conditions. The design point analysis sets the temperature-entropy diagram of engine cycle and defines the size of engine and its components to meet the cycle requirements. The VariFlow code is used for engine's performance simulation which splits the gas turbine model into several control volumes (named blocks), such that each block is designed based on the conditions specified for the design-point conditions. VariFlow then finds engine performance parameters by solving the equations of conservations of energy as well as mass ratio in each block. Additional equations of perfect gas and choked flow at first stage of nozzle are added to close the system of equations [66]. These equations are detailed in [47], [49], and [48] and briefly described for a single-shaft industrial gas turbine shown in Fig. 3.1

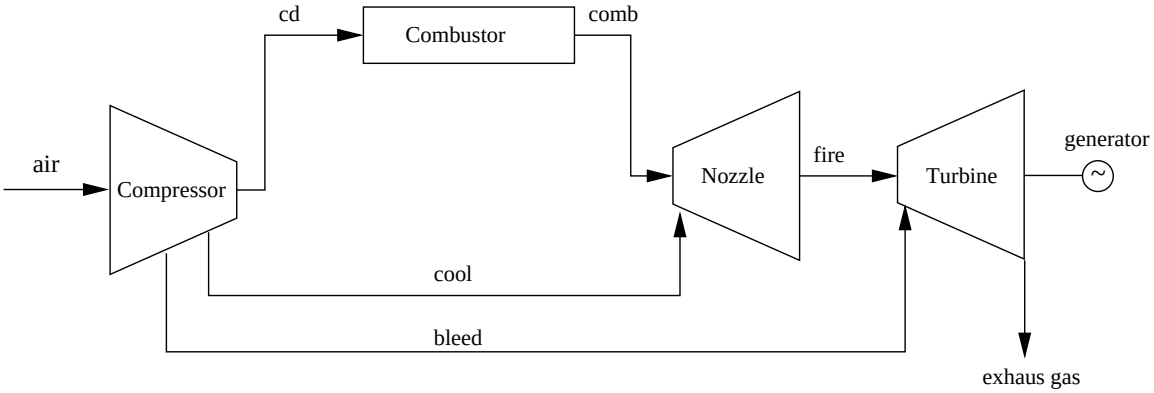

Figure 3.1: A simple gas turbine model.

- Compressor: Air enters the compressor of the gas turbine, where its pressure and temperature rises. Air is extracted from the compressor for cooling the nozzle and turbine blades. The governing equations for conservation of mass and energy are:

$$\dot{m}_{\text{air}} = \dot{m}_{\text{cd}} + \dot{m}_{\text{cool}} + \dot{m}_{\text{bleed}} \tag{3.1}$$

$$\begin{aligned} \dot{m}_{\text{air}}\ \mathrm{C}_{\mathrm{P}_{\text{air}}}\mathtt{T}_{\text{inlet}} + \dot{\mathrm{W}}_{\text{cmp}} = \dot{m}_{\text{cd}}\ \mathrm{C}_{\mathrm{P}_{\text{cd}}}\mathtt{T}_{\text{cd}} + \dot{m}_{\text{cool}}\ \mathrm{C}_{\mathrm{P}_{\text{cool}}}\mathtt{T}_{\text{cool}} \\ + \dot{m}_{\text{bleed}}\ \mathrm{C}_{\mathrm{P}_{\text{bleed}}}\mathtt{T}_{\text{bleed}} \end{aligned} \tag{3.2}$$

  where $\dot{m}$ shows the mass flow rate; $\mathrm{C_P}$ is the specific heat at constant pressure; T is the temperature in K; and $\dot{\mathrm{W}}_{\text{cmp}}$ is the compressor work.

- Combustor: In the combustor, heat is added at nearly constant pressure to the compressed air by the combustion of a fuel. The governing equations for conservation of mass and energy are:

$$\dot{m}_{\text{comb}} = \dot{m}_{\text{cd}} + \dot{m}_{\text{fuel}} \tag{3.3}$$

$$\begin{aligned} \dot{m}_{\text{cd}}\ \mathrm{C}_{\mathrm{P}_{\text{cd}}}(\mathtt{T}_{\text{cd}} - \mathtt{T}_{\text{ref}}) + \dot{m}_{\text{fuel}}\ \eta_{\text{cmb}}(\mathtt{LHV} + \ \mathrm{C}_{\mathrm{P}_{\text{fuel}}}(\mathtt{T}_{\text{fuel}} - \mathtt{T}_{\text{ref}})) \\ = \dot{m}_{\text{comb}}\ \mathrm{C}_{\mathrm{P}_{\text{comb}}}(\mathtt{T}_{\text{comb}} - \mathtt{T}_{\text{ref}}) \end{aligned} \tag{3.4}$$

where η_{cmb} is the combustor efficiency and $\texttt{LHV}$ is the lower heating value.

- Nozzle: The compressor cool air is directed to the nozzle guide vanes, where the hot air from combustor is mixed with the cool air. The governing equations for conservation of mass and energy are:

$$\dot{m}_{\text{fire}} = \dot{m}_{\text{comb}} + \dot{m}_{\text{cool}} \tag{3.5}$$

$$\dot{m}_{\text{comb}}\ \mathrm{C}_{\mathrm{P}_{\text{comb}}}\mathtt{T}_{\text{comb}} + \dot{m}_{\text{cool}}\ \mathrm{C}_{\mathrm{P}_{\text{cool}}}(\mathtt{T}_{\text{cool}} - \Delta\mathtt{T}_{\text{cool}}) = \dot{m}_{\text{fire}}\ \mathrm{C}_{\mathrm{P}_{\text{fire}}}\mathtt{T}_{\text{fire}} \tag{3.6}$$

- Turbine: The hot air is expanded in the turbine and produces work. The governing equations for conservation of mass and energy are:

$$\dot{m}_{\text{exh}} = \dot{m}_{\text{fire}} + \dot{m}_{\text{bleed}} \tag{3.7}$$

$$\dot{m}_{\text{fire}}\ \mathrm{C}_{\mathrm{P}_{\text{fire}}}\mathtt{T}_{\text{fire}} + = \dot{m}_{\text{exh}}\ \mathrm{C}_{\mathrm{P}_{\text{exh}}}\mathtt{T}_{\text{exh}} + \dot{\mathrm{W}}_{\text{gtu}} \tag{3.8}$$

where $\dot{\mathrm{W}}_{\text{gtu}}$ is the turbine work. The balance of powers are written as:

$$\eta_{\text{shaft}}\dot{\mathrm{W}}_{\text{gtu}} = \dot{\mathrm{W}}_{\text{shaft}} + \dot{\mathrm{W}}_{\text{cmp}} \tag{3.9}$$

$$\dot{\mathrm{W}}_{\text{net}} = \eta_{\text{generator}}\dot{\mathrm{W}}_{\text{shaft}} - \dot{\mathrm{W}}_{\text{aux}} \tag{3.10}$$

For a choked nozzle this equation also applies:

$$\dot{m}_{\text{comb}} = C_{\text{noz}}A_{\text{noz}}\frac{\mathrm{P}_{\text{comb}}}{\sqrt{\mathrm{T}_{\text{comb}}}} \tag{3.11}$$

where C_{noz} is chocked flow constant and A_{noz} is the nozzle surface area. The inlet temperature, compressor pressure ratio, and turbine inlet temperature are often given,

therefore:

$$\mathrm{T_{cd}} = \mathrm{T_{air}} + \left[1 + \frac{1}{\eta_{scp}}\left[\left(\frac{\mathrm{P_{cd}}}{\mathrm{P_{exh}}}\right)^{(\gamma_{\mathrm{air}}-1)/\gamma_{\mathrm{air}}} - 1\right]\right] \tag{3.12}$$

$$\mathrm{T_{exh}} = \mathrm{T_{fire}} + \left[1 - \eta_{sgt}\left[1 - \left(\frac{\mathrm{P_{fire}}}{\mathrm{P_{exh}}}\right)^{(1-\gamma_{\mathrm{fire}})/\gamma_{\mathrm{fire}})}\right]\right] \tag{3.13}$$

where η_{scp} and η_{sgt} are compressor and turbine isentropic efficiencies, respectively; γ is the specific heat ratio. Also the compressor extractions are defined as:

$$\dot{m}_{\mathrm{cool}} = \lambda_{\mathrm{cool}}\dot{m}_{\mathrm{air}} \tag{3.14}$$

$$\dot{m}_{\mathrm{bleed}} = \lambda_{\mathrm{bleed}}\dot{m}_{\mathrm{air}} \tag{3.15}$$

$$\mathtt{T}_{\mathrm{cool}} = \delta_{\mathrm{cool}}\mathtt{T}_{\mathrm{cd}} \tag{3.16}$$

$$\mathtt{T}_{\mathrm{bleed}} = \delta_{\mathrm{bleed}}\mathtt{T}_{\mathrm{cd}} \tag{3.17}$$

Finally, the thermal efficiency is calculated as:

$$\eta_{th} = \frac{\dot{\mathrm{W}}_{\mathrm{net}}}{\dot{m}_{\mathrm{fuel}}\ \mathrm{LHV}} \tag{3.18}$$

The solution of Eqs. 3.1-3.18 finds the engine performance parameters.

3.2.2 Gas Turbine Performance Adaptation

In the above equations, several thermodynamic parameters, such as components efficiencies, are often not available. For initial design-point simulations, these parameters may be guessed, but it is high probability that the engine's performance based on these assumptions vary from the actual engine's behavior. Thus, an approach is required to accurately evaluate these parameters. The approach used is to match the engine's model with the performance data obtained from experiment. This process is

called the engine's performance adaptation which enables the operator to obtain the actual engine's performance data. The thermodynamic equations of an arbitrary gas turbine is expressed as:

$$y = h(u, x) \tag{3.19}$$

where $y \in \mathrm{R}^M$ are dependent variables such as temperature and pressure; the $x \in \mathrm{R}^N$ vector contains the component characteristics (i.e. mainly efficiencies and flow capacities); the vector u defines the engine's operating conditions; and the function h includes the aero-thermodynamic equations. In gas-turbine performance simulation, the vector y is found for the given input and operating conditions. The design-point performance adaptation is the inverse operation of performance simulation: the vector x is estimated for some available measurements. According to Li et al [67], the parameters used in the adaptation include:

- To-be-adapted component parameters: These parameters are subset of independent vector of x and not available for design-point performance simulation.
- Target performance parameters: These are also called dependent parameters, measurable, or measured performance parameters [67] and include shaft power, thermal efficiency, pressure, and temperature.

The gas turbine performance equations can be extended around a given initial design point (baseline) by using Taylor series method as:

$$y = y_0 + \frac{\partial h(u, x)}{\partial x}|_0 (x - x_0) + \mathrm{HOT} \tag{3.20}$$

where HOT represents the higher order terms from Taylor expansion and can be neglected for a linear model. The linear performance simulation equations are then written as:

$$\Delta y = H.\Delta x \tag{3.21}$$

where H is named influence coefficient matrix. The linear adaptation process is valid locally around the initial point as shown in Fig. 3.2 (a). For a highly nonlinear model, the to-be-adapted parameters are estimated by using the Newton-Raphson iterative method [68] as shown in Fig. 3.2 (b).

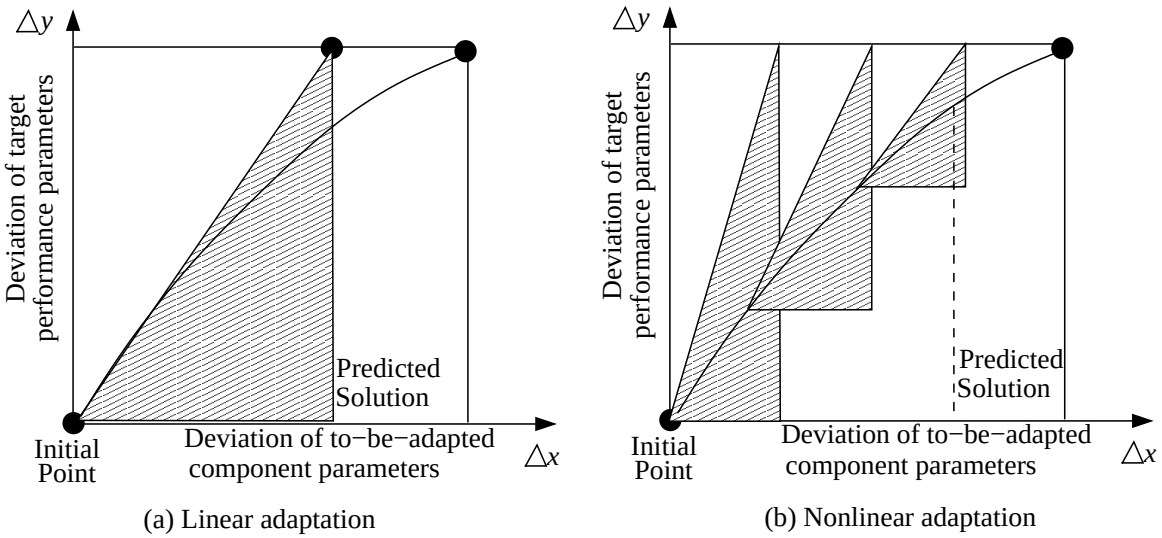

Figure 3.2: Gas turbine performance adaptation.

In the adaptation study, the vector Δy represents the deviation of engine target performance parameters from its initial point. Assuming $N = M$, the deviation of to-be-adapted component parameters from its initial point can be found as:

$$\Delta x = H^{-1}.\Delta y \tag{3.22}$$

where, H^{-1} is named adaptation coefficient matrix. if $N > M$, Eq. 3.22 is underestimated and leads to an infinite number of least-square solution. A pseodoinverse is defined as:

$$H^* = H^T.(H.H^T)^{-1} \tag{3.23}$$

where, T shows the transpose operation. Equation 3.23 provide a solution that is the best in a least-square sense. if $N < M$, Eq. 3.22 is overestimated with $M - N$ redundant equations. A pseodoinverse is defined as:

$$H^* = (H^T.H)^{-1}.H^T \tag{3.24}$$

The solution of Eq. 3.24 also leads to an infinite number of least-square solution. The adaptation method iterates until the root mean squared error (rms) of the difference between predicted and target performance parameters fall below an error threshold. The root mean squared error at each iteration is estimated as:

$$\text{rms} = \sqrt{\frac{\sum_{i=1}^{M}(Y_{i,\text{predicted}} - Y_{i,\text{target}})^2}{M}} \tag{3.25}$$

where M is the number of target performance parameters. Note that the gas turbine performance adaptation problem can also be seen as an optimization problem with an objective to minimize the root mean squared error defined in Eq. 3.25. In this study, the components efficiencies are estimated by using the optimization approach.

3.2.3 VariFlow Solver

The VariFlow source code was written in Fortran by Cranfield University mainly for use in Techno-economical Environmental Risk Analysis. The code is a simple version of TurboMatch program which enables the user to develop a nonlinear thermodynamic mathematical model of the engine's behavior. The TurboMatch code has a library describing the various components of the engine such as INTAKE, COMPRE (representing the compressor or fan), BURNER (representing the combustion chamber),

TURBINE, PREMASS (which indicates the mass flow rate split to model bypass or bleeding air) and etc. In this code, the various components (e.g. compressor, combustor, turbine, nozzle) are identified using station numbers in the inlet and outlet sections. The station numbers begin in the intake's inlet and ends with the nozzle's outlet. Likewise TurboMatch, VariFlow has a library describing the various components of the engine, but the combined mode is limited only to single-shaft industrial gas turbines [64]. Also, some differences between the input data for the VariFlow and TurboMatch are:

1. The turbine and compressor efficiencies in TurboMatch are isentropic, while VariFlow uses polytropic efficiency values.

2. In TurboMatch, the output power is defined as an auxiliary work in turbine module, while VariFlow calculates the output power.

3. VariFlow code allows water mixture with incoming air and hence has been used in many studies of gas turbine cycles with NO_x abatement.

4. TurboMatch uses kerosene as fuel only, but VariFlow allows variety of fuels as a mixture of CH2, CH4, C2H6, C3H8, CO, CO2, H2, H2O, N2 and O2.

The outcome of the engine's simulation code is presented in an output file, and includes the engine's performance such as shaft power, thermal efficiency, and all the stations pressure, temperature and mass flow rates.

3.2.4 Operating Performance Modeling

With the fixed engine geometry from the design-point, the engines must operate effectively over a range of ambient temperature and the load changes. These conditions that geometry is fixed and operating conditions are changing called off-design conditions. The performance parameters of each component are no longer specified in the

off-design, but determined from component maps. These maps have been developed using experimental data from actual rig tests or previous experience and once the component geometry has been decided then a map may be generated to define its performance under all off-design conditions. Zhang and Cai [69] also proposed some equations to model the compressor and turbine maps. For a compressor the operating pressure ratio and efficiency are estimated as:

$$r_c = c_1\dot{N}_c\dot{G}_c^2 + c_2\dot{N}_c\dot{G}_c + c_3\dot{N}_c \tag{3.26}$$

$$\eta_{scp} = \left[1 - c_4(1-\dot{N}_c)^2\right](\dot{N}_c/\dot{G}_c)(2-\dot{N}_c/\dot{G}_c) \tag{3.27}$$

where $r_c = P_2/P_1$ is the compressor pressure ratio; P_1 and P_2 are the compressor inlet and outlet pressures; η_{scp} is the compressor isentropic efficiency; $\dot{N}_c$ is the compressor normalized rotating speed defined as $N\sqrt{\mathrm{T_{std}}/\mathrm{T_{air}}}$ where N is rotational speed, $\mathrm{T_{std}}$ is standard ambient temperate and $\mathrm{T_{air}}$ is actual ambient temperature. $\dot{G}_c$ is normalized mass flow rate and is defined as $\dot{m}_{\mathrm{air}}\sqrt{\mathrm{T_{air}}/\mathrm{T_{std}}}\mathrm{P_{std}}/\ \mathrm{P_{air}}$ where $\dot{m}_{\mathrm{air}}$ is the compressor mass flow rate , $\mathrm{P_{std}}$ is standard ambient pressure and $\mathrm{P_{air}}$ is actual ambient pressure. The coefficients of c_1, c_2, c_3, and c_4 are set based on desired shape and the positions. The operating turbine efficiency can also be estimated as:

$$\eta_{sgt} = \left[1 - t(1-\dot{N}_t)^2\right](\dot{N}_t/\dot{G}_t)(2-\dot{N}_t/\dot{G}_t) \tag{3.28}$$

where η_{sgt} is the compressor isentropic efficiency; $\dot{N}_t$ is the turbine normalized rotating speed; $\dot{G}_c$ is turbine normalized mass flow rate; and t is set based on desired shape and the positions. There are some pre-defined maps in the VariFlow program that are dimensionless in order to avoid having to be presentable with respect to specific values for all influential parameters. It is obvious that the more accurate the performance maps, the more accurate will be the performance predictions [70]. The compressor

map contains information about engine's performance like compressor pressure ratio, mass flow, shaft speed, efficiency, compressor outlet temperature and pressure. However, once two appropriate parameters are defined for the compressor then all others will be found from the compressor map. The off-design modeling in simulation program is based on successive guesses for the off-design operating point on pre-defined component maps: these guesses will be updated by iteration procedure until specified constraints (sometimes called handles) are satisfied. Once the successive iteration is complete, overall cycle parameters such as power and fuel consumption can easily be derived. The off-design operating conditions depend on the handle selection such that the results for the constant turbine inlet temperature vary from the results for constant shaft speed. In VariFlow, turbine inlet temperature changes at off-design conditions but gas turbine always operate at constant shaft speed.

3.3 Baseline Gas Turbine

The power generator considered as a baseline design in this study is one shaft engine inspired by the Alstom GT13-E2 [1] shown in Fig. 3.3. This gas turbine became operational in mid-1997 and has been modified and improved since then. The engine model with a pressure ratio of 16.9:1 is used in this study. Under International Standard Atmosphere (ISA) conditions and maximum shaft speed, this single-shaft gas turbine results in 184.5 MW output power. The available nominal performance parameters of the engine at design-point conditions are given in Table 3.1.

[1] Alstom Power webpage, http://www.power.alstom.com

Figure 3.3: ALSTOM GT13-E2 gas turbine (Alstom Power webpage, http://www.power.alstom.com).

Table 3.1: GT13-E2 measured parameters

Parameter	Actual values
Shaft power, MW	184.5
Exhaust mass flow rate, kg/s	565
Total pressure ratio	16.9
Exit temperature, ^{o}C	505
Thermal efficiency, %	37.8
Gross heat rate, kj/kw.hr	9524

3.4 Performance Prediction Results

3.4.1 Design-Point Performance

A MATLAB call function was written in order to write the VariFlow code input file, launch the code, and get the performance data back. The actual engine has cooled turbine blades, while, this is not considered in the engine performance model. The fuel chosen is natural gas. Also, some required performance parameters are unknown, and here they are estimated in order to bring closer predicted data with available data. In more detail, an adaptation method was used to estimate the compressor isentropic efficiency (η_{scp}), turbine isentropic efficiency (η_{sgt}), combustor pressure loss (ΔP_{cc}), combustor efficiency (η_{cmb}), engine input mass flow rate ($\dot{m}_{\text{air}}$), and turbine entry temperature ($\mathtt{T}_{\text{fire}}$). The target performance parameters include shaft power ($\dot{\mathrm{W}}_{\text{shaft}}$), thermal efficiency ($\eta_{th}$), exhaust mass flow rate ($\dot{m}_{exh}$), exhaust temperature ($\mathtt{T}_{\text{exh}}$), and the gross heat rate ($\dot{m}_{\text{fuel}}$ LHV). A genetic algorithm optimization approach was used to minimize the root mean squared error between predicted and target parameters. The initial and adapted errors are given in Table 3.2. Note that the adapted errors for all parameters are smaller than initial error values. Also, the to-be-adapted performance parameters are calculated and given in Table 3.3. Also, Fig. 3.4 represents the air-gas temperature-pressure distribution along engine parts. The adaptation results in Table 3.2 show a good agreement between simulation model and measured values. The outcome of this study is an engine model which is inspired by real engine with small differences between predicted and observed data. It should be noted that the intention of this study is not to have a very detailed model of real engine, thus, the adapted model is used with confidence for the optimization studies. Appendix B includes the final VariFlow input file.

Table 3.2: Design-point performance adaptation.

Parameter	Initial error, %	Adapted error, %
Shaft power	4.17	-0.33
Exhaust mass flow rate	-0.53	0.17
Exit temperature	-0.29	0.19
Thermal efficiency	4.21	0.39
Gross heat rate	-4.1	-0.41

Table 3.3: To-be-adapted performance parameters.

Parameter	Adapted value	Deviation from initial value, %
Compressor efficiency, %	82.88	-9.9
Turbine efficiency, %	92.78	0.52
Combustor pressure loss	0.102	-30.7
Combustor efficiency, %	95.02	-4.50
Inlet mass flow rate, kg/s	556.8	0.82
Turbine inlet temperature, ^{o}K	1394	1.53

3.4.2 Operating Performance

Ambient temperature changes are the most significant factor affecting the performance of industrial gas turbines. The standard-ambient temperature ($\mathtt{T}_{\mathrm{std}}$) is 15^0C. For an industrial gas turbine running at constant shaft speed (N), the non-dimensional shaft speed, ($N/\sqrt{\mathtt{T}_{\mathrm{air}}/\mathtt{T}_{\mathrm{std}}}$) will be lower in the hotter days, leading to lower pressure and temperature ratios as shown in Fig. 3.5-(a). In addition, the high ambient temperatures decrease the air density. The decrease in inlet air density causes a decrease in the inlet mass flow rate (Fig. 3.5-(b)). The higher the ram temperature, more heat is exhausted to the atmosphere as shown in Fig. 3.5-(c). Therefore, the hotter temperatures lead to a decrease in the efficiency and the net power output as shown in Figs. 3.5-(d) and (e).

3.5 Design-Point Diagrams

The aero-thermodynamic equations of gas turbine cycles in relation to the temperature-entropy diagrams show that the changes in the compressor pressure ratio and turbine inlet temperature strongly affect the engine performance [71] and hence these two parameters are used in this work to maximize the engine cycle performance. The thermal efficiency and specific power typically represent the performance of an industrial gas turbine and considered here. Design-point diagrams based on a 184.5MW-power engine are created by plotting engine performance parameters of thermal efficiency and specific power versus the changes in compressor pressure ratio and turbine inlet temperature and shown in Fig. 3.6. Note that the changes in the values of compressor pressure ratio and TET will result in different engine geometry (size) from baseline engine. Figure. 3.6 shows that for each TET value, there is a corresponding compressor pressure ratio value that maximizes the gas turbine efficiency, such that, the optimum pressure ratio increases with increasing turbine entry temperature. The fact that an optimum thermal efficiency value does exists is because the thermal efficiency depends on both combustor temperature rise and exhaust temperature which the latter shows the heat wastage. Thermal efficiency is maximum where the ratio of combustor temperature rise to exhaust temperature is maximum [71]. This requires to minimum exhaust temperature and hence increasing pressure ratio. However, at very high pressure ratio values, the low combustor temperature rise offsets the low exhaust temperature and therefore thermal efficiency is reduced [71]. Also, Figure. 3.6 shows that there is an optimum pressure ratio value that maximizes specific power. Inspecting trends of efficiency and specific power shows that the specific power is maximized at much lower compressor pressure ratio compared with efficiency.

There are some limitations of how much the compressor pressure ratio and turbine entry temperature change. For example, Soars [71] mentioned that due to mechanical

integrity, the combustor entry temperature must be limited to temperatures between 850 and 950^{o}K, depending on the technology level. Also, if the engine is to be used in a combined cycle power plant, exhaust temperature must be limited to between 800 and 900^{o}K, depending on the technology level of the HRSG. These temperatures are shown in Fig. 3.7 that shows the combustor entry temperature increases with compressor pressure ratio. Note that the turbine entry temperature has no effects on the combustor entry temperature. Figure 3.7-(b) also shows that the exhaust temperature falls with compressor pressure ratio, although the rate of fall becomes smaller at higher pressure ratio values. The exhaust temperature will increase with turbine entry temperature as well. The pressure rise per stage is also limited; a high pressure rise per stage might results in the flow separation and compressor surge [48]. Therefore, a high pressure ratio compressor requires many stages that will rise the production cost and complexity. In addition, the high pressure-ratio compressor tends to increase the casing expansion and distortion [48] that produces energy losses due to the flow around the blade tips.

A surface graph of thermal efficiency and specific power is plotted from a series of pressure ratio and TET values and shown in Fig. 3.8. This figure shows that thermal efficiency is maximized at high compressor pressure ratio and high turbine entry temperature. The specific power is more sensitive to the compressor pressure ratio changes. The specific power is maximized at high turbine entry temperature as well but at a moderate pressure ratio value. The pressure ratio that maximize the thermal efficiency is approximately three times larger than the value that maximizes specific power.

Figure 3.8-(b) shows that the specific power is a nonlinear function of pressure ratio and TET with a global maximum point in the pressure ratio and TET range of interest. Genetic Algorithm (GA) and Expected Improvement Function (EIF) optimization methods are applied to maximize specific power and to compare the

power of each algorithm. In the genetic algorithm, each point is associated with a "fitness" value that defines the probability of survival in the next "generation" such that the higher the fitness, the higher the probability of survival [72]. The genetic algorithm starts with an initial population generally chosen random and then applies three basic operators of reproduction, crossover, and mutation. In the reproduction, the chromosomes to be copied in the next generation are selected based on fitness values. The crossover operator is then applied to produce some new points from crossover between pairs of selected points. Finally, the mutation operator is applied which randomly reverses the value of every bit within a chromosome with a fixed probability. The population size used to find the specific power maximum point has 40 points and the point locations for different generations are shown in Fig. 3.9. Note that how the points concentrate more and more around the global maximum point as generation increases. The EIF optimization also starts from some initial points; the initial points consist of four points at the border of pressure ratio and TET space and one random point as shown in Fig. 3.10. The points at the borders aid in to avoid extrapolation in Kriging. From Kriging predictions, EIF values are found for the design space. A point is then selected where EIF is maximum and this iterates until the maximum EIF falls below a threshold value. The final point locates at the global maximum point. In comparison to GA, EIF needs much less computational cost. More comparisons of these methods will be detailed in Chapter on thermoeconomic optimization.

Figure. 3.6(b) shows that specific power increases with turbine inlet temperature. The maximum specific power in Figs. 3.8-3.10 is located at TET=1800^{o}K at the maximum value of studied range. One might ask for increasing TET further to improve the specific power. This applies with similar assumption that no air is bled from compressor for cooling the turbine blades. However, the materials are limited to the temperature and they need to be cooled to avoid over-heating. Following simulations

consider the bleeding air effects into specific power. The air is bled from compressor to keep the metal temperature below 1488^{o}K. The amount of required bleeding is found from an optimization method to minimize the squared difference between predicted metal temperature and desired temperatures. Note that the amount of bleeding air is zero for all TET values below desired metal temperature and optimization method was used only for higher temperatures. Once the bleeding air amount is known, the VariFlow code was used to predict the specific power. Figure 3.11 shows the surface graph of specific power for a series of pressure ratio and TET values and assuming metal temperature kept below 1488^{o}K. This figure shows that specific power is nearly unchanged from moderate to high turbine inlet temperature values, though they still change with compressor pressure ratio. Therefore, for all subsequent studies, the maximum TET value is set to 1800^{o}K.

In Fig. 3.6, the pressure ratio and TET changes are independent of each other, therefore for each line, the pressure ratio changes but TET is held constant. The trend of efficiency versus power from simulations is compared with general trends of gas turbines in Fig. 3.12. The figure shows that the simulation trends are very different from expected ones. The issue in simulations is that it does not take into account the correlation functions existing between actual engine parameters. The pressure ratio, turbine inlet temperature, and air mass flow of commercial gas turbines are correlated and follow a global trend regardless of the manufacturer [73]. These trends are shown in Fig. 3.13. Figure 3.13-(a) shows pressure ratio and turbine entry temperature as a function of output power. The points in the figure correspond to real gas turbines and lines represent the linear regression trends. The real gas turbine data can be separated to low and high power engines. Figure 3.13-(a) shows that the pressure ratio and turbine entry temperature trends are different for these two types of engines. Figure 3.13-(b) also shows that the mass flow rate changes with engine output power (size). In summary, the turbine entry temperature, pressure ratio, and

mass flow rate will increase with increasing the engine power. The simulation results were updated with taking into account the correlation functions shown in Fig. 3.13 and then simulation trends are compared with the engine data and an approximation trend by Boyce [28] as shown in Fig. 3.14. The figure shows that the simulation trend agree well with engine data now.

As shown earlier, the specific power and thermal efficiency are increased with increasing turbine inlet temperature, therefore there has been a great interest in industry to use higher turbine inlet temperatures. The highest allowed TET for uncooled blade is approximately 1250-1300^{o}K, while depending on the cooling system, this temperature can reach to 1800^{o}K for a cooled blade [74]. The cooling air usually is extracted from the exit stage of high-pressure compressor and carried by ducts to the guide vanes and rotor of hight-pressure turbine. The air extraction from compressor significantly changes the engine performance. The thermal efficiency and specific power changes with amount of bled air are shown in Fig. 3.15 that shows both thermal efficiency and specific power fall with increase in amount of bled air from the compressor of engine. Therefore, the cooling system should be designed to minimize the use of compressor bleed air [75]. The required amount of bled air depends on the allowable metal temperature and turbine inlet temperature as shown in Fig. 3.16 that shows more air needs to be extracted for cooling if the turbine inlet temperature increase. The amount of cooling air would be less for higher maximum metal temperature.

In general, emissions of NOx and CO are the main sources of changing air quality and therefore are considered in this work. Unfortunately, the VariFlow code has no tools for predicting these emissions, instead the semi-empirical equations by Rizk and Mongia [41] were used to estimate the NOx and CO changes with compressor pressure ratio and TET. The NOx emissions (in ppm) are shown in Fig. 3.17 for a constant TET scenario and for correlation functions detailed by Valdes et al. [73].

Figure 3.17 shows that the Nox emissions fall with increasing pressure ratio if TET is held constant. It is also shown that for an engine following the global trends of engines in the market, increasing pressure ratio will rise the NOx emissions. In these correlation function, TET increases with an increase in pressure ratio, and this will significantly increase the NOx emissions. The CO changes are shown in Fig. 3.18 that shows CO emissions are reduced by increasing the compressor pressure ratio.

3.6 Conclusions

The performance prediction of an industrial gas turbine was described in this chapter. The gas turbine considered is a single-shaft engine inspired by the Alstom GT13-E2 with 184.5 MW output power. An adaptation technique was used to estimate the compressor efficiency, combustor efficiency, combustor pressure loss, and turbine efficiency. This technique is based on the minmization of differences between engine predictions and available measurements from manufacture. The adaption method allows us to have an engine model with close predictions with actual engine to be used for subsequent studies. The adapted model was then used to predict the operating performance. In this study, the engine parts are designed and fixed but the ambient temperature changes. The predictions are based on guess and iteration method of using some pre-defined component maps. The results showed that the normalized shaft speed will be lower in the hotter days, leading to lower pressure and temperature ratios in the compressor. In addition, the high ambient temperatures decrease the air density and hence the inlet mass flow rate. The hotter temperatures causes decreasing of efficiency and the net power output as well.

The design point diagrams were created and shown in this chapter. These included the plots of efficiency and specific power versus compressor pressure ratio and turbine entry temperature. The results showed that there is a compressor pressure ratio

that maximizes the efficiency and specific power. For low turbine entry temperature values, the pressure ratio that maximizes efficiency is around three times larger than the pressure ratio that maximizes the specific power. The plots also showed that the optimum pressure ratio increases with an increase in turbine inlet temperature.

Two optimization methods of GA and EIF were used to find the optimum point of specific power in the operating range of interest. Both methods accurately found the global point in the compressor pressure ratio and turbine entry temperature space, though EIF needed less computational cost. The results showed that efficiency and specific power are improved by increasing turbine entry temperature, but at high temperatures, the effects of cooling air from compressor leads to a decrease in the efficiency and specific power.

Some correlation functions were described to relate design parameter of available engines. The simulation results using these functions showed that prediction trends agree well with efficiency-power trend of available engines.

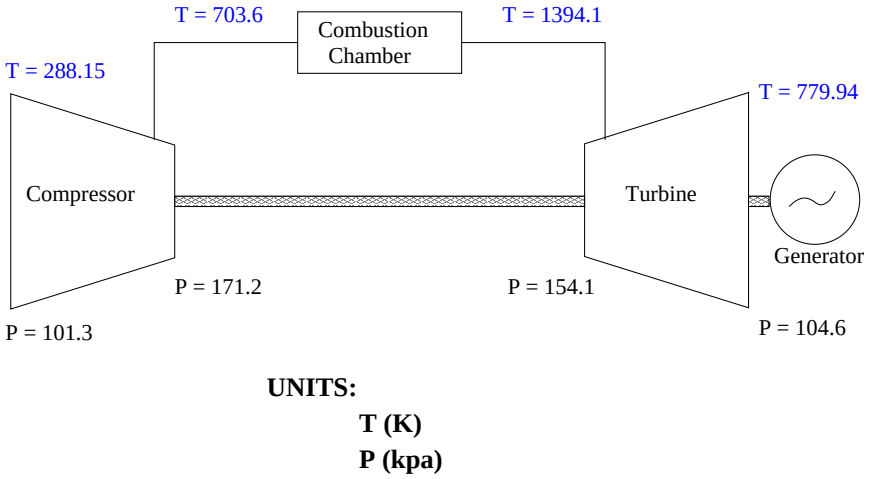

Figure 3.4: The baseline-engine temperature-pressure distribution.

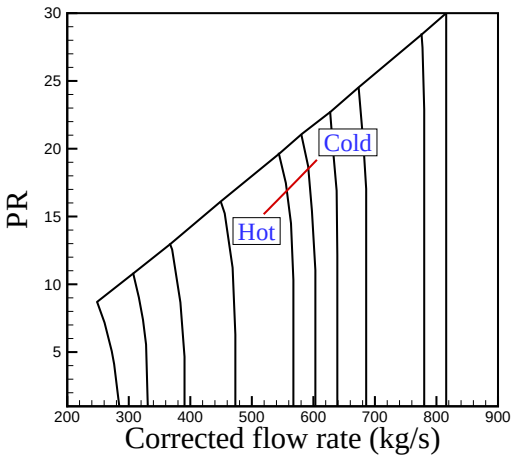

(a) Operating Line

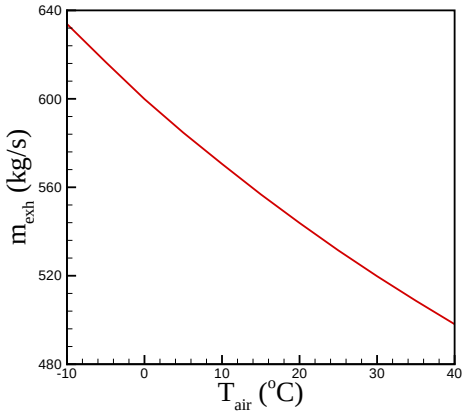

(b) Exhaust Flow

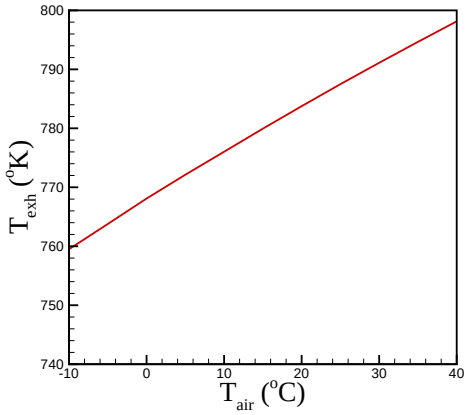

(c) Exhaust Temperature

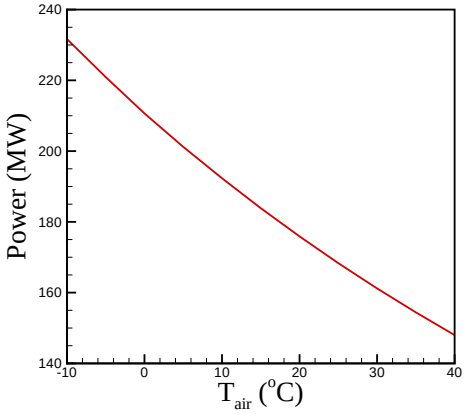

(d) Shaft Power

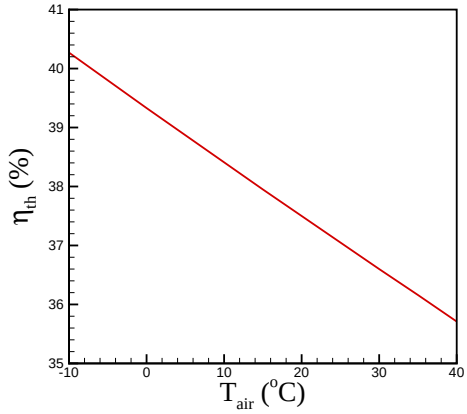

(e) Thermal Efficiency

Figure 3.5: The 184 power engine off design performance prediction. In (a) corrected flow rate is: $\dot{m}_{\text{air}}\sqrt{\text{T}_{\text{air}}/\text{T}_{\text{std}}}$

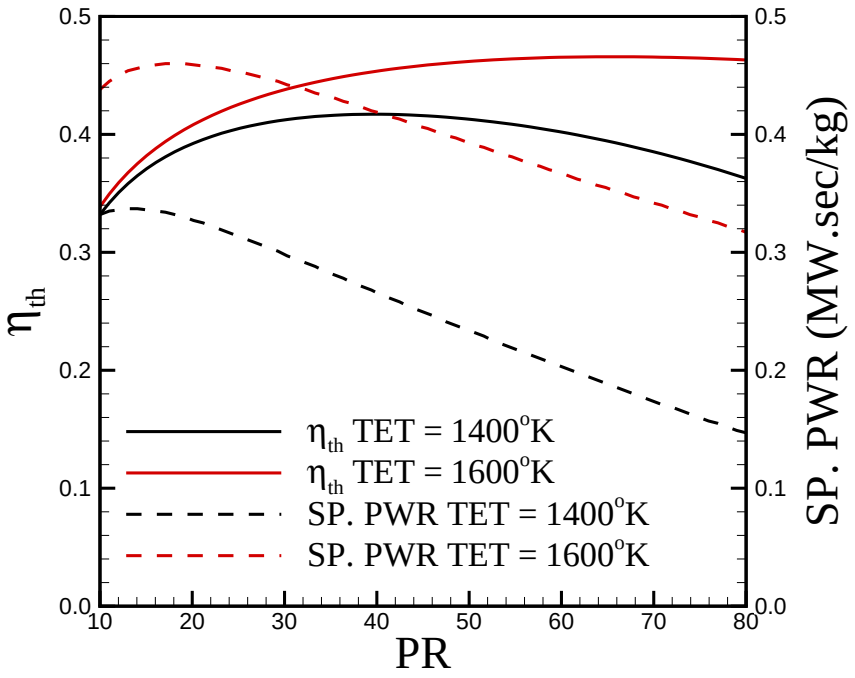

Figure 3.6: Thermal efficiency and specific power design diagrams.

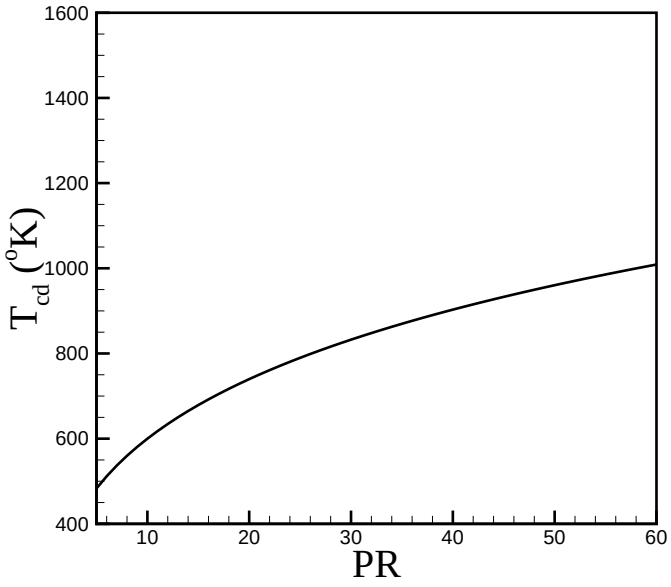

(a) The combustor entry temperature

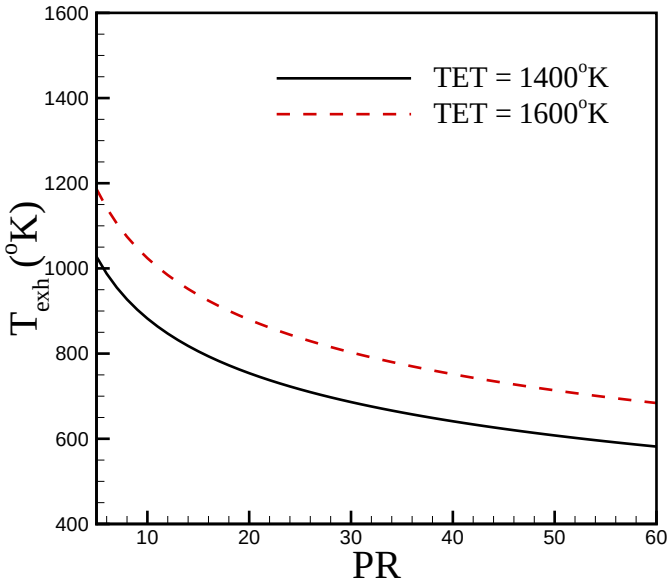

(b) Exhaust temperature

Figure 3.7: The combustor entry temperature and the exhaust temperature design diagrams.

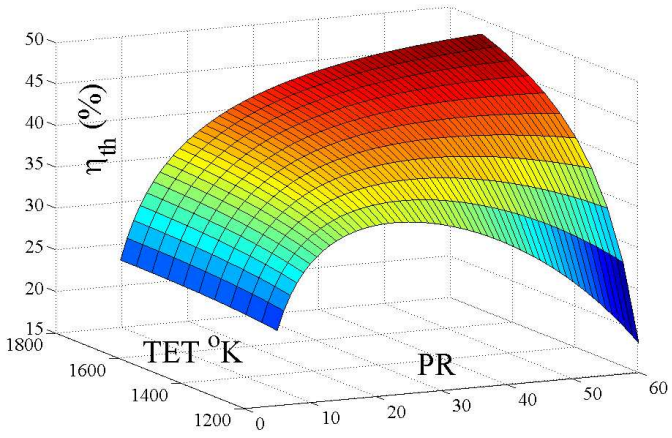

(a) Thermal Efficiency

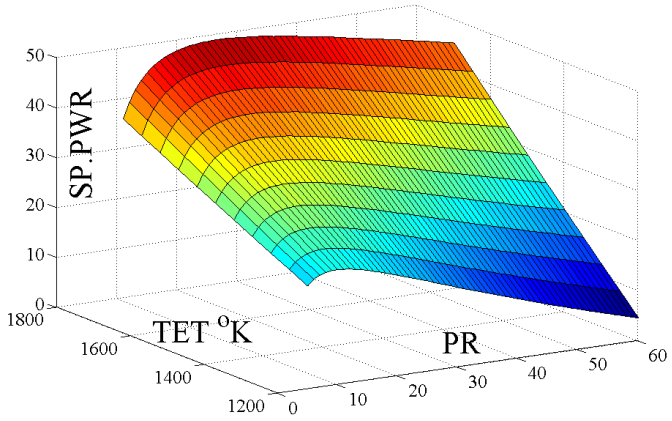

(b) Specific Power

Figure 3.8: Thermal efficiency and specific power surface graphs.

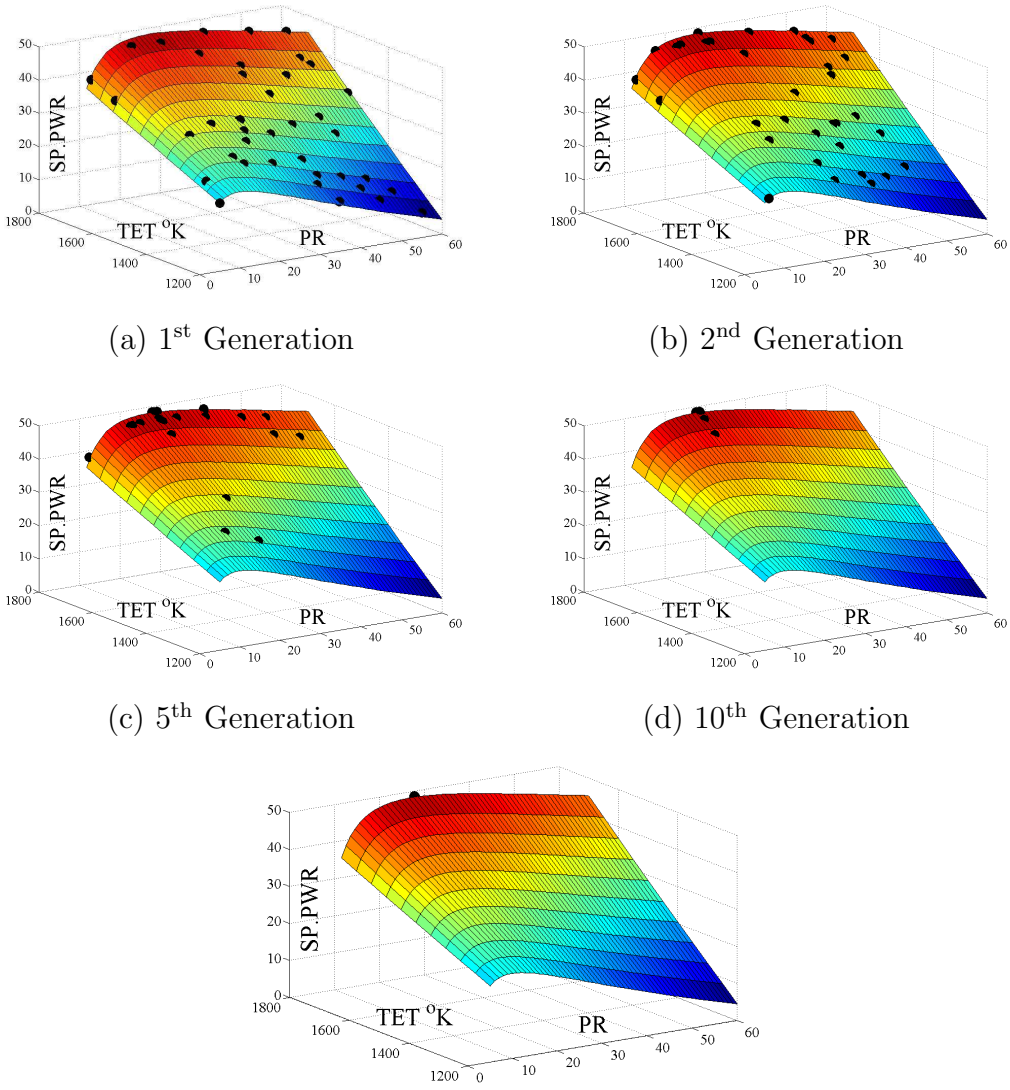

(a) 1st Generation

(b) 2nd Generation

(c) 5th Generation

(d) 10th Generation

(e) Optimal Point

Figure 3.9: Genetic algorithm optimization of specific power.

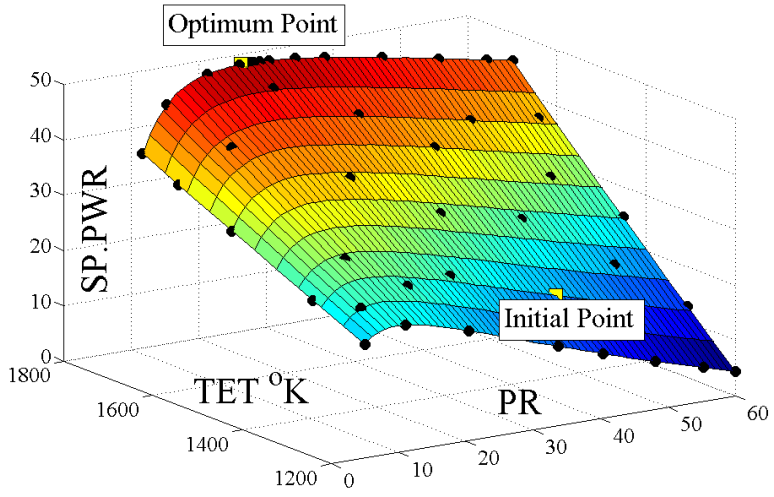

Figure 3.10: EIF optimization of specific power.

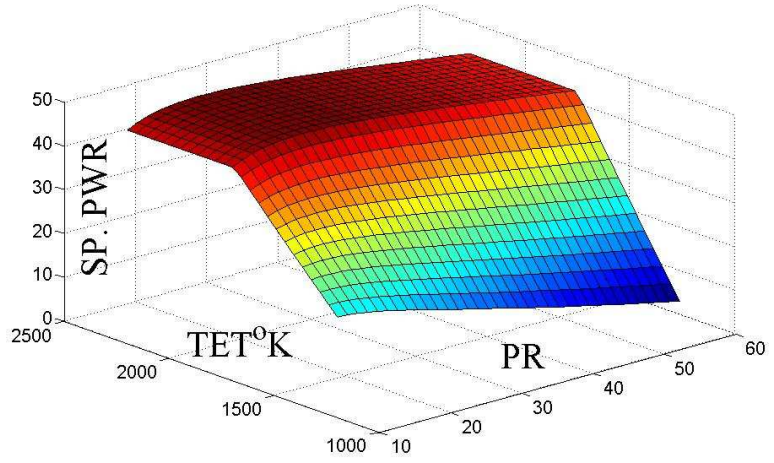

Figure 3.11: Specific power surface graph with a maximum metal temperature of 1488^{o}K.

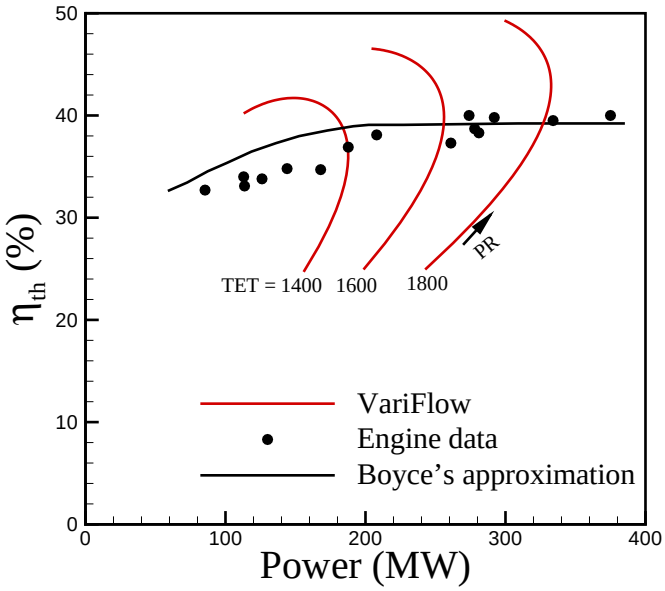

Figure 3.12: Issues of simulation trends for constant TET case.

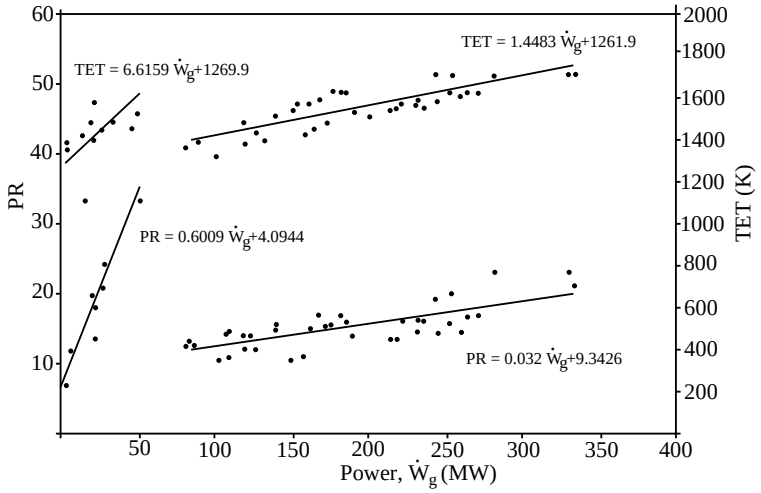

(a) TET and PR trends

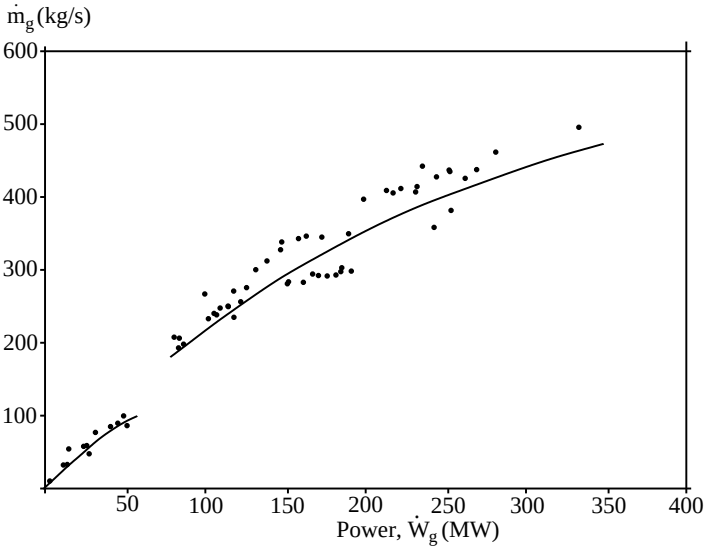

(b) Mass flow rate trend

Figure 3.13: Existing trends of engine parameters for commercial gas turbines. Points corresponds to real gas turbines and lines represent the linear regression trends.

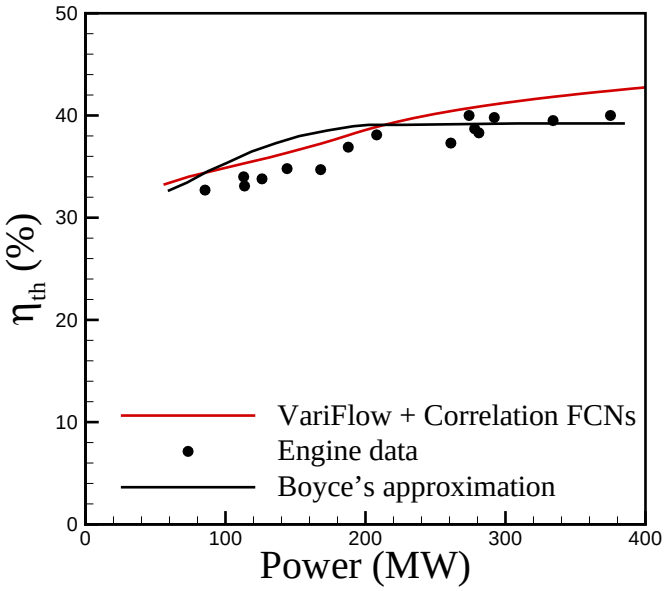

Figure 3.14: Simulation trends for constant TET case using correlation functions.

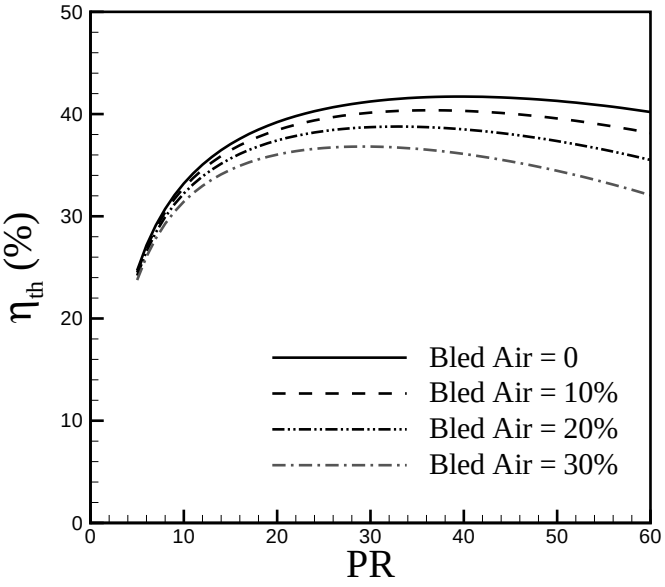

(a) Thermal Efficiency

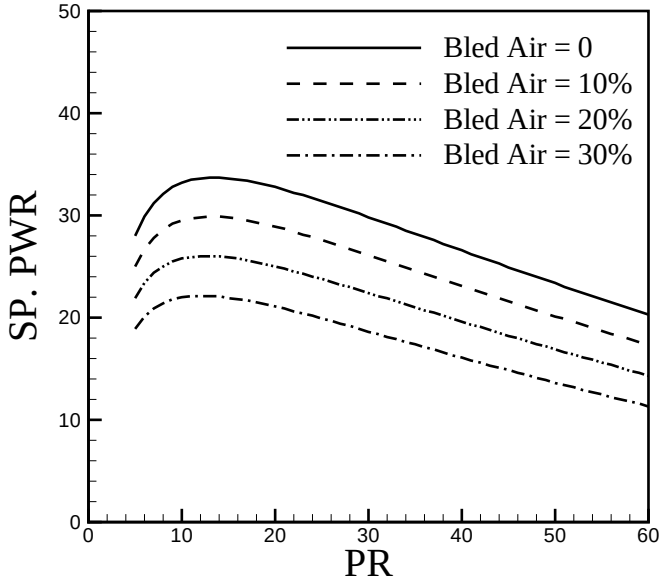

(b) Specific Power

Figure 3.15: Thermal efficiency and specific power trends with compressor bleeding air.

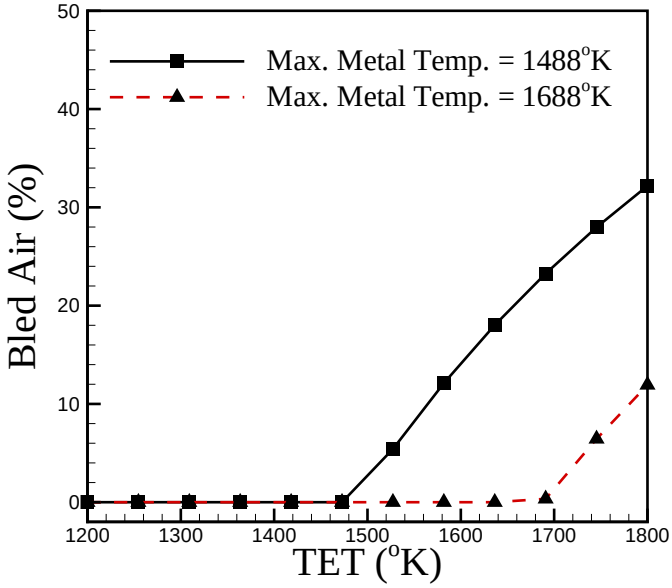

Figure 3.16: Required compressor bleeding air versus TET.

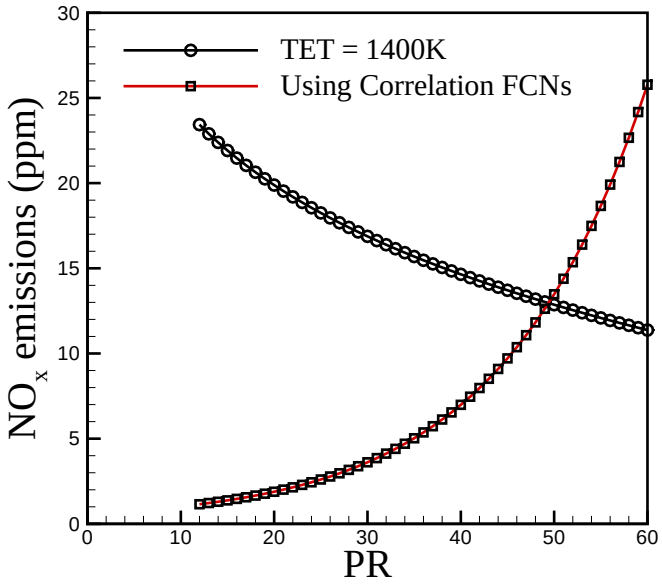

Figure 3.17: NO_x emissions.

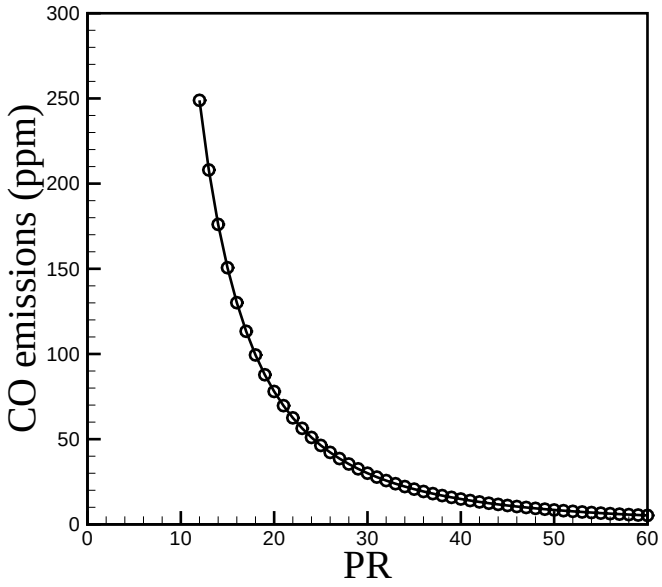

Figure 3.18: CO emissions. TET = $1400^o K$

Chapter 4

GAS TURBINE CAPITAL COST FORMULATION

4.1 Introduction

The mathematical modeling of capital investment is the focus of this chapter. The accurate prediction of gas turbine capital cost aids in creating reliable models for thermoeconomic analysis and optimization of simple and combined gas-turbine cycles. Several semi-empirical equations have been proposed to estimate the cost of gas turbine's components of compressor, combustor, and turbine. These equations are based on data collected over many years from different engines. It should be noted that the gas turbine economics vary with time as technology changes from time to time [76], such that in recent years, the cost of gas turbines has fallen due to advances in technology [23]. Therefore, the equation descriptions had been kept unchanged but the cost coefficients had been modified several times based on the technological improvements in gas turbines [33, 8, 77, 78].

The objective of this chapter is to provide some criteria to select a low-cost gas turbine power plant. The economic of gas turbines can be compared using the operating

income which is:

$$\text{Operating income} = \text{Total Revenue} - \text{Total operating expenses} \tag{4.1}$$

where total revenue is directly related to the electricity cost and output power. The total operating expenses include the initial investment, operating and maintenance, and cost of fuel consumption. The revenue and initial investment increase with increasing the gas turbine power, however the revenue has a larger rate of increase than investment [76]. Therefore, a large gas turbine power plant makes more operating income in its lifetime than a small gas turbine plant assuming a fixed life-time and operating hours per year. In this work, capital cost per kw (so-called unit of capital cost) has been used to compare the competing gas turbine power plants. The capital cost here refers to the initial investment, operating and maintenance, and interest rate.

In this chapter the equations for modeling gas turbine components are presented. The total cost is then estimated by adding the cost of each component. The cost sensitivity to the engine size is then studied. The cost values will then be validated against the general cost trend of gas turbines in the market. The problem of using the cost model for predicting the cost of different size engines is addressed. An updated cost model is proposed and validated for use in thermoeconomic study.

4.2 Capital Cost

Capital cost is regarded as the sum of capital investment (purchased equipment cost or initial cost), operating (excluding fuel) and the maintenance costs [30]. According to Frangopoulos and Caralis [79], the capital cost can be calculated as:

$$C_z = \beta C_0 + C_{\mathrm{OM}} \tag{4.2}$$

where C_0 and C_{OM} show the initial investment and operating and maintenance in US$, respectively. β is a capital charge factor that relates to the discount rate on capital and the life of the plant. The capital charge factor (β) is used to take into account the cost recovery of the plant purchased equipment cost during plant lifetime and can be estimated as:

$$\begin{aligned}\beta = {} & (l-1) + l.\mathrm{CFR}(N_L, r).\mathrm{PWF}(N_{min}, 0, d) - t_i\phi_i \\ & - l.t_i\{[r - \mathrm{CRF}(N_L, r)].\mathrm{PWF}(N_{min}, r, d) + \mathrm{CRF}(N_L, r).\mathrm{PWF}(N_{min}, 0, d)\} \\ & - \frac{t_i}{N_D}.\mathrm{PWF}(N'_{min}, 0, d) - \frac{v_s}{(1+d)^{N_e}}\end{aligned} \quad (4.3)$$

where, l is the loan to initial investment ratio; CFR is capital recovery factor and is function of loan period (N_L) and the loan interest rate (r); PWF is present worth factor and depends on the years which loan payment contribute to the analysis (N_{min}), discount rate (d) and the years which depreciation contributes to the analysis (N'_{min}); t_i is income tax rate; ϕ_i is part of the initial investment deductible from first-year income tax; N_D is depreciation life time in years; v_s is ratio of salvage value at the end of period of analysis to initial investment; and N_e is period of economic analysis in years. More detailed descriptions of these terms are given by Duffie and Beckman [80]. In the present work, the annual fixed change rate percent was defined and used for estimating the capital cost instead of estimating the terms in Eq. 4.3.

The operating and maintenance costs are the charges that occur during electricity generation and can be separated into fixed and variable costs. Thissen and Herder [81] estimated these costs for a conventional gas turbine; these estimates are given in Table 4.1. It should be noted that the operating and maintenance costs depend on the fuel type such that the costs associated with kerosene are higher than costs associated with natural gas [28]. In Eq. 4.2, the initial investment is a “one-time” cost

but operating and maintenance costs are continuing during the life of the system [8]. Therefore the annualized capital cost is defined in Eq. 4.4 and used here.

Table 4.1: Gas turbine capital cost estimates (Thissen and Herder, 2003)

	Units	Values
Capital cost	\$/kw	500
Fixed O&M cost	\$/kw	15
Variable O&M cost	c\$/kwhr	0.55

$$\dot{C}_z = \frac{\beta C_0 + C_{\mathrm{OM}}}{N} = \frac{C_0 \times FCR \times \Phi_r}{N} \tag{4.4}$$

where, FCR is the annual fixed change rate percent with standard value of 18.2 percent, Φ_r is maintenance factor with standard value of 1.06, N is number of operating hours per year and C_0 shows the capital investment (or purchased equipment cost) in US\$. Annualized capital cost is denoted by $\dot{C}_z$ and expressed in US\$/h. However, the capital investment still needs to be calculated. The capital investment changes with engine design parameters. For example, as the compressor pressure ratio is increased, more compressor stages are needed and this adds to the initial cost [82]. The compressor cost also increases with increasing isentropic efficiencies. Also, the initial cost increases with turbine entry temperature because of using special alloys and advanced cooling techniques for the turbine blades and vanes [8]. Kreith and West [24] related the capital cost of simple and combined gas turbine power plants to the output power as:

$$\text{Gas Turbine Capital Cost} = \$43,200,000 \;.\; (\dot{W}_g/100)^{0.7} \tag{4.5}$$

$$\text{Combined Cycle Capital Cost} = \$5,040,000 \;.\; (\dot{W}_g)^{0.6} \tag{4.6}$$

where $\dot{W}_g$ is the plant output power in MW. For thermoeconomic study, the initial cost needs to be correlated to gas turbine design parameters of compressor pressure ratio, turbine entry temperature, isentropic efficiencies, and gas mass flow rate [83]. These correlation functions are described in this chapter.

4.3 Cost Modeling and Problems

For effective implementation of capital cost (or PEC) in thermoeconomic optimization problem, correlations between capital cost and the size and performance of system are required. The capital cost significantly changes with the design of turbine and compressor [84]. Table 4.2 shows some of the effects of designs changes into gas turbine cost. To estimate these effects, the functions proposed by El-sayed and Tribus [33] and modified by von Spakovski and Frangopolous [27] and used by Agazzani *et al.* [31] and Massardo and Scialo [32] were implemented. These functions consist of the cost of compressor, combustor, and turbine and are as follows:

$$C^{\$}_{cmp} = \frac{c_{11}}{c_{12} - \eta_{scp}} r_c \ln(r_c) \dot{m}_a \tag{4.7a}$$

$$C^{\$}_{cmb} = \frac{c_{21}}{c_{22} - \alpha} [1 + \exp(c_{23} \mathrm{T}_3 - c_{24})] \dot{m}_a \tag{4.7b}$$

$$C^{\$}_{gtu} = \frac{c_{31}}{c_{32} - \eta_{sgt}} \ln(r_c) [1 + \exp(c_{33} \mathrm{T}_3 - c_{34}] \dot{m}_g \tag{4.7c}$$

where c_{ij} coefficients are given in Appendix A. In Eqs. 4.7, $r_c = P_2/P_1 = P_3/P_4$ is the compressor or turbine pressure ratio, and $\alpha = P_3/P_2$ is the combustor pressure ratio, where, P_1, P_2, P_3 and P_4 present the air and gas pressure at the inlet and outlet of compressor and turbine, respectively; η_{scp} and η_{sgt} denote the compressor and turbine isentropic efficiencies, respectively; T_3 is the maximum gas turbine temperature in Kelvin, while $\dot{m}_a$ and $\dot{m}_g$ are compressor entering air and gas mass flow rates in

Table 4.2: Economics of power plants (Kensett, 1990)

Part	Low Cost	High Cost
Compressor	Single stage centrifugal	
		Multistage axial
Turbine	No blade cooling	
		Advanced blade cooling

kg/s, respectively. The purchased equipment cost is then calculated as the sum of all component costs, i.e.:

$$C_0 = C_{cmp} + C_{cmb} + C_{gtu} \tag{4.8}$$

It is more common to use capital cost in terms of $/kw, so-called unit capital cost, to compare the cost of different power plants. The unit capital cost shows the cost of delivering a kw of electric power to the final customer. Table 4.3 compares the initial cost per kilowatt of various types of power plants. Table 4.3 shows that the gas turbines offer relatively low unit capital cost, ranging in $300-$500/kW, makes them the best economic choice for peaking power. Next choice is a combined-cycle power plant with initial costs of $600-$900/kW. Nuclear power plants are the most expensive plants with initial costs of $1,800-$2,000/kW as shown in Table 4.3.

Table 4.3: Economics of power plants (Boyce, 2002)

Type of Plant	Capital Cost (US$/kW)
SCGT (1371^{o}C, natural gas fired)	200 - 350
Regenerative gas turbine (natural gas fired)	375 - 575
Combined-cycle gas turbine	600 - 900
Steam plant coal fired	800 - 1,000
Combined-cycle coal gasification	1,200 - 1,400
Nuclear power	1,800 - 2,000

The cost trends of engine components along with total engine are shown in Fig. 4.1. Note that the combustor cost is negligible compared to the costs of compressor and

turbine. Figure 4.1 shows that the compressor cost linearly increases with compressor pressure ratio. The higher pressure ratio requires more compressor stages and this adds to the cost. The turbine cost also increases with increasing compressor pressure ratio, although the rate of increase is smaller than compressor.

Note that for a given power output the greater the efficiency the higher the capital cost of plant [84]. Figure 4.2 shows the trend of increase in compressor and turbine cost with increasing component efficiencies. Figure 4.2(a) shows that the compressor cost suddenly start to increase as compressor efficiency increases above 0.85. Note that c_{12} in Eq. 4.7 was assumed 0.9 and as the compressor efficiency becomes close to this value, the compressor cost predictions tend to infinity. Turbine cost also increases with turbine efficiency as shown in Fig. 4.2(b).

According to Kensett [84] the greater the output of the gas turbine the lower the capital cost/kW (unit capital cost). Regardless of the manufacturer, the unit capital cost of engines in the market follows a general trend as shown in Fig. 4.3. This figure shows the unit capital cost (capital cost/kw) is large for small engines and then falls as the plant size is increased. Figure 4.3 shows the gas turbine unit capital cost is relatively insensitive to the plant size for medium and large engines. Figure shows that cost predictions from Eqs. 4.7 and varying the compressor pressure ratio do not match the general cost trends. The problem of this modeling is that it does not take into account the correlation functions existing between actual engine parameters such as pressure ratio, mass flow, and TET.

4.4 An Updated Cost Model

The pressure ratio, turbine inlet temperature, and air mass flow rate of commercial gas turbines are correlated and follow a global trend regardless of the manufacturer [73]. These trends are shown in Fig. 4.5. Figure 4.5-(a) shows pressure ratio and turbine

entry temperature as a function of output power. The points in the figure correspond to real gas turbines and lines represent the linear regression trends. The real gas turbine data can be separated to low and high power engines. Figure 4.5-(a) shows that the pressure ratio and turbine entry temperature trends are different for these two types of engines. Figure 4.5-(b) also shows that the mass flow rate changes with engine output power (size). In summary, the turbine entry temperature, pressure ratio, and mass flow rate will increase with increasing the engine power. Manninen and Zhu [20] developed some equations for predicting engine performance and cost trends with output power. These equations are:

$$\dot{m}_{exh} = 2.9 \times \dot{W}_g \tag{4.9}$$

$$T_{exh} = 0.4 \times \dot{W}_g + 493.42 \tag{4.10}$$

$$C^{\$} = 195.5 \times \dot{W}_g + 2529.2 \tag{4.11}$$

where $\dot{m}_{exh}$ is the exhaust mass flow rate in kg/s; T_{exh} is gas exhaust temperature in ^{o}K; $C^{\$}$ is the capital cost; and $\dot{W}_g$ is the gas turbine power in MW. The cost model was updated with taking into account the correlation functions using these equations and then predictions are compared with the engine data and an approximation trend by Boyce [28] and Valdes [73] as shown in Fig. 4.6. The figure shows that the simulation trend agree well with engine data now for engines with output power above 100MW. For thermoeconomic study only engine designs with power larger than 100MW are considered.

Once the purchase equipment cost models were developed and validated, they could be used to estimate the annualized capital cost in Eq. 4.4. The annualized cost depends on the operating hours in a year. Figure 4.7 shows the effects of operating hours into the cost values. The cost increases as the operating hours becomes smaller

as shown in Fig. 4.7.

4.5 Sensitivity Analysis

The exact values of c_{ij} coefficients are usually unknown. Besides, these coefficients may vary with time as technology development changes. It is therefore important to perform a sensitivity analysis for the cost predictions to estimate the effects of changes in these coefficients. A sensitivity analysis was performed in order to find the cost coefficients that have most effects in capital cost. The cost coefficients were changed one percent around nominal values given in Appendix A and then capital cost changes were calculated. The partial derivatives of capital cost are defined as the ratio of capital cost to coefficient changes and shown in Fig. 4.8. For linear sensitivities, the coefficients correspond only to a positive change, but for nonlinear terms, derivatives with positive and negative numbers are shown in Fig. 4.8. The results show that among all the coefficients, only coefficients of c_{12}, c_{23}, c_{32}, and c_{33} are capable of significantly changing the capital cost around nominal values given in Appendix A. These coefficients are related to the costs of isentropic efficiencies and turbine entry temperature. This suggests that in order to reduce the cost of gas turbine, one might design an engine with reduced component efficiencies or turbine entry temperature.

4.6 Conclusions

The accurate prediction of gas turbine capital cost aids in creating reliable models for thermoeconomic analysis and optimization of simple and combined gas turbine power plants. The capital cost includes initial investment, operating and maintenance, and interest rate. The cost is annualized using operating hours per year. Some equations

were provided in order to estimate the initial investment of compressor, combustor, and turbine. However, it was shown that by using these equations, the cost predictions do not match with available engine prices. The problem of this modeling is that it does not take into account the correlation functions existing between actual engine parameters such as pressure ratio, mass flow, and TET. Using these correlations, the cost predictions match well with available data. In order to estimate the effects of cost coefficient changes into capital cost, a sensitivity analysis was performed. The sensitivity analysis results showed that capital cost predictions are very sensitive to the coefficients related to component efficiencies and turbine entry temperature.

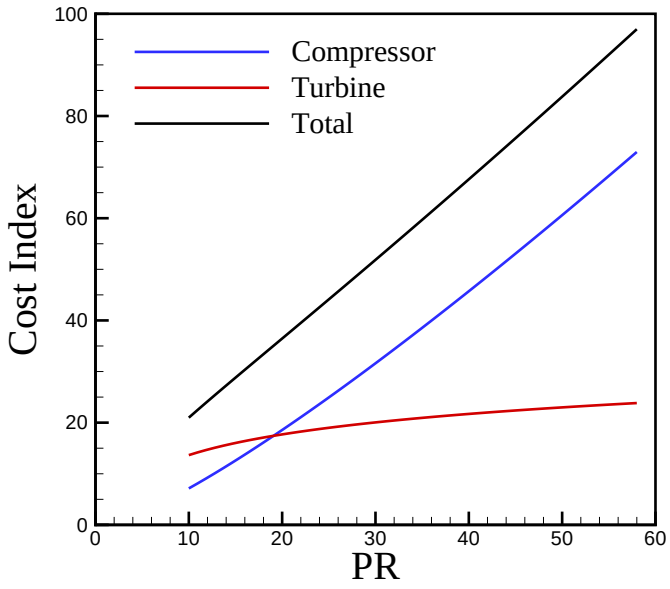

Figure 4.1: Gas turbine cost index trend with compressor pressure ratio.

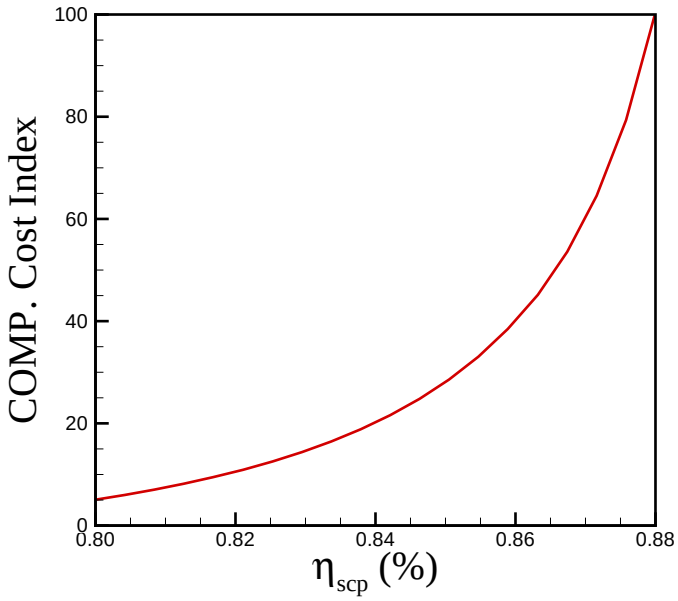

(a) Compressor cost

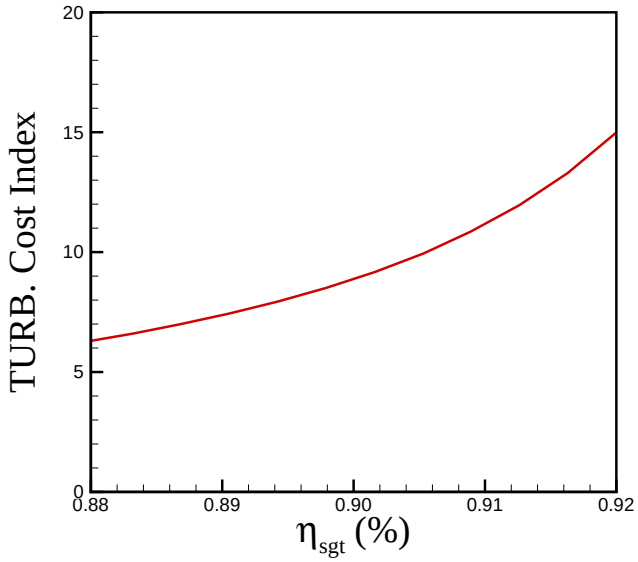

(b) Turbine cost

Figure 4.2: Compressor and turbine cost index changes with component efficiencies.

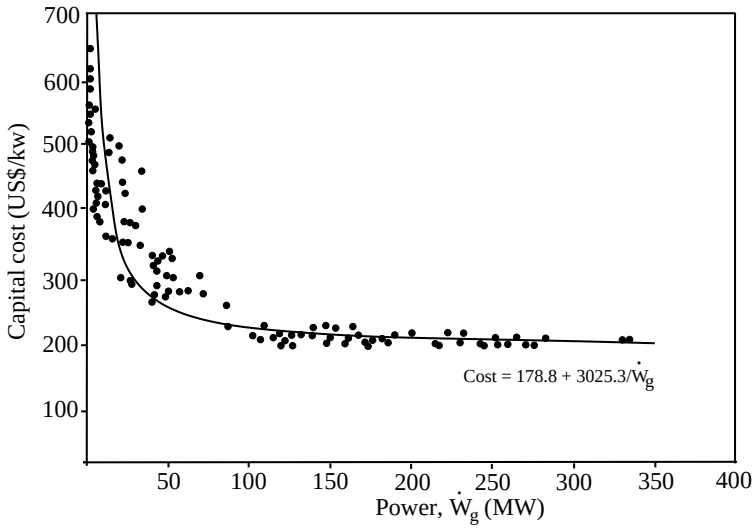

Figure 4.3: Existing trends between capital cost and plant power.

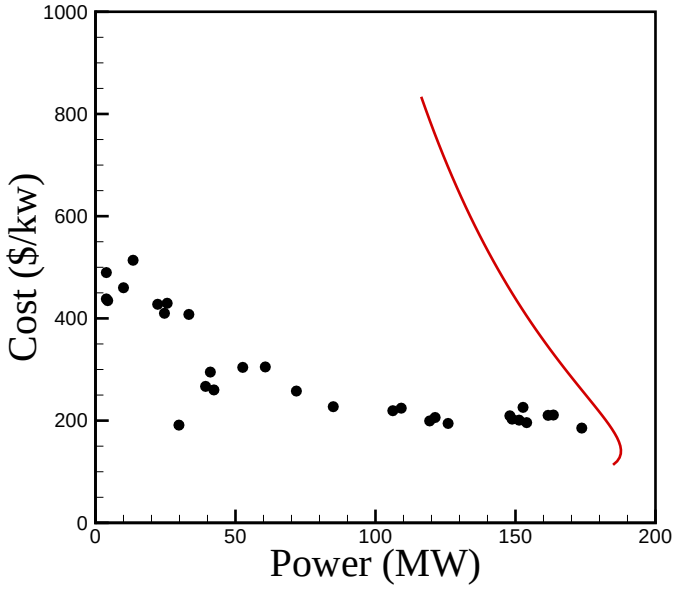

Figure 4.4: Issues of gas turbine cost modeling.

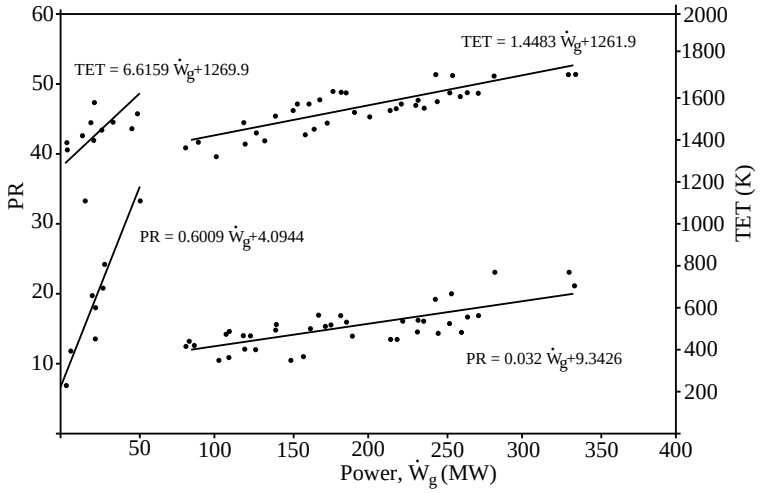

(a) TET and PR trends

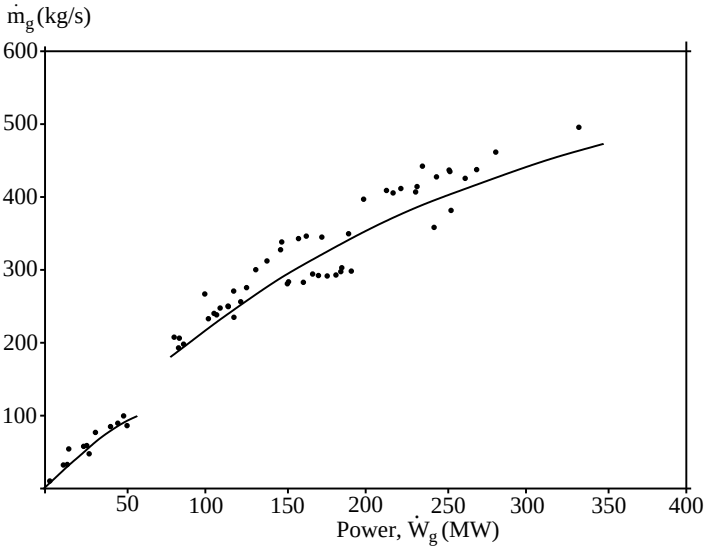

(b) Mass flow rate trend

Figure 4.5: Existing trends of engine parameters for commercial gas turbines. Points corresponds to real gas turbines and lines represent the linear regression trends.

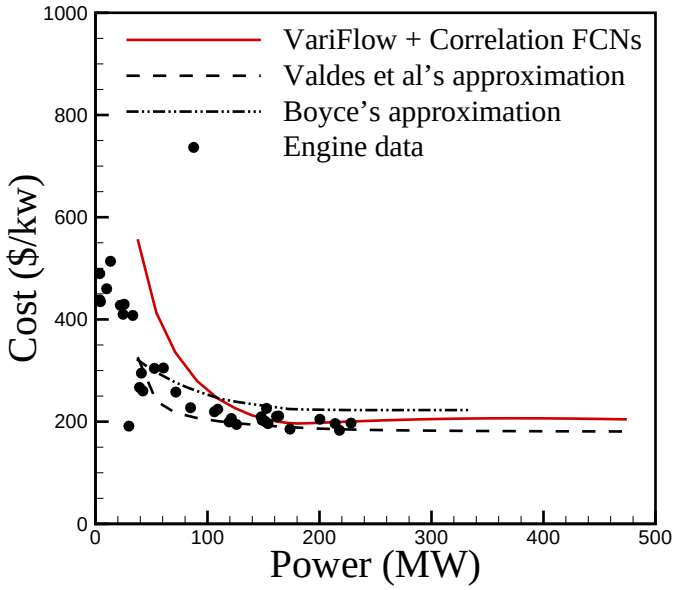

Figure 4.6: An updated model of gas turbine cost.

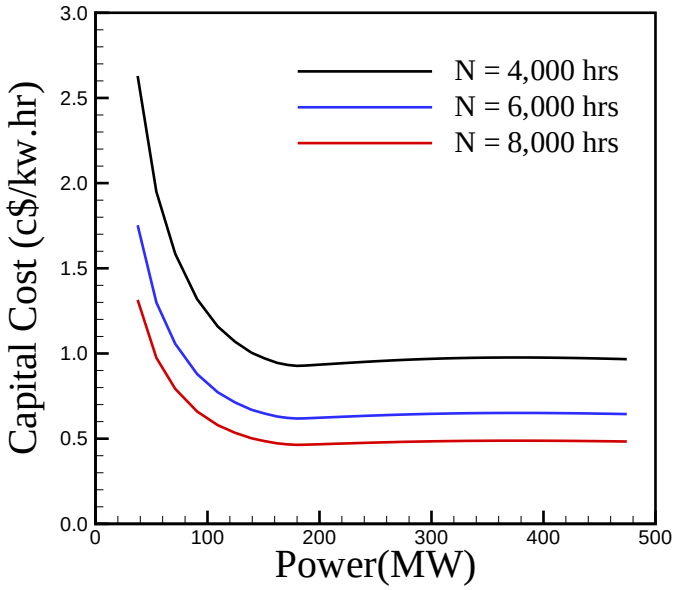

Figure 4.7: Effects of operating hours into annualized capital cost.

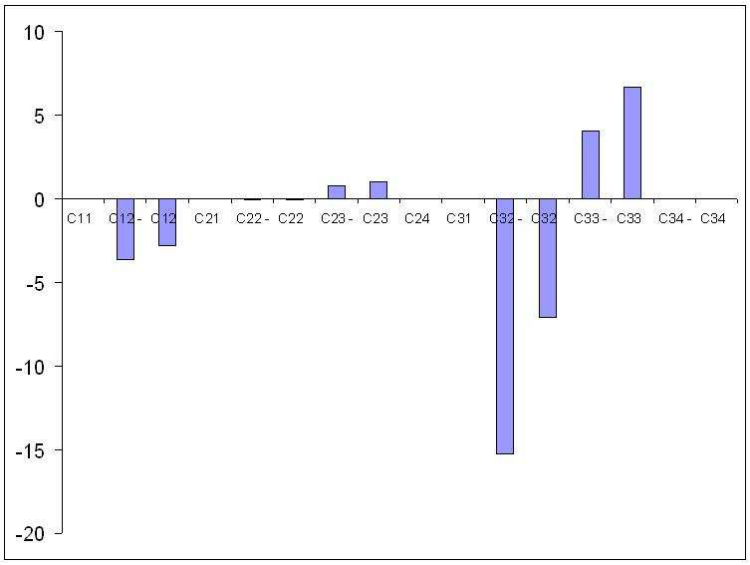

Figure 4.8: Sensitivity analysis of the cost model.

Chapter 5

COMBINED CYCLE PERFORMANCE PREDICTION

5.1 Introduction

A combined-cycle power plant has cycles with different working fluids that drive a synchronized generator. The plant efficiency of combined cycle is considerably larger than each cycle alone. The cycle operating at higher temperatures is called topping cycle. The waste heat produced by topping cycle is used in the second cycle that operates at lower temperature and therefore is named bottoming cycle. A combined gas and steam power plant consists of gas turbine, steam turbine, and a Heat Recovery Steam Generator (HRSG). The exhaust gas from gas turbine with a temperature ranging from 500^o-600^oC is used for steam production. Water from steam turbine enters HRSG economizer as a subcooled liquid. The water temperature is increased in the economizer until the liquid becomes saturated. At this point, the minimum temperature difference between the water in the steam cycle and the exhaust gas occurs and is called the "pinch point". Typical pinch point values are from 8^o to 15^oC. The saturated steam is superheated to the final temperature in the superheater

section. This steam is then expanded through the steam turbine and generates power. The stack gas temperature in HRSG is reduced to a temperature ranging from 80^o to 150^oC. The cycle thermal efficiency can reach up to 40% considerably larger than gas turbine efficiency with typical efficiencies of 35%.

The gas turbine used in this study is based on 184.5 MW power engine described in Chapter 3. The selection of HRSG configuration is the focus of this chapter. The configurations that have been considered include single-, dual-, and triple-pressure HRSG configurations. It is desirable that selected HRSG extracts maximum useful work for given exhaust gas conditions. However, the selected system needs to minimize number of heat exchanger units and reduce the construction cost [85]. In this chapter the steam turbine, HRSG, and gas turbine combined cycles are briefly described. The integration of 184.5 MW power engine with single-, dual-, and triple-pressure HRSGs is investigated. The cycle performance is also studied for operating conditions, where the ambient temperature changes.

5.2 Steam Turbine Cycle Modeling

The steam turbine main components are shown in Fig. 5.1 (a). Feedwater is pumped into the boiler where the heat is added to the water. In the boiler, water changes to superheated steam with typical temperature of 540^oC [86]. The mechanical work is extracted in turbine from boiler outlet steam to drive a shaft for electricity generation. The turbine exhaust is steam/water mixture which is cooled in the condenser. The steam turbine operates on the Rankine Cycle as shown in Fig. 5.1. In Fig. 5.1 (b) the process $1-2$ corresponds to the feeding pump, where the water is pressurized and sent to the boiler; process $2-3$ shows the heat addition in the boiler where the steam is generated; process $3-4$ is the steam expansion in the turbine, where the work is produced; and the process $4-1$ corresponds to the heat released in the condenser,

where the steam is condensed back to the water. The typical boiler in steam plant are water-tube types which help to increase the heat exchange area [87]. The feed-pump work is usually much smaller than turbine work and can be neglected in the performance calculations [88]. The thermodynamic equations of this cycle have been detailed in Chapter 2. Note that the operating temperatures in the steam cycle are much lower than those in gas turbines

The main steam cycle parameters are the live-steam pressure (boiler pressure), condenser pressure, and boiler outlet steam temperature. An increase in the boiler pressure raises the temperature at which evaporation occurs. This results in an increase in the average temperature heat added to the steam and hence improves the cycle efficiency [89]. The cycle performance is also improved by increasing the live steam temperature [90]. However, the maximum allowed boiler pressure and steam temperature are limited by the materials used in the boiler. Besides for a constant live steam temperature, the increased boiler pressure increases the moisture content in the turbine exit that causes major corrosion and erosion problems [91], while the acceptable moisture content is around 10% [28]. The boiler outlet steam is typically superheated dry steam, which its temperature changes the moisture content in the turbine exit, such that higher the steam temperature, the smaller the moisture content. The moisture content problem can be corrected using a reheat, in which the steam is partially expanded through a turbine section and then heat is added again to the steam before expanded in other turbine sections [70]. The lower condenser pressure also improved the cycle efficiency. The steam plant efficiency is defined as:

$$\eta_{st} = \frac{\dot{W}_{st}}{\dot{Q}_{boiler}} \tag{5.1}$$

where $\dot{W}_{st}$ is the power and $\dot{Q}_{boiler}$ is the heat transferred in the boiler. The typical efficiency values of steam plant are in the range of 30% to 40% [28].

5.3 Heat Recovery Steam Generator

A simple gas turbine discards most of the added heat into atmosphere with temperatures in range of 430 to 590^{o}C. These temperatures are higher than operating temperatures in the steam cycle and some of the wasted energy could be recovered in a heat recovery steam generator (often named waste-heat boiler), where heat is transferred from the gas turbine exhaust to water flowing in the tubes to generate steam in a combined cycle. Two typical HRSG types are unfired and supplementary-fired. In the unfired type, the heat of exhaust gas is used to raise steam in HRSG. Since, the gas exhaust temperature is smaller than flame temperature, the unfired HRSGs have less recovery efficiency and steam temperatures than supplementary-fired configurations [92]. In supplementary-fired HRSG, additional fuel can be sprayed into the exhaust stream to increase efficiency further and increase steam temperature to 850-900^oC [71]. HRSG can have multiple stages of steam pressures and temperatures; typical configurations are single-, dual-, and triple-pressure level configurations [93]. The pressure levels are named low pressure (LP), intermediate pressure (IP) and high pressure (HP) (Fig. 5.2), where, each pressure level consists of three heat exchangers or heating elements of economizer, evaporator, and superheater [94]. The feed water is first pre-heated in the economizer and then enters into a drum, where the water flows to the bottom. Heat is added to the water in the evaporator and the water/steam mixture returns to the drum, where the water and steam are separated. The saturated steam is then heated in the superheater where it reaches the live steam temperature [95]. The superhot steam is then expanded in the steam turbine for power generation.

The parts of a single-pressure HRSG are shown in Fig. 5.3. Also, Fig. 5.4 shows the temperature-heat diagram of a single-pressure HRSG. The temperature difference between gas exhaust stream and water/steam flow varies along the HRSG as shown

in Fig. 5.4. The minimum temperature difference is named pinch point, which is the difference between evaporator steam outlet temperature and the exhaust gas temperature at that physical location in the HRSG. A common range for pinch-point temperature is 8^o to 15^oC. Another important design parameter is approach point which is the temperature difference between the saturation temperature and the temperature of the leaving water in the economizer. The energy balance equations of HRSG are:

$$\dot{m}_g C_p(\mathrm{T}_1 - \mathrm{T}_3) = \dot{m}_w(h_a - h_c) \tag{5.2}$$

$$\dot{m}_g C_p(\mathrm{T}_3 - \mathrm{T}_4) = \dot{m}_w(h_d - h_e) \tag{5.3}$$

where C_p is the gas specific heat at constant pressure and can be estimated using Eqs. 2.44- 2.45; T_1 and T_4 are the inlet and outlet gas temperatures, respectively. $\dot{m}_g$ and $\dot{m}_w$ are the gas and steam mass flow rates; h_a is the steam enthalpy at superheat exit, h_c is the saturated water enthalpy in the evaporator, h_d is the water enthalpy in the economizer exit, and h_e is the feedwater enthalpy. It should be noted that the heat transfer between approach and pinch points are assumed small and neglected in the above equations. The HRSG efficiency is then defined as:

$$\eta_{\mathrm{HRSG}} = \frac{\mathrm{T}_1 - \mathrm{T}_4}{\mathrm{T}_1 - \mathrm{T}_{air}} \tag{5.4}$$

where T_{air} is ambient temperature. The outlet gas temperature (stack temperature) has direct effects into the HRSG efficiency, because it shows the amount of wasted heat, therefore, it is essential to reduce stack temperature to increase the cycle efficiency. The stack temperature of single-pressure HRSG is typically high and hence it produces low efficiencies. The stack temperature can be decreased by using a multiple-pressure steam generator, although this adds to the initial cost [96]. A

steam turbine connected to a modern gas turbine using a single-pressure HRSG can produce up to 25% of total power of plant, while this ratio increases another 10% by using dual-pressure HRSG, and a 3% additional increase might be obtained using triple-pressure HRSG [97]. Nowadays, multiple-pressure steam generator are used to improve efficiency. The temperature-heat and temperature-entropy diagrams of a dual-pressure HRSG are also shown in Fig. 5.5.

5.4 Combined Cycle Modeling

The combination of a gas turbine with air as working fluid and a steam turbine with water as working fluid offers cycles with higher efficiencies and power compared with single cycle alone as shown in Fig. 5.6. Nowadays, advanced combined cycles with multiple-pressure steam generator could reach thermal efficiency up to 58% [44, 98]. According to Sanjay [99] the use of combined cycles for power generation will increase from 570 GW in 1999 to 2935 GW in 2020. In a gas/steam cycle, the hot exhaust gases from gas turbine are used to produce high-pressure steam in the steam plant as shown in Fig.5.7. Therefore, such a cycle provides power with less environmental pollution compared with conventional coal-fired steam turbine plants. In particular, the need to reduce the greenhouse gases has made combined cycle power plants a promising choice to produce energy because of their high efficiency and the use of low-carbon fuels [44]. Petchers [100] and Colpier and Corlando [101] detailed advantages of combined cycles compared to conventional oil, coal and nuclear plants as:

- High thermal efficiency,
- Low emissions,
- Low capital cost and construction times,
- Lower risk,

- Fast start-up,

- Small space requirements than for equivalent coal or nuclear stations.

While a gas turbine performance is improved at high temperature region, a steam turbine cycle has a good performance at low temperature region [102]. Therefore, the combination of the gas and steam turbines using heat recovery steam generator benefits from the high-temperature and low-temperature parts of both cycles. The combined cycle performance depends on the performance of all its systems: gas turbine, HRSG, and steam turbine. The gas turbine performance in a simple cycle could be optimized by selecting the best compressor pressure ratio and turbine entry temperature. However, an optimum gas turbine for simple cycle is different from an optimum gas turbine for a combined cycle [25]. The steam turbine performance could be optimized by selecting the best boiler pressure, condenser pressure, and boiler outlet steam temperature for given steam mass flow rate. However, in a combined cycle, the steam mass flow rate is determined from the HRSG performance. Higher the steam pressure in HRSG, the smaller steam mass flow rate [28]. The efficiency of a combined cycle performance should be improved by optimizing the interactions between gas and steam sections. This is a very complex task because combined cycle parameters are interdependent [103] and any changes in design parameters of each cycle affects the overall power and efficiency [104]. The combined cycle efficiency is defined as:

$$\eta_{cc} = \eta_{gt} \times (\dot{W}_{gt} + \dot{W}_{st})/\dot{W}_{gt} \tag{5.5}$$

where η_{gt} is the gas turbine thermal efficiency; $\dot{W}_{gt}$ and $\dot{W}_{st}$ are gas turbine and steam turbine output power, respectively.

5.5 Analysis

Careful consideration is required in order to select the gas turbine for a combined cycle power plant. For example, single-pressure-level HRSGs are preferred for gas turbine engines with power less than 100 MW [76]. Large size gas turbines have been used in combined cycles with two-pressure-level HRSG. A three-pressure-level HRSG is efficient with very large size engines as well [76]. The effects of HRSG type into combined cycle performance using a 184.5 MW power engine is detailed below.

5.5.1 Single-Pressure HRSG Combined Power Plant

Design-Point Performance

A gas/steam combined cycle with a single-pressure HRSG shown in Fig. 5.4 is considered. The operating parameters of the cycle are summarized in Table 5.1. The topping cycle used in this work is a 184MW gas turbine described in the Chapter 3. The gas turbine at design point conditions has a compressor pressure ratio of 16.9, turbine inlet temperature of 1394^{o}K, and exhaust mass flow rate of 565 kg/s. The steam (bottoming) plant has a condenser pressure of 0.05 bar. For a single-pressure HRSG, the steam is generated in a pressure of 70 bar. The pinch and approach temperatures at design conditions are 10^oC and 5^oC, respectively. The live steam temperature is determined using a superheat pinch temperature, which is the difference between the gas inlet temperature and the live steam temperature:

$$\mathrm{T}_a = \mathrm{T}_1 - \Delta\mathrm{T}_{sh} \tag{5.6}$$

where T_a is the live-steam temperature; T_1 is the gas turbine exhaust temperature; and $\Delta\mathrm{T}_{sh}$ is the superheat pinch temperature and is assumed 20^oC.

The Tera code first determines the saturation temperature of $\mathrm{T}_s(p)$ at given boiler

Table 5.1: Single-pressure HRSG design parameters.

Parameter	Value	Parameter	Value
Compressor PR	16.9	Superheat pinch temperature, ^{o}C	20
Turbine entry temperature, ^{o}K	1394	Pinch temperature, ^{o}C	10
Gas turbine mass flow rate, kg/s	556	Approach temperature, ^{o}C	5
Boiler pressure, bar	70	Steam turbine efficiency, %	90
Condenser pressure, bar	0.05		

pressure of $P = 70$ bar using the Mollier Diagram. This temperature is $\mathrm{T}_s(p) = 285.8^oC$. From assumed pinch point temperature difference of $\Delta\mathrm{T}_p = 10^oC$, the pinch point on the gas side is:

$$\mathrm{T}_3 = \mathrm{T}_s(p) + \Delta\mathrm{T}_p = 295.8^oC \tag{5.7}$$

The gas turbine exhaust temperature (T_1) is 506.7^oC, therefore, the heat transferred above the pinch is:

$$\dot{Q}_{1-3} = C_p\dot{m}_g(\mathrm{T}_1 - \mathrm{T}_3) = 119kj/s \tag{5.8}$$

where C_p is the gas specific heat at constant pressure and $\dot{m}_g = 556kg/s$ is gas turbine exhaust mass flow rate. This amount of heat is captured by the water/steam circuit in the evaporator and superheater sections. The live steam temperature (T_a) is 486^oC from Eq. 5.6. The water mass flow $\dot{m}_w$ is then determined as:

$$\dot{m}_w = \frac{\dot{Q}_{1-3}}{h_a - h_c} = 55.9kg/s \tag{5.9}$$

where h denotes water enthalpy value. The heat transferred below the pinch is given by the water side energy balance as:

$$\dot{Q}_{3-4} = \dot{Q}_{e-d} = \dot{m}_w \times (h_d - h_e) \tag{5.10}$$

where e subscript denotes feedwater and d subscript corresponds to the approach point temperature and can be found as:

$$\mathrm{T}_d = \mathrm{T}_c + \Delta\mathrm{T}_a = 280.5^oC \tag{5.11}$$

The stack temperature of T_4 can be calculated as

$$\mathrm{T}_4 = \mathrm{T}_3 - \frac{\dot{Q}_{3-4}}{C_p \times \dot{m}_g} = 184.4^oC \tag{5.12}$$

The HRSG data are then used to find the steam plant performance data including thermal efficiency and output power. The VariFlow code also reports the engine performance data. The combined cycle power is then found by adding the powers from both cycles. The thermal efficiency is also found from Eq. 5.5. The overall performance predictions are summarized in Table 5.2 which shows combined cycle has an efficiency of 52.7% higher than each single cycle alone. The single-pressure HRSG has quite high stack temperature of 184^oC. Another issue is the relatively high moisture content in the turbine exit which is around 15%. Figure 5.8 also shows the temperature-heat diagram of HRSG at standard ambient temperature and gas turbine operating at design point conditions.

Table 5.2: Single-pressure HRSG performance prediction .

Parameter	Value	Parameter	Value
GT power, MW	184.0	CC power, MW	250
GT efficiency, %	37.9	Stack temperature, ^{o}C	184
GT exhaust temperature ,^{o}K	506	CC efficiency, %	52.7
Steam power, MW	66	Steam quality, %	85
Steam efficiency, %	36.3		

Design Point Diagrams

According to Horlock [26], the optimum pressure ratio for a combined cycle is different from a simple gas turbine cycle. Figure 5.9 shows the typical trends of plant efficiencies with pressure ratio changes. The optimum pressure ratio that maximizes combined cycle efficiency is relatively smaller than of a simple gas turbine cycle as shown in Fig.5.9. This optimum pressure ratio also changes with maximum temperature and HRSG operating conditions. In this section, the combined cycle with a single-pressure level HRSG has been studied parametrically to find the maximum output and efficiency.

Design point diagrams are first created by plotting combined cycle performance parameters of thermal efficiency and output power versus the changes in gas turbine compressor pressure ratio and turbine inlet temperature and shown in Fig. 5.10. Figure. 5.10(a) shows that combined cycle efficiency is substantially larger than gas turbine efficiencies. There is an optimum pressure ratio value that maximizes the efficiency for each TET value, such that, the optimum pressure ratio increases with turbine entry temperature as shown in Fig. 5.10(a). This figure also shows that the optimum efficiency of a combined cycle occurs at lower pressure ratio values compared with the gas turbine. Increasing the compressor pressure ratio leads in a fall in exhaust temperature as shown in Fig. 3.7 (b). Therefore, the live steam temperature will be lowered and hence the steam cycle and combined cycle efficiencies. Figure. 5.10(b) shows that increasing compressor pressure ratio results in a fall in the combined cycle power as well.

Figure. 5.11 shows the changes in HRSG cycle efficiency with compressor pressure ratio and turbine inlet temperature, such that the HRSG efficiency significantly falls with increasing pressure ratio. The lower turbine entry temperature also results in lower HRSG efficiency as shown in Fig. 5.11. Increasing the compressor pressure ratio leads in a fall in exhaust temperature (T_1) and hence the HRSG efficiency is

reduced using Eq. 5.4. A lower gas temperature flowing in the HRSG reduces the heat transferred to water/steam and hence smaller steam mass flow rate is needed for constant boiler pressure. The effects of compressor pressure ratio and turbine inlet temperature into steam mass flow rate are shown in Fig. 5.12. In this figure, the boiler pressure is constant. Figure. 5.13 also shows the effects of compressor pressure ratio and turbine inlet temperature into the steam quality and gas temperature difference in HRSG. The steam quality falls with increasing pressure ratio as shown in Fig. 5.13 (a). Again, an increased pressure ratio flows lower temperature exhaust gases into HRSG and therefore the live-steam temperature will be lower. The lower live-steam temperature for a constant boiler pressure results in a lower steam quality (or increased moisture content). Fig. 5.13 (b) also shows the gas temperature difference in HRSG falls with increasing compressor ratio because a higher pressure ratio results in a lower exhaust gas temperature.

Increasing the boiler pressure raises the saturation temperature of $T_s(p)$ as shown in Fig. 5.14. The heat transferred in HRSG is smaller for larger boiler pressure cycles, therefore the steam mass flow rate is smaller using Eq. 5.9. The sensitivity diagram of combined cycle efficiency with boiler pressure is shown in Fig. 5.15 (a) for two different turbine inlet temperature values. Figure 5.15 (a) shows the combined cycle efficiency increases with boiler pressure for high TET values. For lower TET, there is an optimum boiler pressure that maximizes the combined cycle efficiency. Note that gas turbine efficiency is larger for higher TET, the steam cycle efficiency is also increased with TET, because it produces higher live-steam temperature values. Figure 5.15 (b) shows that steam quality gets worsen for larger boiler pressure values. The gas temperature difference is also smaller for larger boiler pressure values as shown in Fig. 5.15 (c). This is because heat transferred in HRSG become smaller as boiler pressure increases.

The sensitivity diagram of combined cycle efficiency with condenser pressure is also

shown in Fig. 5.16 (a). The combined cycle efficiency falls with increasing condenser pressure for both selected TET values. Fig. 5.16 (b) shows that as condenser pressure increases, the steam turbine power falls and hence the efficiency, however the steam quality is improved by increasing condenser pressure as shown in Fig. 5.16 (c).

A large pinch point temperature reduces the heat transferred in the HRSG and steam mass flow rate, but increases the stack gas temperature as shown in Fig. 5.17. The cycle efficiency, power, and the steam quality change with pinch temperature are shown in Fig. 5.18. The cycle efficiency falls with larger pinch temperature as gas turbine stack temperature is higher for a large pinch temperature value. The power slightly becomes smaller with pinch temperature as shown in Fig. 5.18 (b). The gas temperature difference between inlet and outlet to HRSG falls with large pinch temperature as shown in Fig. 5.18 (c).

Operating Performance

It is assumed now that design parameters (compressor pressure ratio, turbine inlet temperature, boiler pressure, steam mass flow rate, and etc.) are fixed and then ambient temperature changes. The results of Chapter 3 showed that gas turbine efficiency and power decreases at hotter temperatures. The gas turbine exhaust temperature also increases with ambient temperature. The Tera code again used to study the combined cycle operating performance. The ambient temperature range is from -10 to 40^oC. In design point study, the live steam temperature is found from the supreheat approach temperature and the gas turbine exhaust temperature. The mass flow rate is then estimated from the heat transferred in the evaporator and superheater. In operating performance modeling the steam mass flow rate is fixed from design conditions and the live steam temperature is estimated as:

$$h_a = h_d + \frac{\dot{Q}_{1-3}}{\dot{m}_s} \tag{5.13}$$

where $h - a$ shows the enthalpy of steam exit from HRSG. Given the boiler pressure and calculated the enthalpy, the steam exit temperature can be found from the Mollier Diagram. The cycle efficiencies with ambient temperature are shown in Fig. 5.19. This shows that gas turbine efficiency falls at hotter temperatures, but the steam plant efficiency is nearly unchanged with ambient temperature. Note that the boiler pressure and steam mass flow rate are fixed; the live-steam temperature slightly changes because of the gas turbine exhaust changes. The live-steam temperature changes are small and therefore there is no considerable effects into steam plant efficiency. The combined cycle efficiency therefore falls because of smaller gas turbine efficiency. The steam turbine power is unchanged with ambient condition for the assumptions made here but gas turbine power falls because the gas mass flow rate decreases at hotter temperatures. Therefore, the combined cycle power is reduced as well as shown in Fig. 5.20. The HRSG temperature-heat transfer diagram changes with two ambient temperatures is shown in Fig. 5.21. The heat transferred to water/steam is smaller at hot temperatures; this is because the gas mass flow rate is smaller at hot temperatures. Although, the gas turbine exhaust is higher for hot temperatures, but because of fixed steam mass flow rate and lower heat transferred, the live-steam temperature becomes smaller. Note that the saturation temperature is fixed by constant boiler pressure. Figure 5.21 shows that the hot temperatures helps to a more reduced stack gas temperature which improves HRSG cycle efficiency but this is compensated by the fall in gas turbine efficiency. The hot temperature causes the smaller live-steam temperature (again because the heat transferred is smaller for a fixed steam mass flow rate and saturation temperature). The lower live-steam temperature makes the steam quality worsen as shown in Fig. 5.22.

5.5.2 Dual-Pressure HRSG Combined Power Plant

In this section, a dual-pressure-level HRSG is combined with a steam turbine and the 184.5MW-power gas turbine described in Chapter 3. The gas turbine exhaust has a mass flow rate of 565 kg/s at a temperature of 506^{o}C at design-point conditions. The exhaust gas enters the HRSG, where heat is transferred to water in steam turbine and super-hot steam is generated. In a dual-pressure HRSG high pressure (HP) and low pressure (LP) super hot steams are generated. These hot steams are expanded in HP and LP turbines with an isentropic efficiency equal to 0.9. The operating pressures for HP and LP steam turbines are 70 bar and 3.89 bar, respectively. After turbines, the steam/water mixture is condensed back to the water at a pressure of 0.05 bar. The pinch and approach temperature differences are assumed to be $\Delta T_p = 10^o$C and $\Delta T_p = 5^o$C. Table 5.3 summarizes gas and steam conditions for the combined cycle as well.

Table 5.3: Dual-pressure HRSG design parameters.

Parameter	Value	Parameter	Value
Compressor PR	16.9	Superheat pinch temperature, ^{o}C	20
Turbine entry temperature, ^{o}K	1394	Pinch temperature, ^{o}C	10
Gas turbine mass flow rate, kg/s	556	Approach temperature, ^{o}C	5
HP pressure, bar	70	Condenser pressure, bar	0.05
LP pressure, bar	3.89	Steam turbine efficiency	90%

In a dual-pressure HRSG, the water flows in HP and LP heat exchangers. Each heat exchanger consists of an economizer, an evaporator, and a superheater. Steam turbine power output of a dual-pressure HRSG is then calculated as:

$$\dot{W}_{st} = \dot{m}_{HP}\Delta h_{HP} + \dot{m}_{LP}\Delta h_{LP} \tag{5.14}$$

where $\dot{m}_{HP}$ and $\dot{m}_{LP}$ denote HP and LP steam mass flow rates. Tera code predicts the

gas and steam/water conditions at each stage of combined cycle. The cycle power and efficiency are then calculated from these predictions. The performance predictions of a dual-pressure HRSG combined with the 184.5MW power gas turbine are given in Table 5.4. It is shown that stack gas temperature has fallen to a temperature around 86^{o}C significantly lower than temperature in single-pressure HRSG. The combined cycle has an output power of 263 MW, slightly larger than combined cycle with a single-pressure HRSG. The steam quality (this is defined as 100%-moisture content (%)) at the exit of HP and LP turbine sections is 100% and 85.15%

Table 5.4: Dual-pressure HRSG performance prediction.

Parameter	Value	Parameter	Value
GT power, MW	184.0	CC power, MW	263
GT efficiency, %	37.9	Stack temperature, ^{o}C	86.42
GT exhaust temperature ,^{o}K	506	CC efficiency, %	54.41
HP turbine power, MW	35.85	HP Steam quality, %	100
LP turbine power, MW	43.90	LP Steam quality, %	85.15
HP steam mass flow rate, kg/s	56.6		
LP steam mass flow rate, kg/s	19.1		

Figue 5.23 compares the effects of compressor pressure ratio into combined cycle powers and efficiencies of a single- and dual-pressure HRSG. Figue 5.23 shows that the a dual-pressure HRSG combined with the 184.5MW-power gas turbine aid in to improve the efficiency and power compared with a single-pressure HRSG. The differences between HRSGs become larger for engines with high compressor pressure ratio. For engines with small pressure ratio values, the single-pressure HRSG has better performance than dual-pressure HRSG as shown in Fig. 5.23. It should be noted that the cost of dual-pressure HRSG is higher than single-pressure HRSG since a dual-pressure HRSG has more heat exchangers.

Figure 5.15 (a) shows that for small TET, there is an optimum boiler pressure that maximizes the combined cycle efficiency using a single-pressure HRSG. The effects of

high pressure into combined cycle efficiency are also shown in Fig. 5.24. The efficiency of a dual-pressure HRSG increases with HP pressure rise.

Finally, the operating performance a dual-pressure HRSG is studied and shown in Fig. 5.25. The ambient temperature range is from -10 to 40^oC. Figure 5.25 shows that efficiency and power of combined cycle with a dual-pressure HRSG falls at hotter temperatures in a similar trend of a combined cycle with a single-pressure HRSG.

5.5.3 Triple-Pressure HRSG Combined Power Plant

Finally, the performance of a triple-pressure combined cycle is studied. The gas turbine again has 184.5 MW output power with an exhaust mass flow rate of 565 kg/s at a temperature of 506^oC at design-point conditions. The power in steam turbine is produced from high-pressure, intermediate-pressure, and low-pressure turbine sections. The operating pressures for HP, IP, and LP steam turbines are 70 bar, 10 bar, and 3.89 bar, respectively. Table 5.5 detail gas and steam conditions for the combined cycle as well as the performance data. Table 5.5 shows that combined cycle efficiency and power are not much changed compare to a dual-pressure combined cycle. Figure 5.26 also shows the effects of pressure ratio into combined cycle efficiency. Again, the improvements from dual-pressure to triple-pressure combined cycle are very small for small to moderate pressure ratio values. From these comparisons, it was decided to use a dual-pressure combined cycle that has improved efficiency and power compared with single-pressure cycles and has less initial cost compared with triple-pressure cycle.

5.6 Conclusions

The results showed that combined cycles has much higher overall efficiency than simple gas turbine. The stack gas temperature by using a single-pressure HRSG

Table 5.5: Triple-pressure HRSG performance prediction .

Parameter	Value	Parameter	Value
GT power, MW	184.0	CC power, MW	265.5
GT efficiency, %	37.9	Stack temperature, ^{o}C	86.2
GT exhaust temperature ,^{o}K	506	CC efficiency, %	54.8
HP pressure, bar	70	HP steam mass flow rate, kg/s	56.6
IP pressure, bar	10	IP steam mass flow rate, kg/s	14.88
LP pressure, bar	3.89	LP steam mass flow rate, kg/s	4.47

is quite high (around 184^{o}C). This temperature falls below 87^oC by using a dual-pressure HRSG and hence that significantly improve the combined cycle efficiency. A three-pressure HRSG result in comparatively little efficiency improvements compared with dual-pressure HRSG and is larger and has more expensive heat exchangers. The finding showed the best HRSG type selection to combine the 184.5MW gas turbine with steam turbine is a dual-pressure HRSG. The design-point diagrams showed that the optimum pressure ratio of combined cycles are much smaller than simple gas turbine cycles. The optimum pressure ratio increases with turbine entry temperature for both cycles.

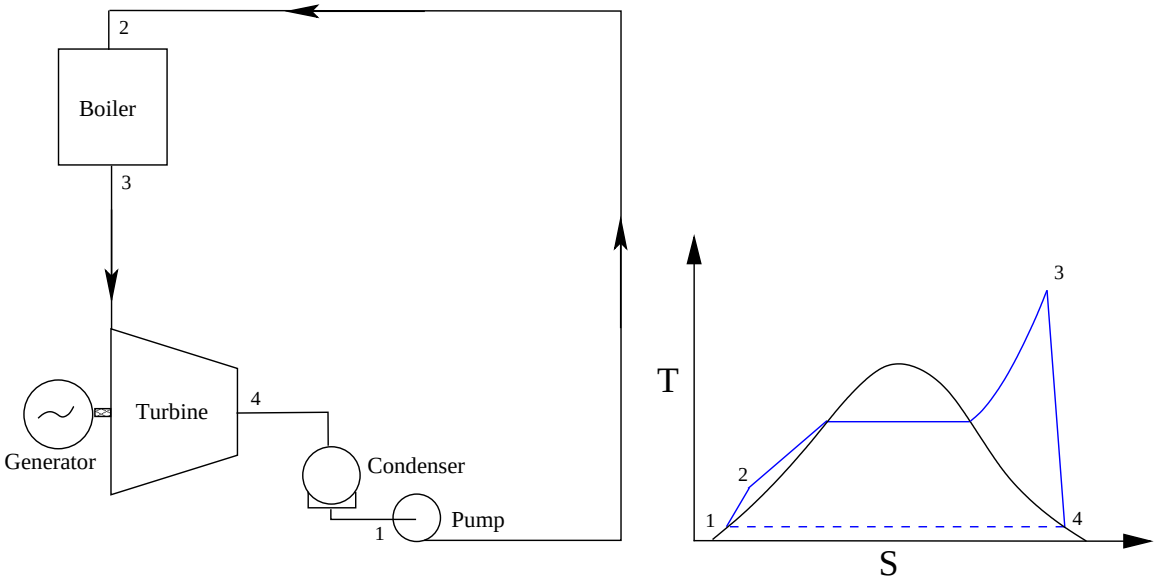

(a) Steam Turbine (b) T−S Diagram

Figure 5.1: Steam turbine components and temperature-entropy diagram.

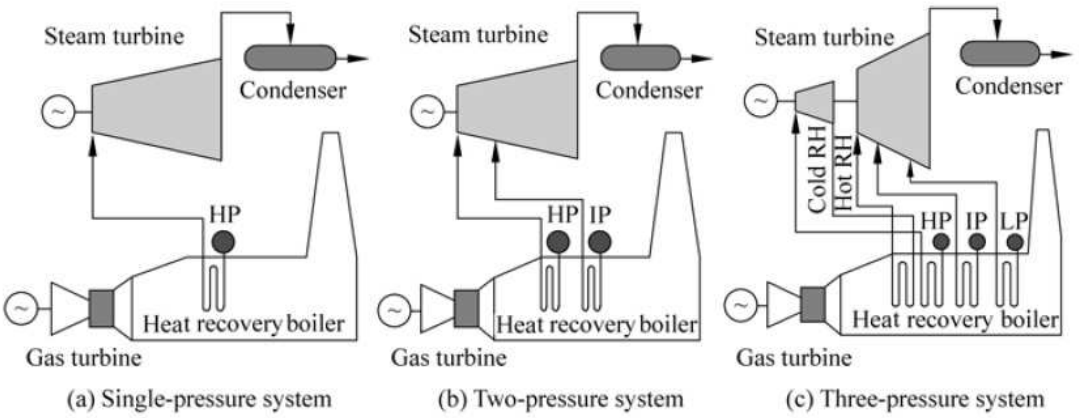

Figure 5.2: HRSG Types (Xiaotao et al, 2005).

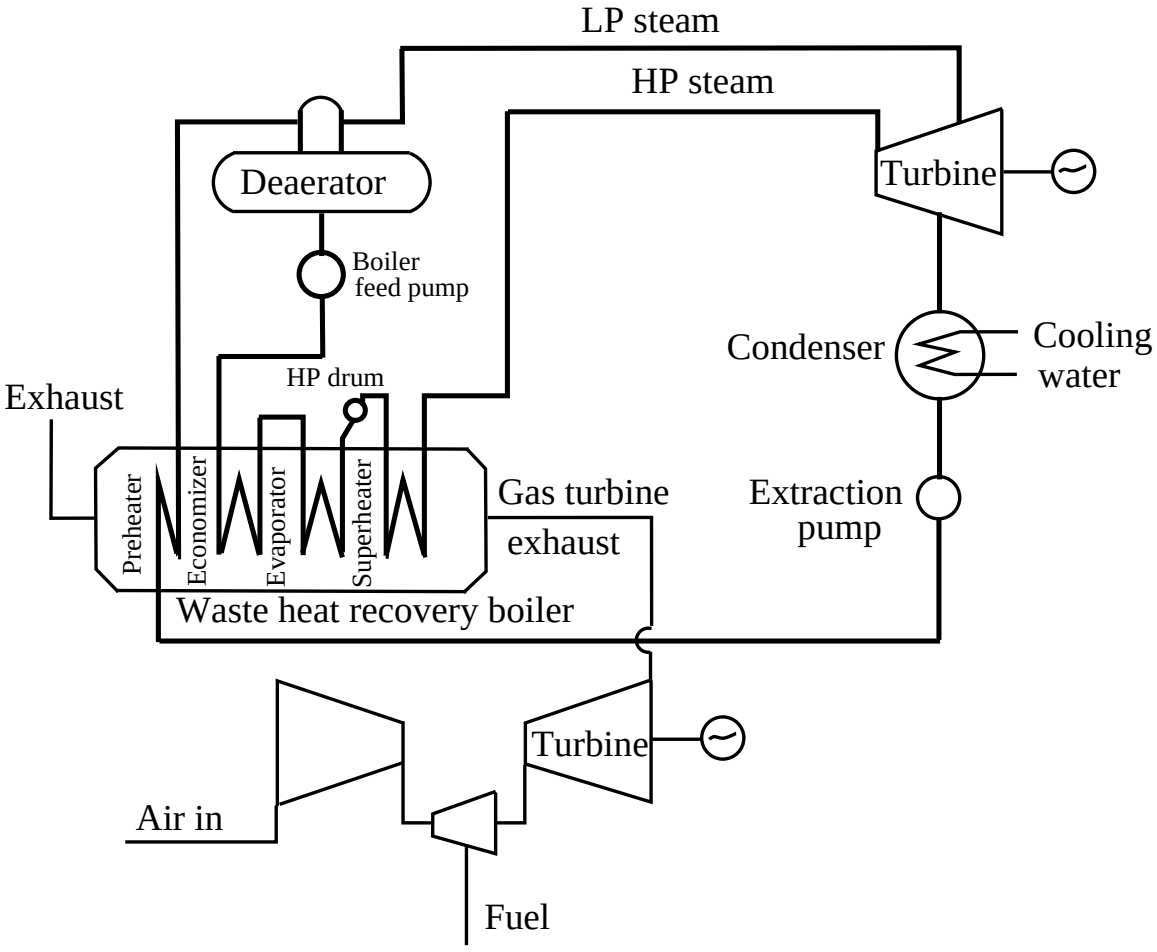

Figure 5.3: Single-pressure HRSG components.

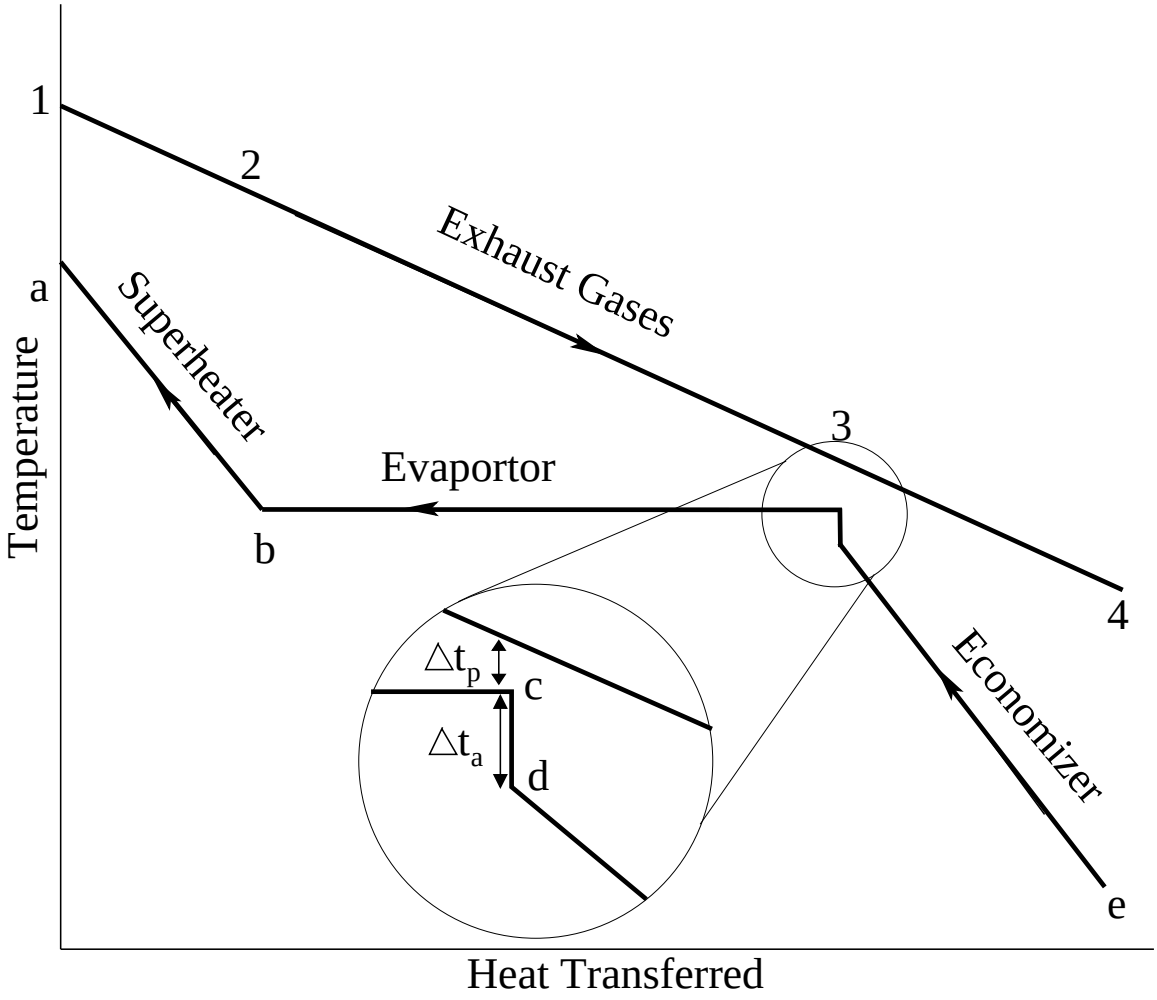

Figure 5.4: Single-pressure HRSG thermodynamic model.

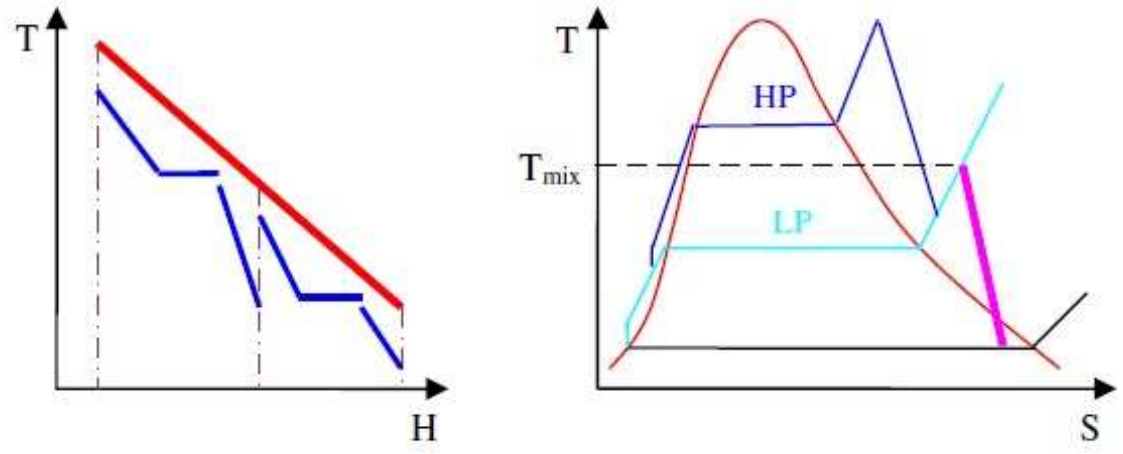

Figure 5.5: Dual-pressure HRSG thermodynamic model (Mohagheghi and Shayegan, 2009).

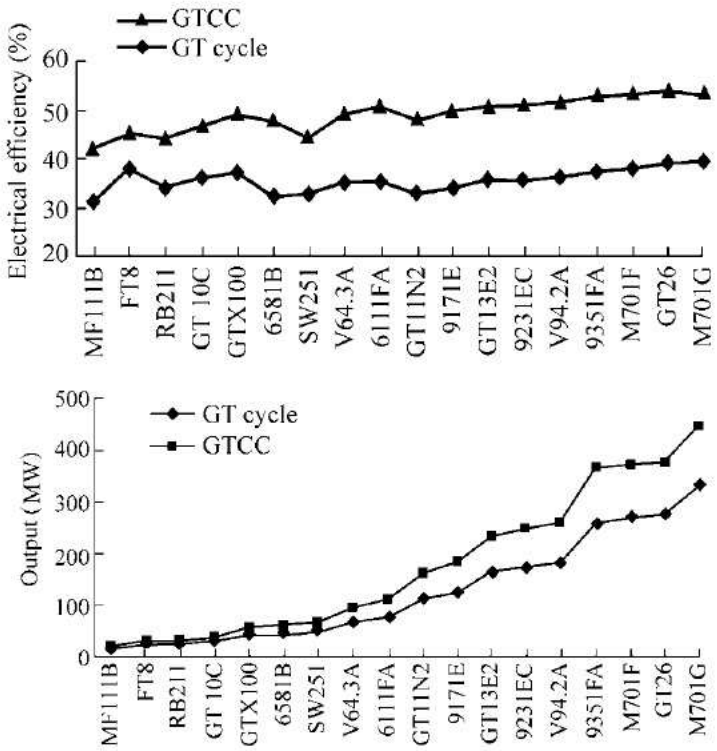

Figure 5.6: Comparison of gas turbine and gas turbine combined cycle performance (Xiaotao et al, 2005).

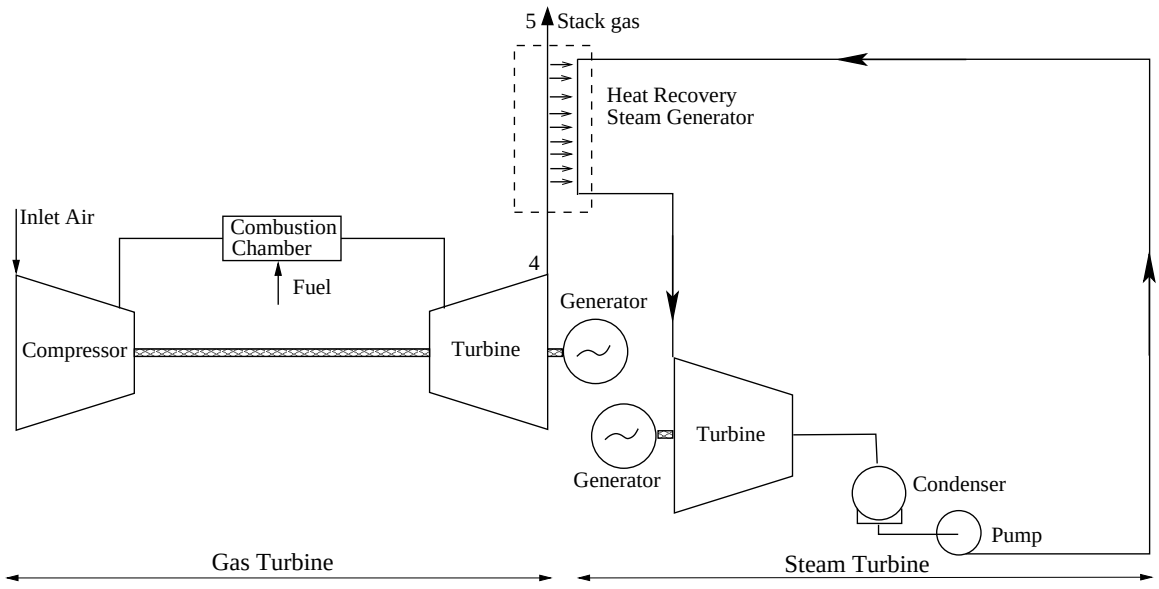

Figure 5.7: Combined gas and steam turbine cycle power plant.

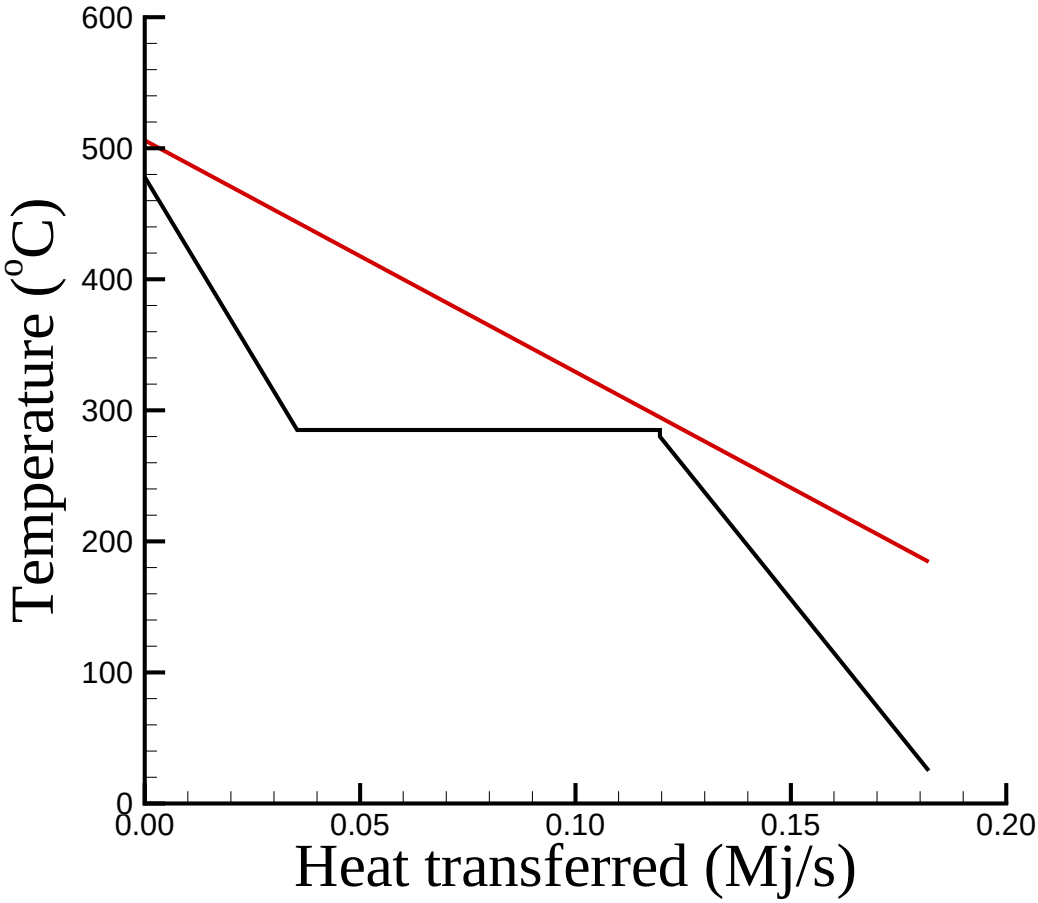

Figure 5.8: Single-pressure HRSG temperature-heat diagram at standard ambient temperature.

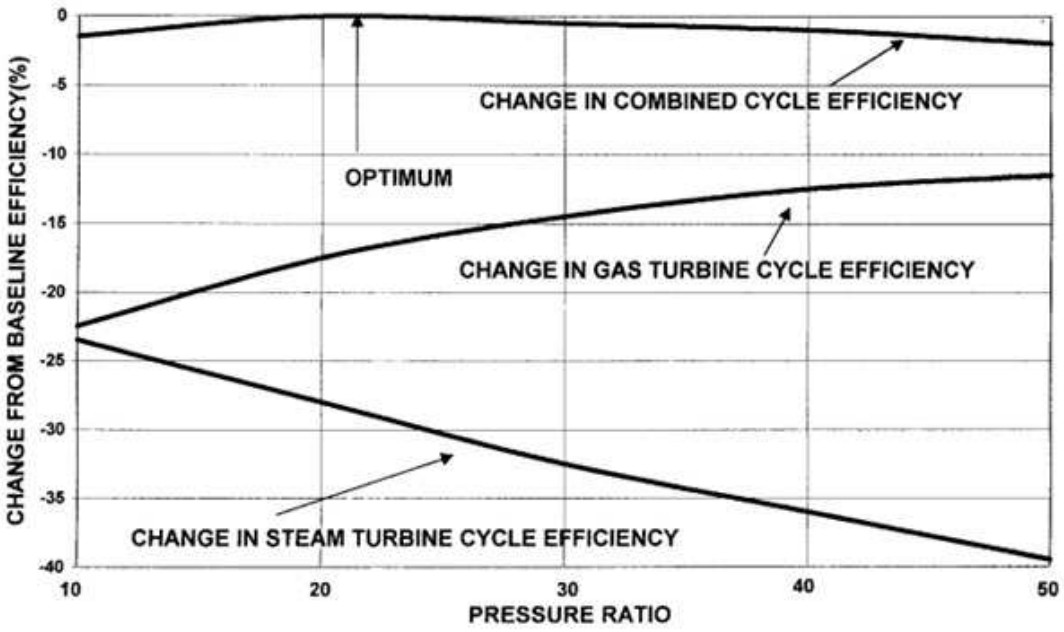

Figure 5.9: Effects of compressor pressure ratio changes into efficiency of gas turbine, steam turbine, and combined cycle (Horlock, 2003).

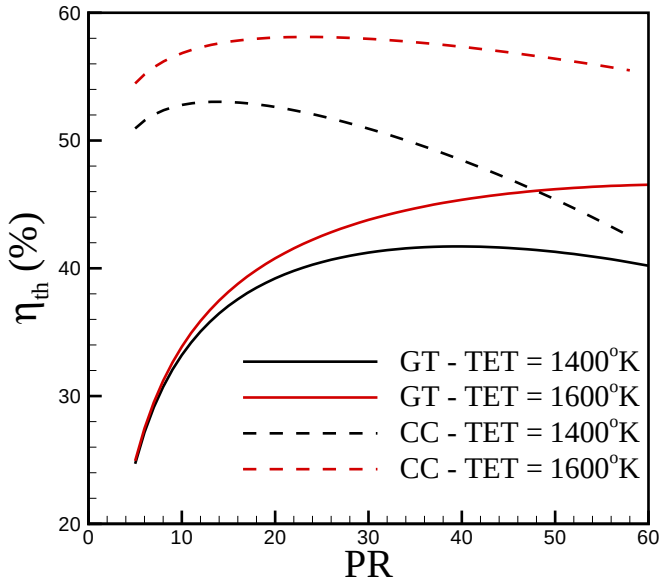

(a) Thermal efficiency

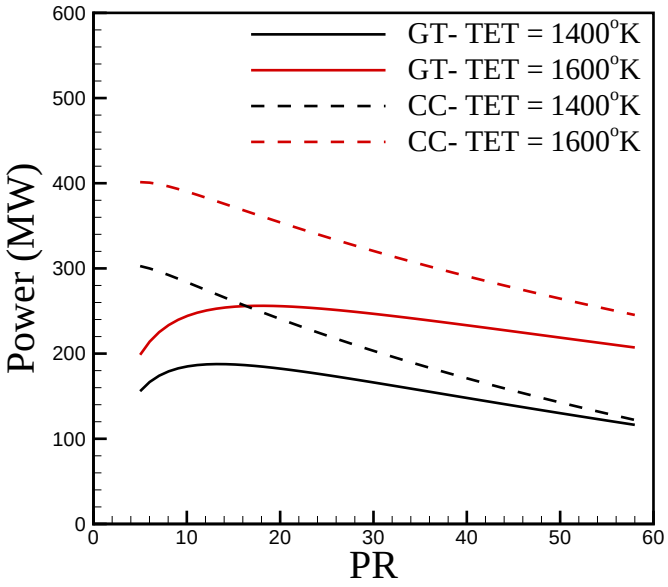

(b) Power

Figure 5.10: Thermal efficiency and power design diagrams of simple and combined gas turbines- The combined cycle consists of a single-pressure HRSG.

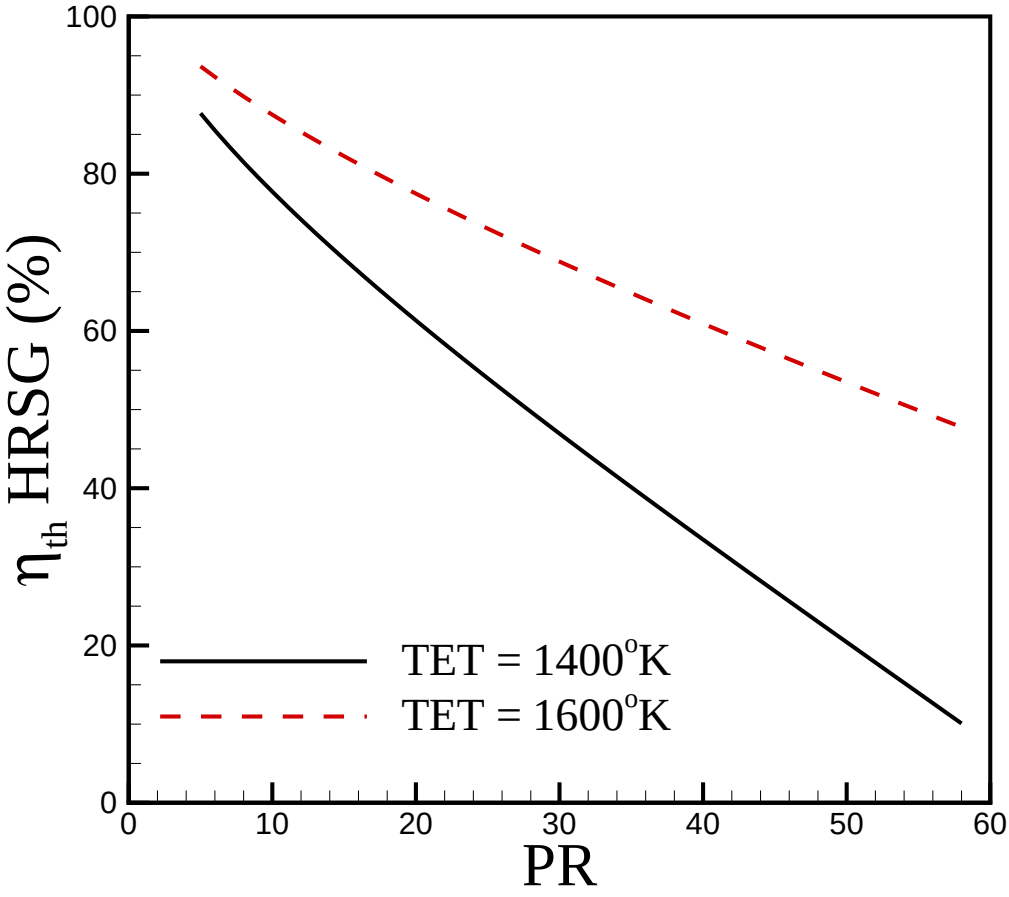

Figure 5.11: Single-pressure HRSG efficiency changes with compressor pressure ratio.

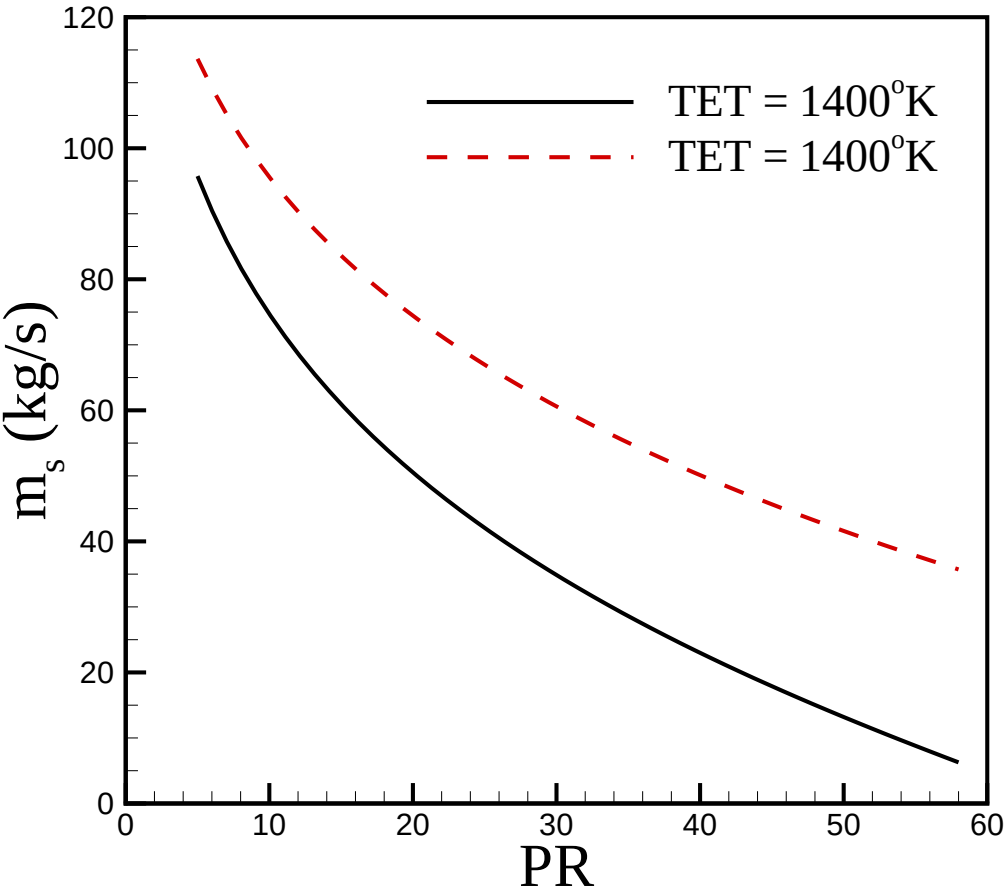

Figure 5.12: Steam mass flow rate changes with compressor pressure ratio. The combined cycle consists of a single-pressure HRSG.

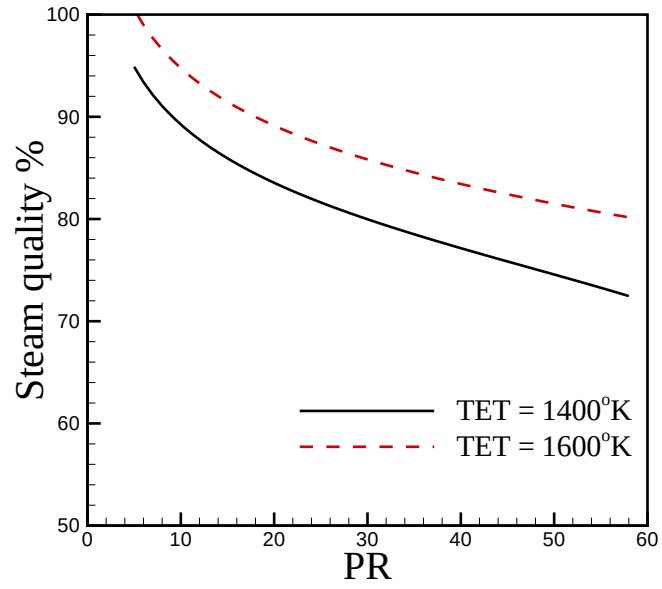

(a) Steam quality

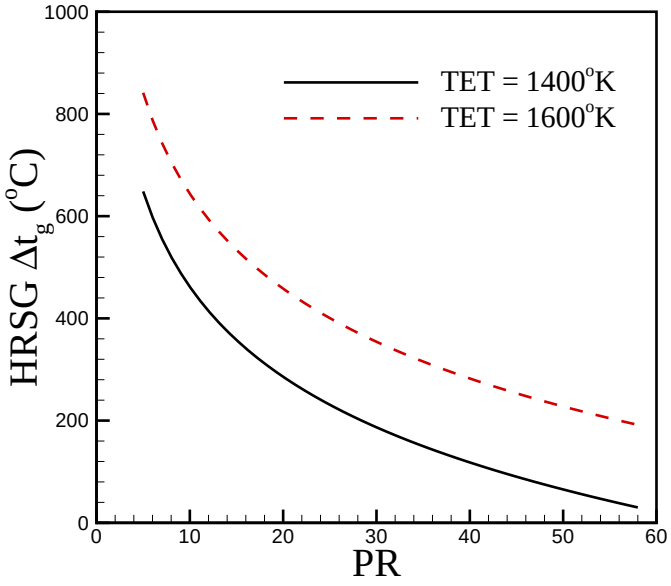

(b) HRSG gat temperature difference

Figure 5.13: Steam quality and gas temperature difference design diagrams with compressor pressure ratio- The combined cycle consists of a single-pressure HRSG.

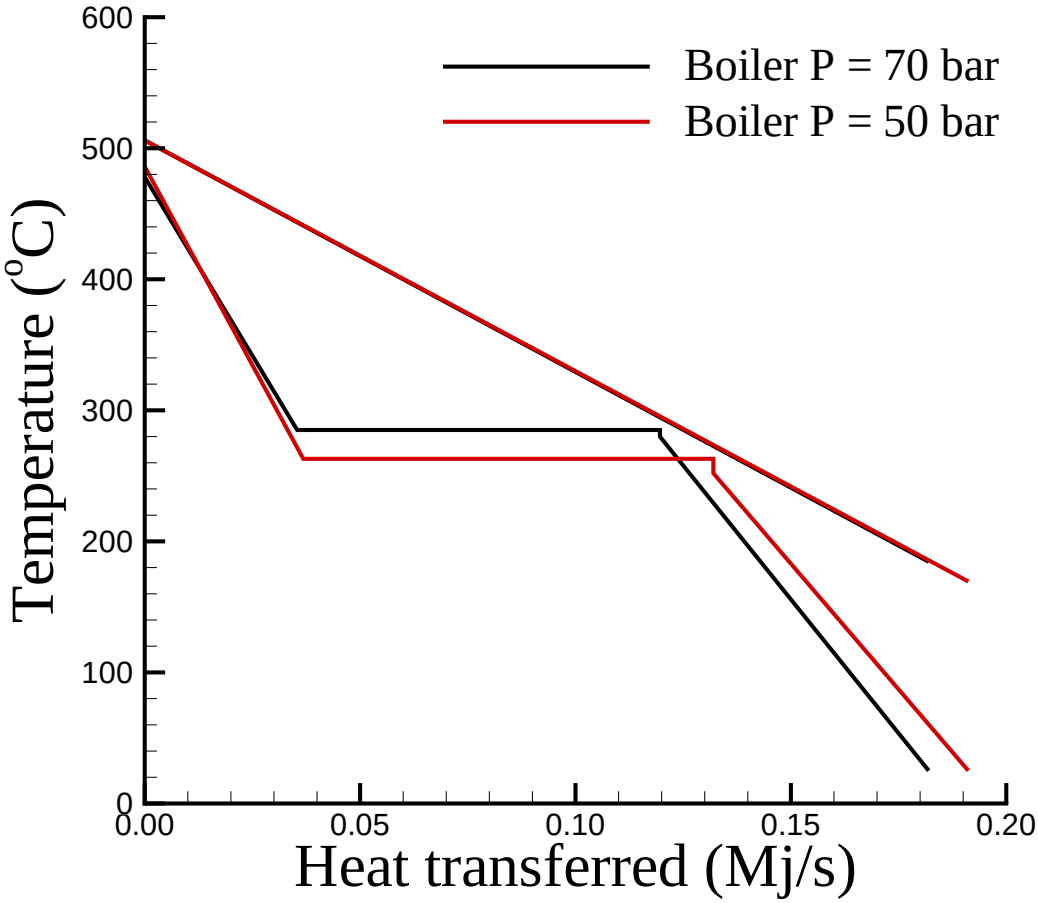

Figure 5.14: Single-pressure HRSG temperature-heat diagram changes with boiler pressure.

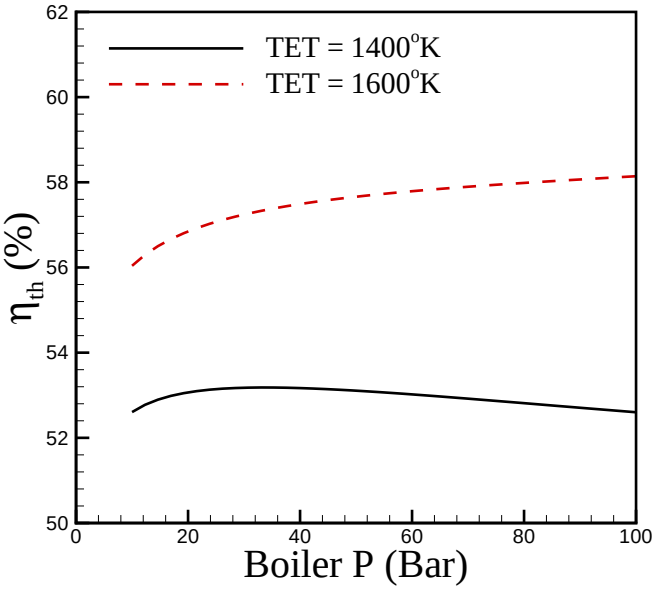

(a) Efficiency

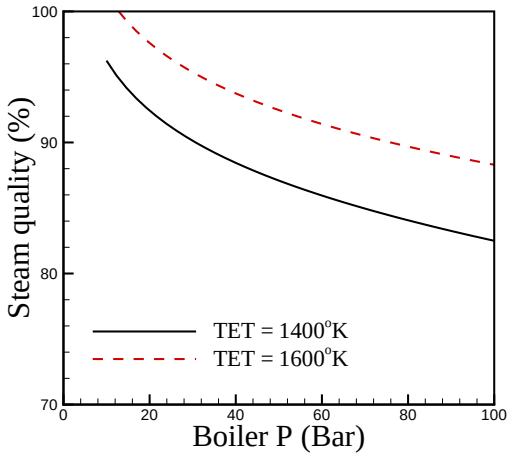

(b) Steam quality

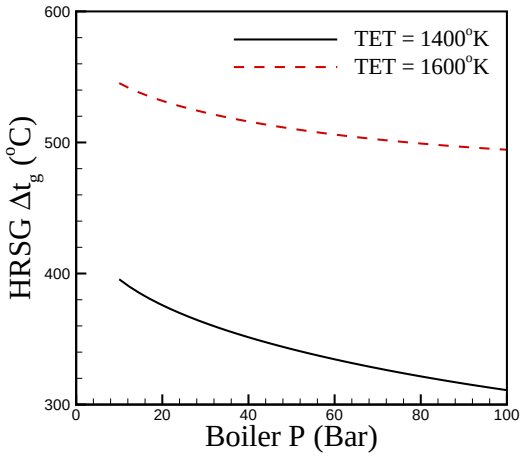

(c) HRSG gat temperature difference

Figure 5.15: Combined cycle design diagrams with boiler pressure- The combined cycle consists of a single-pressure HRSG.

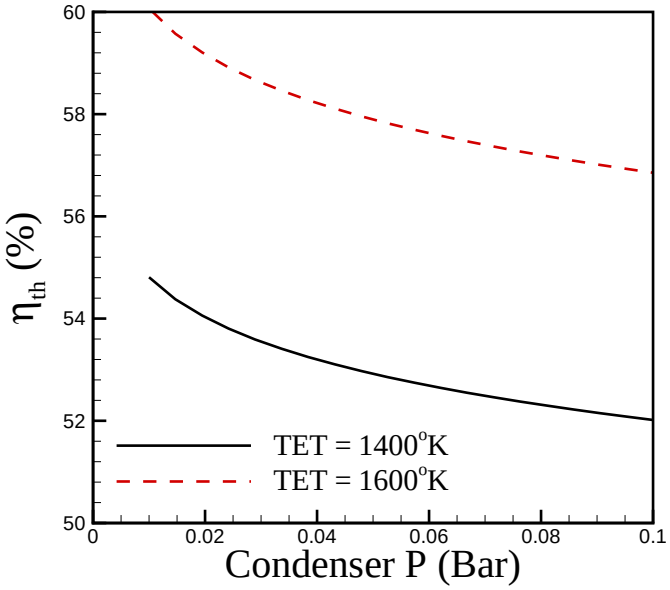

(a) Efficiency

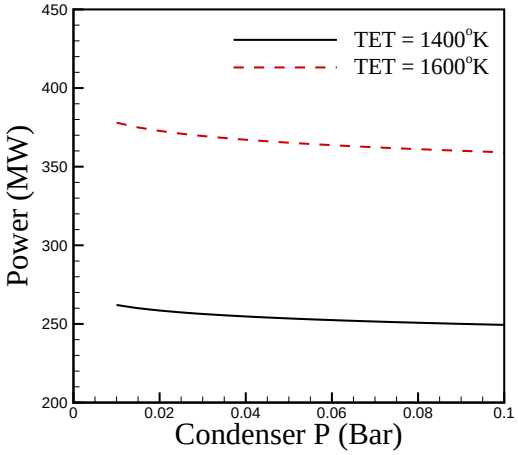

(b) Power

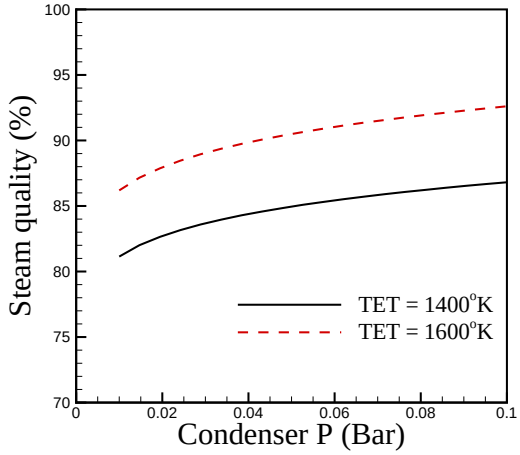

(c) Steam Quality

Figure 5.16: Combined cycle design diagrams with condenser pressure- The combined cycle consists of a single-pressure HRSG.

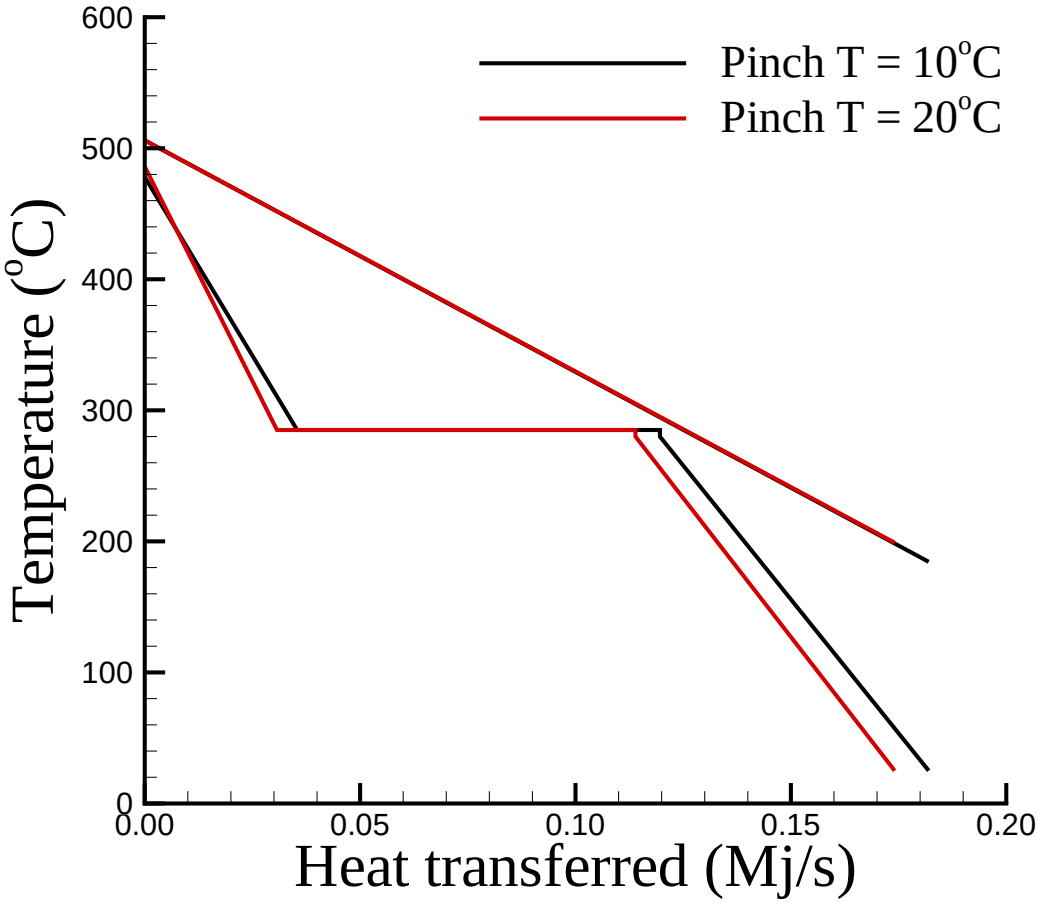

Figure 5.17: Single-pressure HRSG temperature-heat diagram changes with pinch temperature.

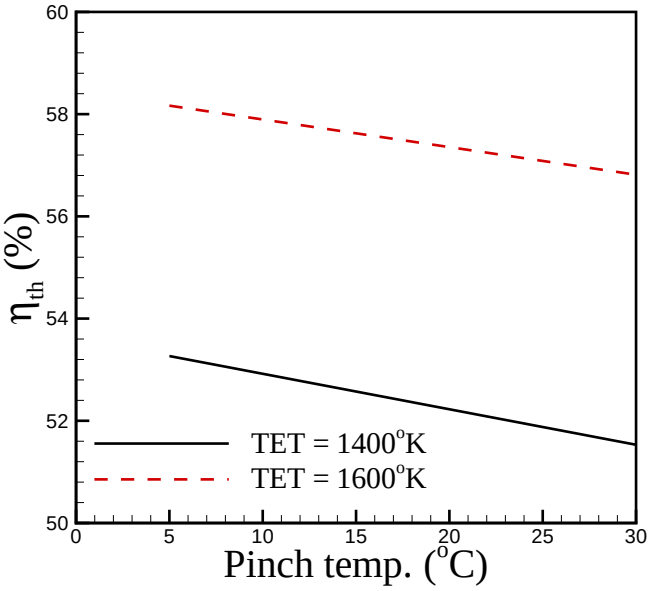

(a) Efficiency

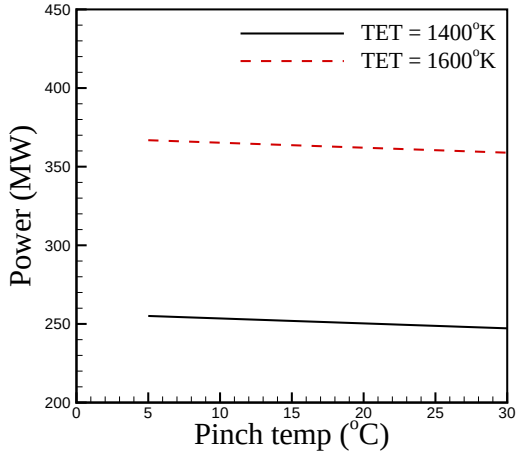

(b) Power

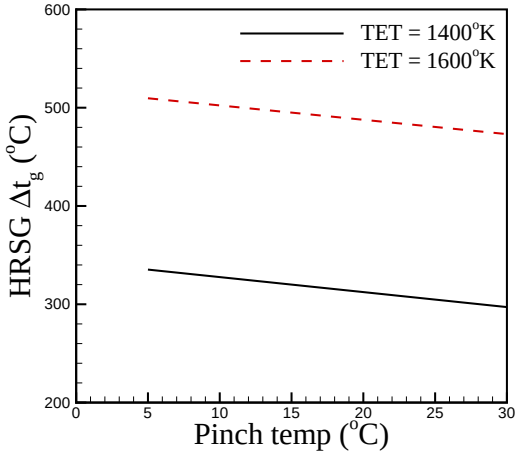

(c) HRSG gat temperature difference

Figure 5.18: Combined cycle design diagrams with pinch temperature- The combined cycle consists of a single-pressure HRSG.

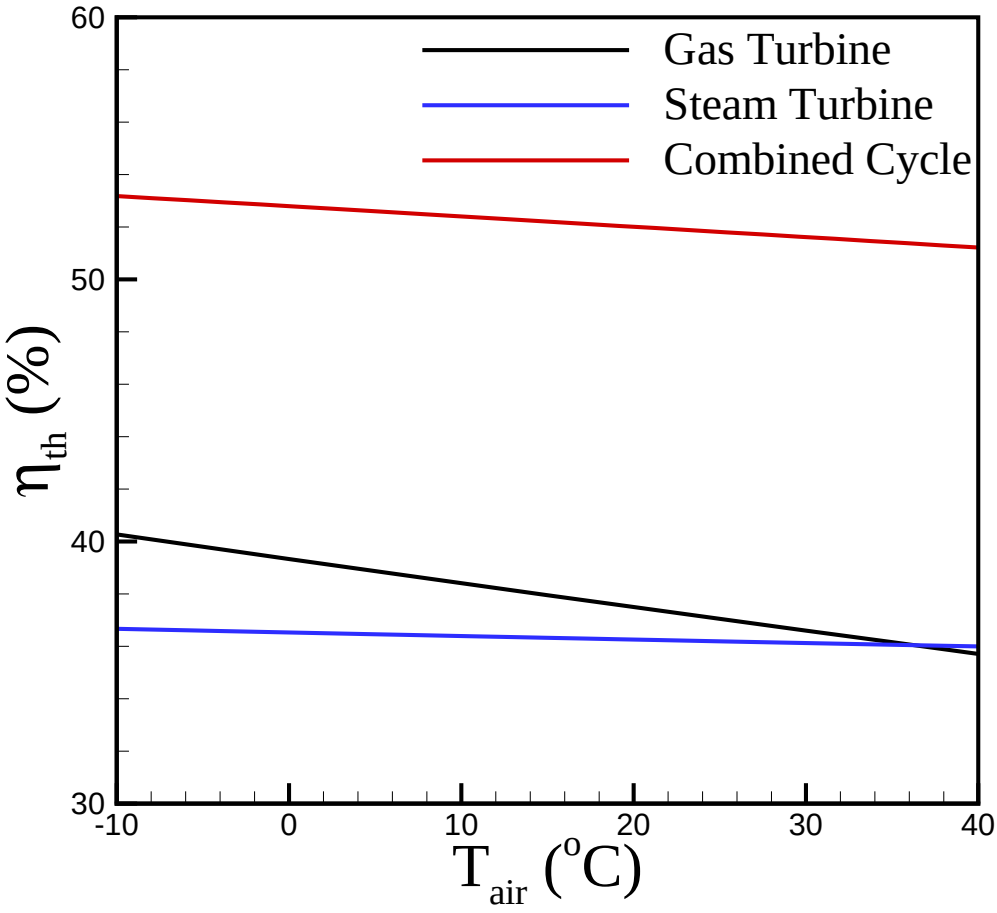

Figure 5.19: Gas turbine, steam turbine, and combined cycle thermal efficiency changes with ambient temperature. The combined cycle consists of a single-pressure HRSG.

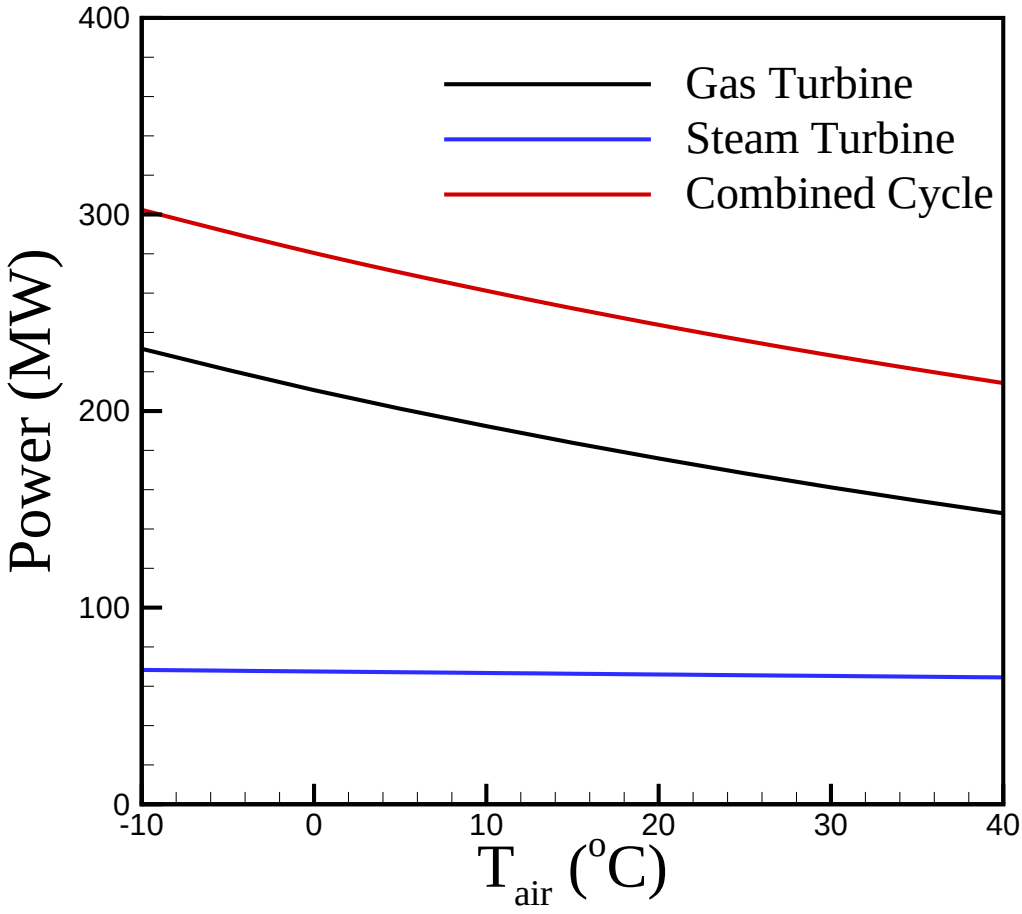

Figure 5.20: Gas turbine, steam turbine, and combined cycle output power changes with ambient temperature. The combined cycle consists of a single-pressure HRSG.

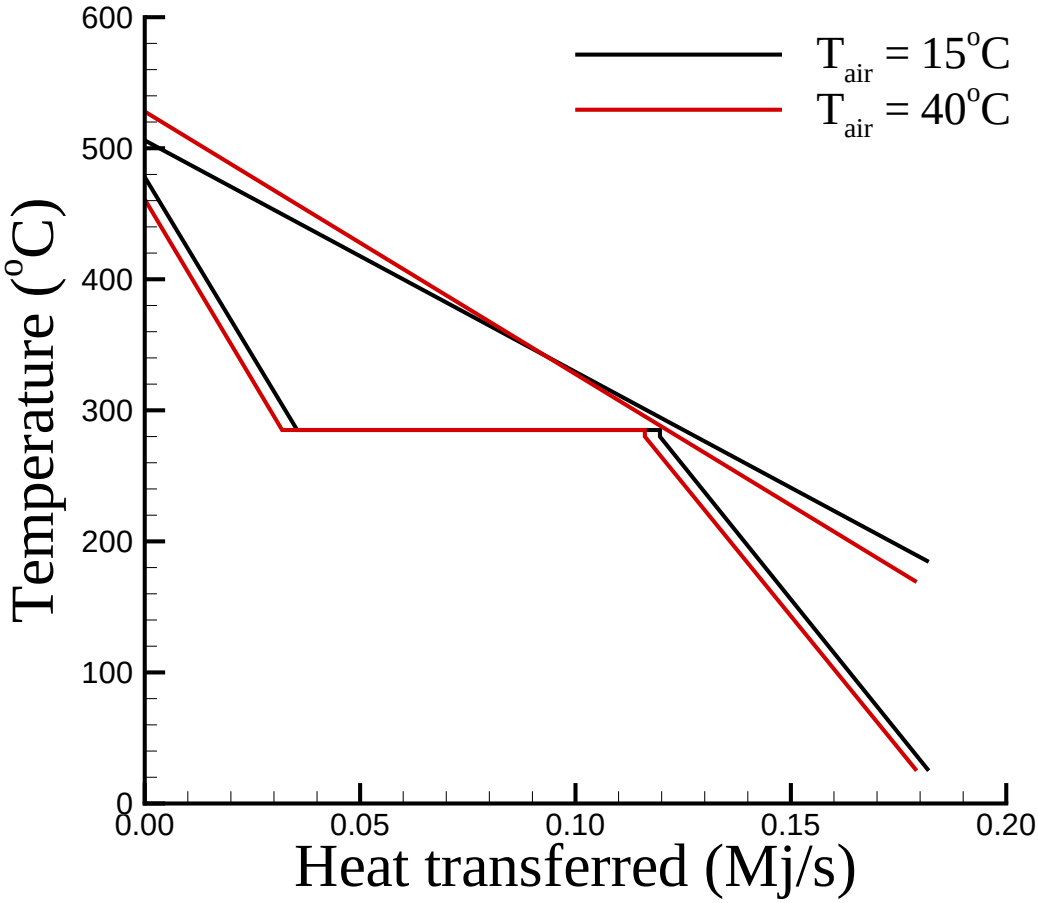

Figure 5.21: Single-pressure HRSG temperature-heat diagram changes with ambient temperature.

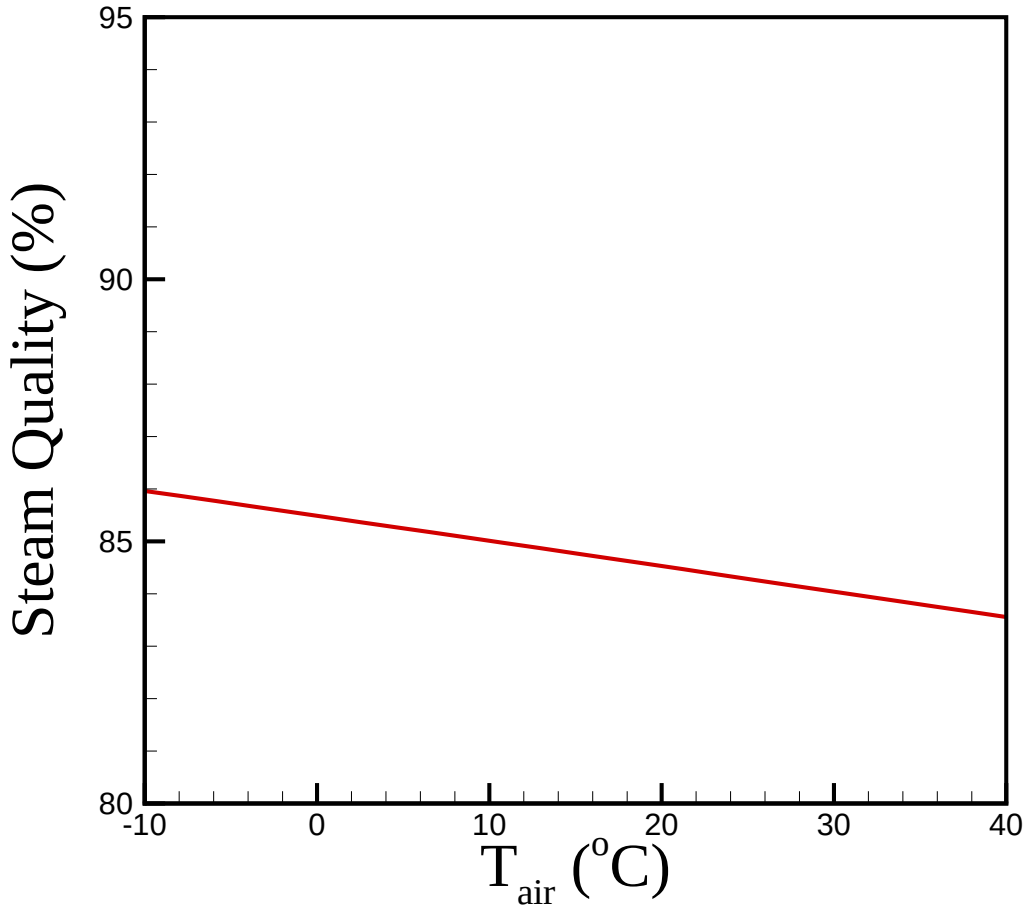

Figure 5.22: Turbine exit steam quality changes with ambient temperature. The combined cycle consists of a single-pressure HRSG.

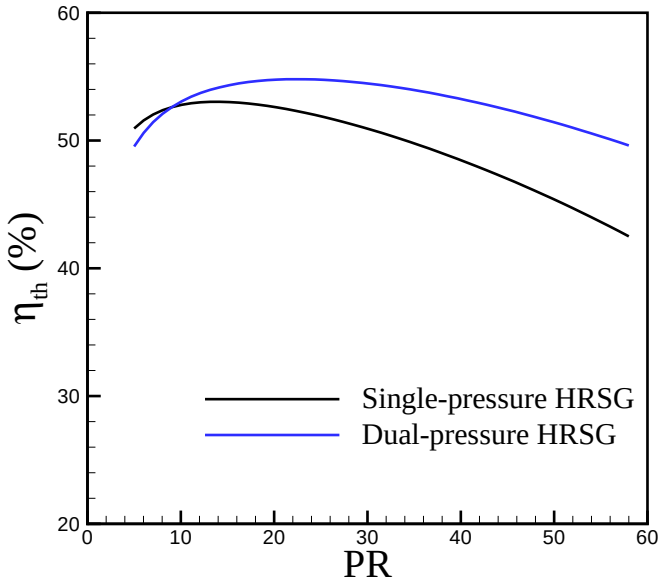

(a) Thermal efficiency

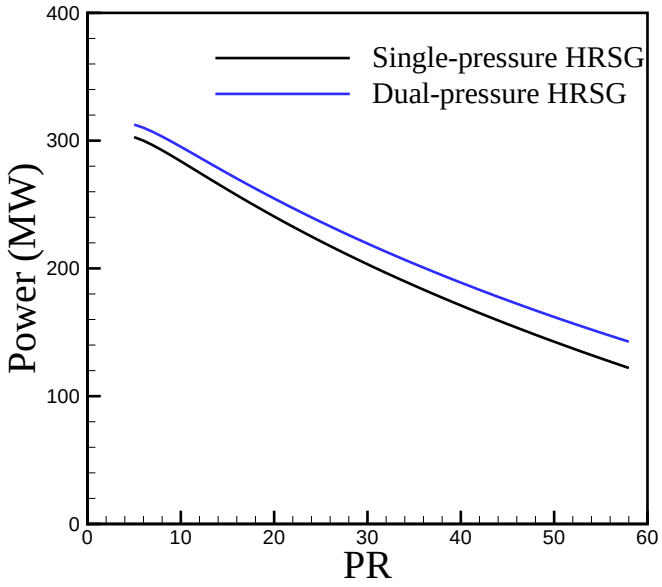

(b) Power

Figure 5.23: Thermal efficiency and power design diagrams of single and dual-pressure combined cycles.

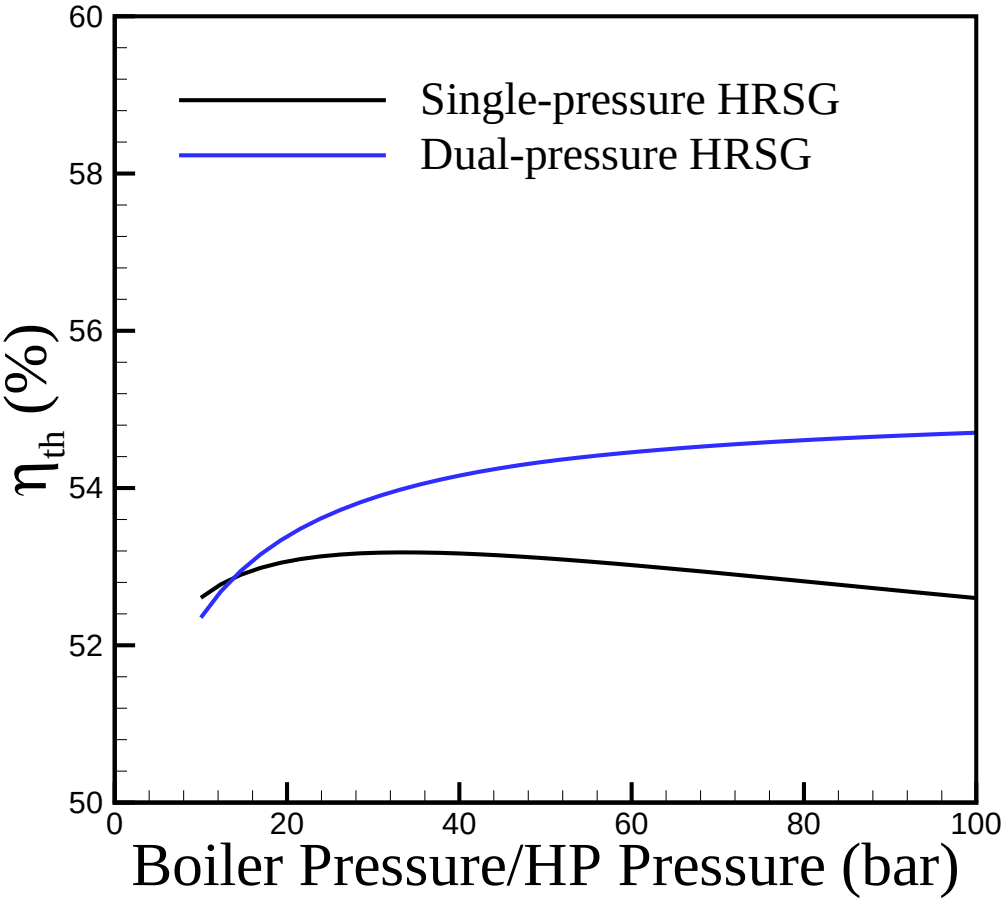

Figure 5.24: Combined cycle efficiency changes with boiler pressure/HP pressure. TET = 1400^{o}K.

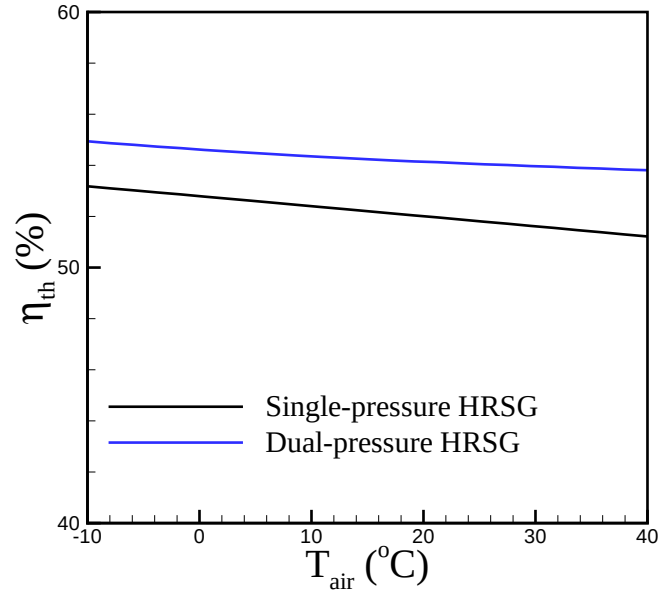

(a) Thermal efficiency

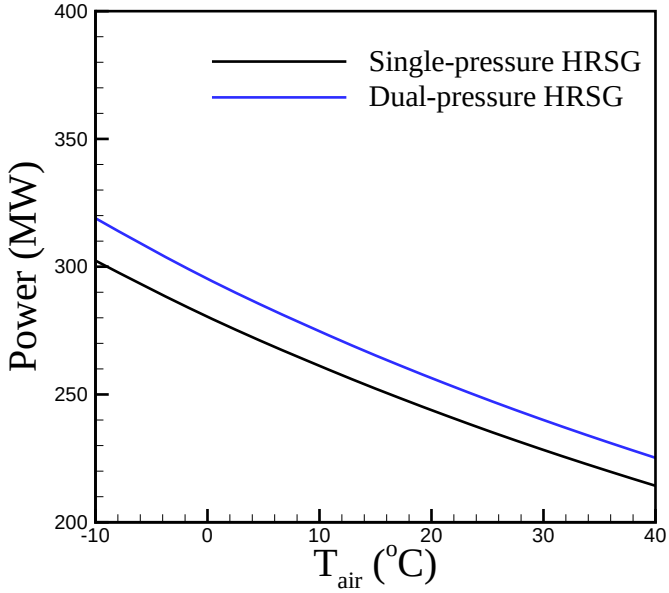

(b) Power

Figure 5.25: Operating performance of combined cycle.

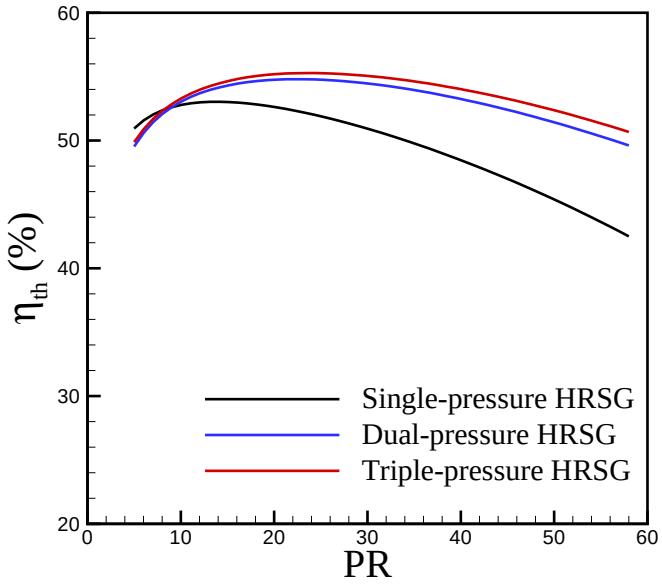

(a) Thermal efficiency

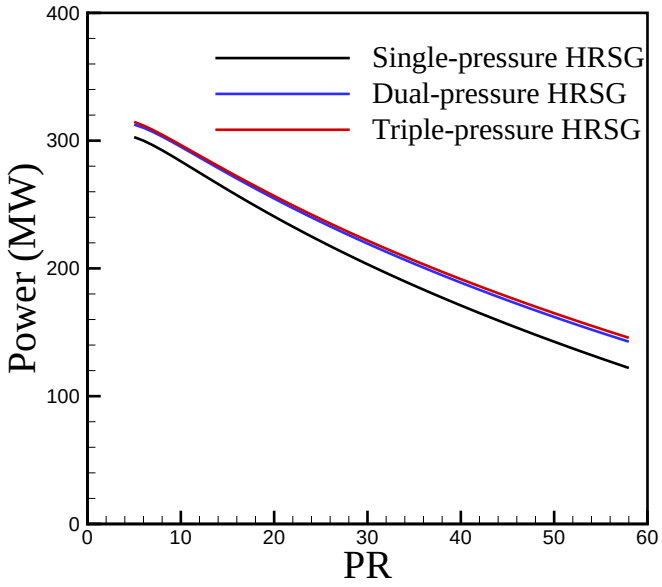

(b) Power

Figure 5.26: Thermal efficiency and power design diagrams of single and triple-pressure combined cycles.

Chapter 6

THERMOECONOMIC OPTIMIZATION

6.1 Introduction

The emphasis of this chapter is on the thermodynamic and thermoeconomic optimization of simple and combined gas-turbine cycles. The optimization methods include golden section search, genetic algorithm, simulated annealing, and expected improvement function based on Kriging modeling. The optimization problem begins with a simple single-variable optimization and then goes on for multiple-variable optimization including some design constraints. All optimization variables are limited to an upper and lower bound defined from reasonable ranges of variables. In single-variable thermodynamic optimization, a pressure ratio is determined to maximize efficiency, while in thermoeconomic optimization the objective function is to minimize the unit cost of producing electricity. This cost consists of thermodynamic performance via fuel consumption and power, along with investment cost, operating and maintenance cost, and pollution damage cost. The sum of these costs is named the total cost [13].

The results of different optimization methods are compared to show the power of

each method. Then optimization problem has been extended to find an optimum point in the pressure ratio and turbine entry temperature design space. Similar optimization problems are solved in the design spaces of pressure ratio-HP pressure, pressure ratio-LP pressure, pressure ratio-condenser pressure, and pressure ratio-Pinch temperature difference as well. This is followed by a multiple-variable optimization including all considered variables. A constrained optimization problem is also defined to limit turbine metal temperature and steam quality at the exit section of steam turbine. A scenario is defined for the operating condition of power plant in its lifetime. The optimization problem is solved again to take into account the changes in the operating conditions. The outcome of this study is to find design parameters associated with a high-efficiency and cost-effective power plant.

6.2 Single-Variable Optimization

A single-variable optimization problem is considered to maximize the efficiency and minimize the cost of producing electricity. The input variable (sometimes called decision variable) of optimization is compressor pressure ratio. The cycles considered include a simple and combined gas turbine power plant based on a gas turbine with 184.5MW output power. The combined cycle has a dual-pressure HRSG as described on Chapter 5. The classical optimization methods based on golden section search are explored to find the optimum pressure ratio. Also advanced global optimizers of genetic algorithm and simulated annealing are tested. Finally, a new optimization method based on expected improvement function is applied to this problem.

6.2.1 Thermodynamic Optimization

At a given turbine entry temperature of 1400^oK, the effects on the thermal efficiency of the simple and combined cycle from increasing compressor pressure ratio are shown

in Fig. 6.1. The gas turbine used in both cycles is based on the 184.5MW-power gas turbine used in this study. The HRSG used is a dual-pressure type with design parameters given in Table 5.3. Figure 6.1 shows that the increase in compressor pressure ratio leads to a rise in efficiencies, however, the further increase of pressure ratio beyond a certain value of pressure ratio, results in lowering the efficiency. Figure 6.1 also shows that the optimum simple cycle pressure ratio is different from optimum combined cycle pressure ratio. In the present study, different optimization methods are proposed to find the optimum pressure ratio for simple and combined cycle. The optimization results are shown in Tables 6.1 and 6.2 for simple and combined cycle, respectively.

Tables 6.1 and 6.2 give the optimal pressure ratio, average run-time and maximum calculated thermal efficiency for each algorithm. The golden section search optimization divides the range of input variable into two separate subintervals using the golden ratio [105]. The optimization method then selects the subinterval that contains the optimal solution and divides it into two more subintervals. The method iterates until the final interval length is less than the tolerance defined. This method is very useful to find the optimal point of a single-variable optimization problem. The fminbnd optimization is also based on golden section search but it benefits from a parabolic interpolation method as well that helps to accelerate the optimiztaion [106]. The genetic algorithm and expected improvement methods have been described in Chapter 2. The parameters of genetic algorithm are set to the default values in MATLAB [107]. For expected improvement function, four initial samples were defined; two random samples and two at the upper and lower bound of pressure ratio as shown in Fig. 6.2 (a). A universal-type Kriging is developed and used to predict expected improvement function for all the pressure values in the range of interest. This function is shown in Fig. 6.2 (d). A new sample is defined at a location where expected improvement function is maximized as shown in Fig. 6.2 (b). The Kriging

model and expected improvement function are again created for the new samples as shown in Fig. 6.2 (e). This process iterates until maximum expected improvement function falls below a set threshold. The pressure ratio that maximizes expected improvement function at the final iteration is the optimal value. This value is shown in Fig. 6.2 (h).

Tables 6.1 and 6.2 show that all optimization methods found approximately similar optimal solutions that maximizes efficiencies. The optimal pressure ratio for simple cycle is around 39 with an efficiency of 41.7%. The optimal pressure ratio for combined cycle is around 22.5 with an efficiency of 54.8%. This again shows that optimal pressure ratio of combined cycle is smaller than optimal pressure of simple cycle. Tables 6.1 and 6.2 also show that the expected improvement function and fminbnd method have the smallest average run-time amongst all methods used.

Table 6.1: Thermodynamic optimization of gas turbine.

Optimization Method	Time (s)	Opt. PR	Opt. η_{th}
Golden Section Search	58	38.66	41.71
MATLAB *fminbnd* function	28	39.88	41.71
Genetic Algorithm	1222	40.02	41.71
Simulated Annealing	677	38.85	41.71
Expected Improvement Function	24	39.27	41.71

Table 6.2: Thermodynamic optimization of combined gas/steam plant.

Optimization Method	Time (s)	Opt. PR	Opt. η_{th}
Golden Section Search	59	23.18	54.80
MATLAB *fminbnd* function	30	22.61	54.81
Genetic Algorithm	1299	22.57	54.81
Simulated Annealing	734	22.22	54.81
Expected Improvement Function	47	23.32	54.80

Tables 6.3 and 6.4 show the gas turbine and combined cycle performance data at optimal pressure ratio and for maximum thermal efficiency. The gas turbine power for

maximum efficiency is smaller than power of baseline engine as shown in Table 6.3. The exhaust gas temperature is significantly lower than exhaust gas temperature of baseline engine that confirms the new engine is more efficient. The efficiency of baseline design was 37.8% while the efficiency of the new engine is 41.7%.

The combined cycle power for a maximum-efficiency design is smaller than the baseline as well. However the efficiency is improved from 54.4% to 54.8%. The gas turbine for optimum efficiency combined cycle has 178.7 MW power with a thermal efficiency of 39.9%. The engine has exhaust temperature of 460^{o}C much higher than gas exhaust temperature of optimum efficiency simple gas turbine.

Table 6.3: Optimum-thermodynamic gas turbine performance predictions using Genetic Algorithm.

Parameter	Predicted value
Shaft power, MW	150.20
Exhaust mass flow rate, kg/s	564.3
Exit temperature, ^{o}C	372.7
Thermal efficiency, %	41.71
Gross heat rate, kj/kw.hr	8631

Table 6.4: Optimum-thermodynamic combined cycle performance predictions using Genetic Algorithm.

Parameter	Value	Parameter	Value
GT power, MW	178.7	CC power, MW	245
GT efficiency, %	39.9	Stack temperature, ^{o}C	92.75
GT exhaust temperature ,^{o}C	460	CC efficiency, %	54.81
HP turbine power, MW	27.4	HP steam mass flow rate, kg/s	46.6
LP turbine power, MW	39.1	LP steam mass flow rate, kg/s	21.7

6.2.2 Thermoeconomic Optimization

The goal of thermoeconomic optimization is to minimize a cost objective function that couples thermodynamic and economic models with environmental considerations. The objective function for thermoeconomic optimization is the unit price of producing electricity by the plant, denoted by $\dot{C}_E$ expressed in US$/kwh. For a design-type optimization, this function remains unchanged within time and is defined as:

$$\dot{C_E} = \frac{\beta C_0}{\dot{W}_g\ N} + \frac{C_{\text{fuel}}}{\dot{W}_g\ N} + \frac{C_{\text{OM}}}{\dot{W}_g\ N} + \frac{C_{\text{NO}_\text{x}}}{\dot{W}_g\ N} + \frac{C_{\text{CO}}}{\dot{W}_g\ N} \tag{6.1}$$

Each annualized cost per output power is denoted as $\dot{\Gamma}$, therefore:

$$\dot{C_E} = \dot{\Gamma}_z + \dot{\Gamma}_{\text{fuel}} + \dot{\Gamma}_{\text{NO}_\text{x}} + \dot{\Gamma}_{\text{CO}} \tag{6.2}$$

where, $\dot{\Gamma}_z = (\beta C_0 + C_{\text{OM}})/(\dot{W}_g\ N)$. The objective of design-type thermoeconomic optimization is to find design variables that minimize $\dot{C_E}$ such that:

$$\begin{aligned} \text{minimize: } \dot{C_E} &= \dot{C_E}(x, y) \\ \text{subject to: } h_j(x, y) &= 0 \quad \text{j=1,...J (equality constraints)} \\ g_k(x, y) &\geq 0 \quad \text{k=1,...K (inequality constraints)} \\ \text{where, } x &= \{x_i\} \ \text{i=1,...I (independent variables)} \\ y &= \{y_j\} \ \text{j=1,...J (dependent variables)} \end{aligned} \tag{6.3}$$

where, x denotes decision variables and is compressor pressure ratio here. The correlations between cost terms in Eq. 6.1 have been established earlier. The fuel flow and power are directly calculated from VariFlow code during optimization. At a given turbine entry temperature of 1400^{o}K, the estimation of function $\dot{C_E}$ is shown for the

simple and combined cycle in Fig. 6.3. Again, the gas turbine used in both cycles is based on the 184.5MW-power gas turbine used in this study and HRSG type in combined cycle is a dual-pressure type.

It should be noted that it is desirable to have the smallest cost of producing electricity. Figure 6.3 shows that the cost of producing electricity is very large for engines with small pressure ratio. These engines have very large capital cost per kw costs and low efficiencies. Figure 6.3 shows that combined cycle cost is signifiable lower than simple cycle. This suggests that combined cycle will produce more profits compared with simple cycles. The cost of simple and combined cycles slightly increases with increasing pressure ratio for engines with moderate to high compressor pressure ratio values. For these engines and assumed cost coefficients, the efficiency is dominant factor since the capital cots nearly remains unchanged for medium and large size engines.

Tables 6.5 and 6.6 show the optimization results to minimize the cost function of the simple and combined cycles. The optimal pressure ratio for simple cycle is around 38 with an electricity producing cost of 3.5827 C$/kw.hr. The optimum pressure ratio is not much different from optimum pressure ratio that maximized efficiency. This is again because capital cost is nearly unchanged with increasing pressure ratio from moderate to high values and efficiency effects are dominant in the cost. The optimal pressure ratio for combined cycle is also round 27 with a electricity producing cost of 2.7519 C$/kw.hr.

Tables 6.7 and 6.8 show the gas turbine and combined cycle performance data at optimal pressure ratio and for minimum electricity producing cost. The gas turbine power is 148.8 MW with an efficiency of 41.5% as shown in Table 6.7. The efficiency of optimal-cost engine is slightly smaller than the efficiency of optimal-efficiency engine. The optimal-cost combined cycle has 225.6MW power and efficiency of 54.48%. Gas turbine in this cycle has 168.8MW power and 40.76% efficiency.

Table 6.5: Unit price of producing electricity optimization of gas turbine.

Optimization Method	Opt. PR	Opt. $\dot{C}_E$ C$/kw.hr
Golden Section Search	38.37	3.5827
MATLAB *fminbnd* function	38.03	3.5827
Genetic Algorithm	38.15	3.5828
Simulated Annealing	38.36	3.5827
Expected Improvement Function	38.17	3.5832

Table 6.6: Thermoeconomic optimization of combined gas/steam plant.

Optimization Method	Opt. PR	Opt. $\dot{C}_E$ C$/kw.hr
Golden Section Search	26.71	2.7519
MATLAB *fminbnd* function	26.98	2.7519
Genetic Algorithm	27.18	2.7520
Simulated Annealing	26.90	2.7519
Expected Improvement Function	27.69	2.7524

Table 6.7: Optimum-thermoecnomic gas turbine performance predictions using Genetic Algorithm.

Parameter	Predicted value
Shaft power, MW	148.87
Exhaust mass flow rate, kg/s	564.3
Exit temperature, ^{o}C	372.0
Thermal efficiency, %	41.55
Gross heat rate, kj/kw.hr	8664

Table 6.8: Optimum-thermoeconomic combined cycle performance predictions using Genetic Algorithm.

Parameter	Value	Parameter	Value
GT power, MW	168.8	CC power, MW	225.6
GT efficiency, %	40.76	Stack temperature, ^{o}C	98.00
GT exhaust temperature ,^{o}K	425.6	CC efficiency, %	54.48
HP turbine power, MW	21.4	HP steam mass flow rate, kg/s	38.5
LP turbine power, MW	35.4	LP steam mass flow rate, kg/s	23.9

6.3 Multiple-Variable Optimization

The optimization problem is now extended to a multiple-variable problem, where, the objective is to find minimum of $f(x)$. For thermodynamic study, f is $-1 \times \eta_{th}$ and for thermoeconomic study it corresponds to $\dot{C}_E$. The vector of x consists of decision variables. To start solving this problem, it is assumed that x includes compressor pressure ratio and turbine entry temperature. The range of TET is from 1200^oK to 1800^oK as well. Figure 6.4 shows the surface graph of thermal efficiency for simple and combined cycle plotted for pressure ratio and TET values in the range of interest. This figure shows that thermal efficiencies are maximized at high compressor pressure ratio and high turbine entry temperatures. This is also found by optimization methods. Figure 6.5 also shows the surface graph of electivity producing cost for simple and combined cycle plotted for pressure ratio. Likewise thermal efficiency, the cost is minimized at high turbine inlet temperature and compressor pressure ratio.

A three-dimensional plot of electricity producing cost is shown in Fig 6.5 for simple and combined cycle. This figure shows the cost function changes with two variables of pressure ratio and turbine entry temperature. As expected, Fig 6.5 shows that cost associated with the combined cycle is much smaller than simple cycle cost. This is mainly due to improved efficiency and increased power in a combined cycle. Likewise efficiency surface plots, the minimum cost occurs at maximum turbine entry temperature and pressure ratio values. Cost of producing electricity has the effects of capital cost and efficiency. Capital cost is nearly unchanged for large power plants (higher TET and PR) but efficiency assuming no bleeding air is improved at high turbine entry temperatures and pressure ratio values. Therefore the cost is reduced at these conditions. The effects of bleeding air for engines with high TET will be detailed later in this chapter.

The next optimization problem is to minimize the cost of producing electricity

in pressure ratio and high pressure steam design space. The surface graph of cost is plotted and shown in Fig. 6.6. In this figure, the objective function of z-axis refers to cost of producing electivity. Fig. 6.6 shows that there is a minimum point in the plot. Optimization methods of genetic algorithm and expected improvement function are used to find the minimum point. Table 6.9 shows the run time, optimal point, and minimum cost value for each method. Both methods found the minimum point closely (pressure ratio around 27.5 and high pressure around 86 bar), however, expected improvement function has less computational time to find the point. In the genetic algorithm optimizer, each point is associated with a "fitness" value that defines the probability of survival in the next "generation" such that the higher the fitness, the higher the probability of survival. The genetic algorithm starts with an initial population generally chosen random and then applies three basic operators of reproduction, crossover, and mutation. In the reproduction, the chromosomes to be copied in the next generation are selected based on fitness values. The crossover operator is then applied to produce some new points from crossover between pairs of selected points. Finally, the mutation operator is applied which randomly reverses the value of every bit within a chromosome with a fixed probability. The population size used to find the specific power maximum point has 40 points and the point locations for different generations are shown in Fig. 6.7. Note that how the points converge to the global minimum point as generation increases.

Table 6.9: Thermoeconomic optimization of combined gas/steam plant.

Optimization Method	Time (s)	Opt. PR	Opt. HP	Opt. $\dot{C}_E$ C$/kw.hr
Genetic Algorithm	5612	27.46	86.63	2.4041
Expected Improvement Function	949	27.83	86.43	2.4043

Table 6.10 shows the gas turbine and combined cycle performance data at optimal point found from genetic algorithm. The gas turbine power is smaller than baseline

engine but it has a better efficiency as shown in Table 6.10. This is to have a lower exhaust gas temperature and heat waste compared with baseline engine. The optimal engine also has increased power and efficency compared with the cycle performance data in Table 5.4.

Table 6.10: Optimum-thermoeconomic combined cycle performance predictions using Genetic Algorithm.

Parameter	Value	Parameter	Value
GT power, MW	168.31	CC power, MW	224.3
GT efficiency, %	40.81	Stack temperature, ^{o}C	97.88
GT exhaust temperature ,^{o}K	423.9	CC efficiency, %	54.39
HP turbine power, MW	20.6	HP steam mass flow rate, kg/s	35.8
LP turbine power, MW	35.4	LP steam mass flow rate, kg/s	26.7

The surface plot of cost with pressure ratio and low pressure is shown in Fig. 6.8. LP ranges from 2 to 20 bar. Inspection of the graph shows that there is a global minimum point in a region which has moderate pressure ratio and small LP values. The optimizer based on expected improvement function is tested to find this global minimum point. The method converges to a point with pressure ratio of 28.14 and LP of 4.56 bar with an objective function of 2.4046 C$/kw.hr. The optimal cycle has a gar turbine with a greater pressure ratio compared with the baseline gas turbine. LP pressure is also slightly higher than the value used in baseline combined cycle. The found optimum point is shown in Fig. 6.9. Besides, Table 6.11 shows the combined cycle performance data for the optimum design.

Effects of varying pressure ratio and condenser pressure on the cost are shown in Fig. 6.10 as well. The condenser pressure ranges from 0.01 to 0.1 bar. The lower condenser pressure also improved the cycle efficiency and hence reduce the cost as shown in Fig. 6.10. The optimizer is again used to find this global minimum point. The method converges to a point with pressure ratio of 27.86 and condenser pressure of 0.01 bar with an objective function of 2.3072 C$/kw.hr. Table 6.12 details the

Table 6.11: Optimum-thermoeconomic combined cycle performance predictions using Genetic Algorithm.

Parameter	Value	Parameter	Value
Compressor PR	28.14	LP pressure, bar	4.56
GT power, MW	167.12	CC power, MW	222.4
GT efficiency, %	40.90	Stack temperature, ^oC	102.7
GT exhaust temperature ,^oK	419.9	CC efficiency, %	54.43
HP turbine power, MW	19.5	HP steam mass flow rate, kg/s	37.1
LP turbine power, MW	35.7	LP steam mass flow rate, kg/s	23.5
Objective function	2.4046		

performance data of the cycle using these minimum data.

Table 6.12: Optimum-thermoeconomic combined cycle performance predictions using Genetic Algorithm.

Parameter	Value	Parameter	Value
Compressor PR	27.86	Conds. pressure, bar	0.01
GT power, MW	167.61	CC power, MW	232.8
GT efficiency, %	40.86	Stack temperature, ^oC	98.6
GT exhaust temperature ,^oK	421.6	CC efficiency, %	56.75
HP turbine power, MW	20.7	HP steam mass flow rate, kg/s	37.5
LP turbine power, MW	44.5	LP steam mass flow rate, kg/s	24.10
Objective function	2.3072		

Pinch point is defined as the difference between the gas temperature leaving the evaporator and the saturation temperature of the water for given boiler pressure in the steam cycle [100]. Figure 6.11 shows the effects of pinch temperature difference on the cost predictions. The lower and upper bounds of pinch temperature are 5^oC and 30^oC, respectively. A large pinch point temperature reduces the heat transferred in the HRSG and steam mass flow rate, but increases the stack gas temperature. The cycle efficiency falls with larger pinch temperature as gas turbine stack temperature is higher for a large pinch temperature value. The power slightly becomes smaller with pinch temperature as well. The optimization method found a global minimum

point with a pressure ratio of 28.75 and pinch point temperature of 5.19^{o}C with a minimum cost of 2.4006 C$/kw.hr. Table 6.13 details the performance data of the cycle using these minimum data.

Table 6.13: Optimum-thermoeconomic combined cycle performance predictions using Genetic Algorithm.

Parameter	Value	Parameter	Value
Compressor PR	28.75	Pinch temp, ^oC	5.19
GT power, MW	166.03	CC power, MW	221.6
GT efficiency, %	40.98	Stack temperature, ^{o}C	93.6
GT exhaust temperature ,^{o}K	416.5	CC efficiency, %	54.70
HP turbine power, MW	20.6	HP steam mass flow rate, kg/s	37.7
LP turbine power, MW	35.0	LP steam mass flow rate, kg/s	24.2
Objective function	2.4006		

The optimization problem is then extended to include all the variables of interest. These variables are listed in Table . The computational effort for such a problem grows singingly because of the large number of independent variables. The objective function is again the cost of producing electricity. Table compares the optimum point with initial solution. The optimum point has the maximum turbine entry temperature in the range. This is because, the thermal efficiency is significantly improved by increasing this temperature. The optimum cycle also has a HP value around the upper bound of variable. The optimum condenser pressure, LP, and pinch temperature tend to be around lower bound of variable range. Table 6.15 gives the performance data of optimum cycle as well. Note the high achieved thermal efficiencies for gas turbine and combined cycles. These high efficiencies aid in to reduce the cost; the cost at minimum point is 2.0129 C$/kw.hr.

Table 6.14: Thermoeconomic optimization of combined gas/steam plant.

Parameter	Original value	Optimum Value
Compressor PR	14.61	47.33
Turbine entry temperature, ^oK	1394	1800
HRSG high pressure, bar	70	99.99
HRSG low pressure, bar	3.89	3.76
Condenser pressure, bar	0.05	0.0126
Pinch temperature, ^oC	10	5.53

Table 6.15: Optimum-thermoeconomic combined cycle performance predictions using Genetic Algorithm.

Parameter	Value	Parameter	Value
GT power, MW	314.0	CC power, MW	424.4
GT efficiency, %	48.08	Stack temperature, ^{o}C	73.1
GT exhaust temperature ,^{o}K	560.7	CC efficiency, %	64.9
HP turbine power, MW	49.7	HP steam mass flow rate, kg/s	67.3
LP turbine power, MW	60.8	LP steam mass flow rate, kg/s	18.7
Objective function	2.0129		

6.4 Constrained Optimization

Many practical applications have some design constraints for example material melting temperature or corrosion due to presence of larger amount of water. This section considers the optimization with some given constraints. In earlier problems, it was assumed that no air is bled from compressor for cooling the turbine blades. However, the materials are limited to the temperature and they need to be cooled to avoid over-heating. It is now assumed that the air is bled from compressor to keep the metal temperature below 1488^oK. The amount of required bleeding is found from an optimization method to minimize the squared difference between predicted metal temperature and desired temperatures and therefore depends on the allowable metal temperature. The required bled air against TET and two metal temperature is shown in Fig. 6.12. The figure shows that more air needs to be extracted for cooling if the turbine inlet temperature increase. The amount of cooling air would be less for higher maximum metal temperature.

It should be noted that the amount of bleeding air is zero for all TET values below desired metal temperature. For each selection of independent variables, a corresponding bled air is found to keep the metal temperature below 1488^oK. Tera code then find the plant efficiency and power. The optimization solver was used to find the global minimum with values shown in Table 6.18. The optimum TET is now below the maximum temperature, because the maximum TET requires large amount of bled air as shown in Fig. 6.12. This significantly reduce the cycle efficiency and output power. The performance data corresponding to this optimum point are shown in Table 6.19 that shows combined cycle efficiency is slightly lower than the plant with no bled air assumption.

In next optimization scenario, more limitations are added to select the optimum solution. The steam quality at the steam turbine exit should be above 0.88 and the

Table 6.16: Thermoeconomic optimization of combined gas/steam plant.

Parameter	Original value	Optimum Value
Compressor PR	14.61	40.0
Turbine entry temperature, ^oK	1394	1782
HRSG high pressure, bar	70	99.99
HRSG low pressure, bar	3.89	3.82
Condenser pressure, bar	0.05	0.010
Pinch temperature, ^oC	10	5.02

Table 6.17: Optimum-thermoeconomic combined cycle performance predictions using Genetic Algorithm.

Parameter	Value	Parameter	Value
GT power, MW	205.9	CC power, MW	443.0
GT efficiency, %	44.51	Stack temperature, ^{o}C	88.1
GT exhaust temperature ,^{o}K	443.0	CC efficiency, %	60.3
HP turbine power, MW	24.9	HP steam mass flow rate, kg/s	40.9
LP turbine power, MW	48.2	LP steam mass flow rate, kg/s	26.8
Objective function	2.1637		

combustor entry temperature should be limited as well. The high moisture content could lead in to turbine blade corrosion. Also, Soars [71] mentioned that due to mechanical integrity, the combustor entry temperature must be limited to temperatures between 850 and 950K, depending on the technology level. Table 6.18 shows the optimum point which has much smaller pressure ratio compared with earlier problems. The HP is also smaller in order to satisfy the constraints. Note that the steam quality is improved in the new design compared with initial one. Table 6.19 also shows the performance data for the optimum point.

Table 6.18: Thermoeconomic optimization of combined gas/steam plant.

Parameter	Original value	Optimum Value
Compressor PR	14.61	25.9
Turbine entry temperature, ^oK	1394	1751
HRSG high pressure, bar	70	15.6
HRSG low pressure, bar	3.89	2.00
Condenser pressure, bar	0.05	0.040
Pinch temperature, ^oC	10	14.6
Comp. exit temperature, ^oK	703	797
LP turbine steam quality, %	85.1	91.4

Table 6.19: Optimum-thermoeconomic combined cycle performance predictions using Genetic Algorithm.

Parameter	Value	Parameter	Value
GT power, MW	215.4	CC power, MW	288.6
GT efficiency, %	42.02	Stack temperature, ^{o}C	83.0
GT exhaust temperature ,^{o}K	501.8	CC efficiency, %	56.30
HP turbine power, MW	32.2	HP steam mass flow rate, kg/s	63.1
LP turbine power, MW	41.0	LP steam mass flow rate, kg/s	10.3
Objective function	2.355		

6.5 Operating Optimization

The optimization framework can be easily extended to include operating optimization. For operating-type optimization, the power plants performance will change because of ambient air changes and operating at different loads. Assuming n different values of $\dot{C}_E$ in a year, then optimization is defined as:

$$\begin{aligned} \text{minimize: } \sum_{i=1}^{n} \dot{C}_E &= \sum_{i=1}^{n} \dot{C}_E(x,y) \\ \text{subject to: } h_j(x,y) &= 0 \quad \text{j=1,...J (equality constraints)} \\ g_k(x,y) &\geq 0 \quad \text{k=1,...K (inequality constraints)} \\ \text{where, } x &= \{x_i\} \ \text{i=1,...I (independent variables)} \\ y &= \{y_j\} \ \text{j=1,...J (dependent variables)} \end{aligned} \tag{6.4}$$

where, the cost of producing electricity is estimated as:

$$\dot{C_E} = \frac{\beta C_0}{\sum_{i=1}^{n} \dot{W}_{gi}\ N_i} + \frac{\sum_{i=1}^{n} C_{\text{fuel}i}}{\sum_{i=1}^{n} \dot{W}_{gi}\ N_i} + \frac{C_{\text{OM}}}{\sum_{i=1}^{n} \dot{W}_{gi}\ N_i} + \frac{\sum_{i=1}^{n} C_{\text{NOx}i}}{\sum_{i=1}^{n} \dot{W}_{gi}\ N_i} + \frac{\sum_{i=1}^{n} C_{\text{CO}i}}{\sum_{i=1}^{n} \dot{W}_{gi}\ N_i} \tag{6.5}$$

where index i corresponds to each part load conditions. In order to demonstrate the approach, the thermodynamic optimization of single gas turbine under operating conditions is considered. Three operating scenarios were defined and tested. In the first and second scenarios, the engines operate at fixed temperatures of $\text{T}_{\text{air}} = 0^o\text{C}$ and $\text{T}_{\text{air}} = 30^o\text{C}$, respectively. The objective function (cost of producing electricity) under these conditions were calculated and plotted against objective function at design point in Fig. 6.13. This figures shows that objective function changes with ambient temperature changes such that it is smaller for colder temperatures. The

EIF optimizer again was used to find the minimum cost for each scenario and the results are summarized in Table 6.20. The results show that the engine operating at cold temperature has less cost of producing electricity compared with standard and hot temperature cases. The optimum compressor pressure ratio is also larger for the engine operating at cold temperature as well.

In the third scenario, it is assumed that engine operates at different ambient conditions during its lifetime. The temperature ranges from $T_{air} = -5^oC$ to $T_{air} = 35^oC$. The total operating hours per year was assumed 8,000 hours again. This value was split to smaller hours each corresponding to a temperature in the temperature range. The objective function was estimated using Eq. 6.5 and plotted against cost at design-point conditions in Fig. 6.14. The EIF optimizer again was used to find the minimum cost and the compressor pressure ratio that minimized the cost. The results are shown in Table 6.21 which shows the minimum cost under these assumptions is smaller than cost from design-point. This is likely due to the effects of more hours operating at temperatures below standard temperature. The optimum compressor pressure ratio for minimum cost is larger than optimum pressure ratio at design point as well.

Table 6.20: Unit price of producing electricity optimization of gas turbine under operating conditions.

Case	Opt. PR	Opt. $\dot{C_E}$ C$/kw.hr
Design-point	38.17	3.5832
Operating, $T_{air} = 0^oC$	42.21	3.3768
Operating, $T_{air} = 30^oC$	35.16	3.8095

Table 6.21: Design-point and operating thermoeconomic optimization of gas turbine.

Case	Opt. PR	Opt. $\dot{C}_E$ C$/kw.hr
Design-point	38.17	3.5832
Operating, $T_{air} = -5 - 35^oC$	39.98	3.4445

6.6 Conclusions

A framework was described in this chapter for the thermodynamic and thermoeconomic optimization of simple and combined gas-turbine cycles. Different methods were considered for the optimization. The results showed the benefits of each method. Optimizers based on golden section search are simple to implement and very helpful for single-variable type optimization problems. Genetic algorithm and simulated annealing have a longer runtime than golden section search, but they are well fitted for multi-variable type of optimization. The results showed that an optimization method based on expected improvement function has smallest runtime amongst used methods. This optimizer also ensures that a global maxima or minima is found.

In the single-variable optimization problem, the compressor pressure ratio was assumed as decision variable. The optimization results confirm that used methods can produce accurate and efficient results for thermodynamic and thermoeconomic optimization. The results showed that the optimum pressure ratio values for maximum efficiency is different for the simple and combined gas-turbine cycles. The combined cycle efficiency is maximum at a lower pressure ratio values. The optimization methods were also tested for multi-variable type optimization problems. The solution of constrained optimization was also described to limit turbine metal temperature and moisture content at the exit stage of steam turbine. Finally, the optimization under operating conditions were shown. The results showed that for engines operating at cold temperatures, a larger compressor pressure ratio is required to minimize the

unit cost of producing electricity than an engine operating at standard ambient temperature. This framework can easily be extended to include different scenarios and constraints for optimization.

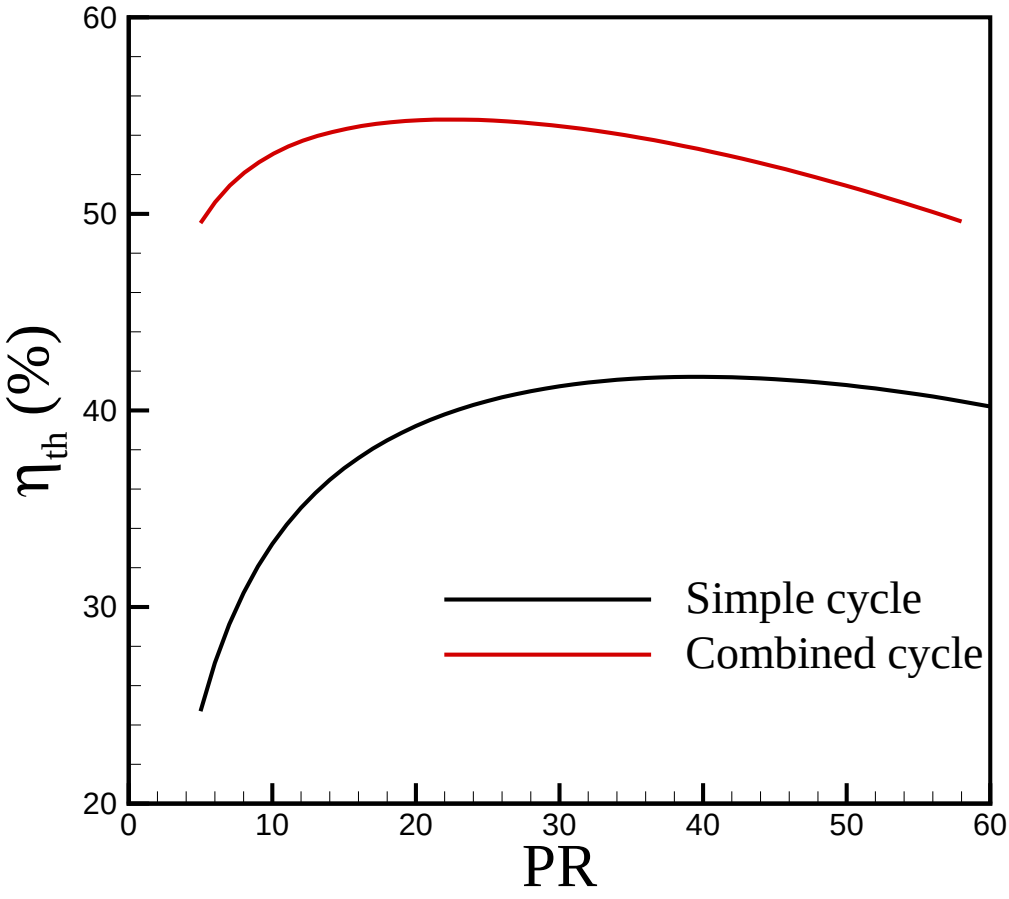

Figure 6.1: Simple and combined cycle efficiencies. TET = 1400^{o}K.

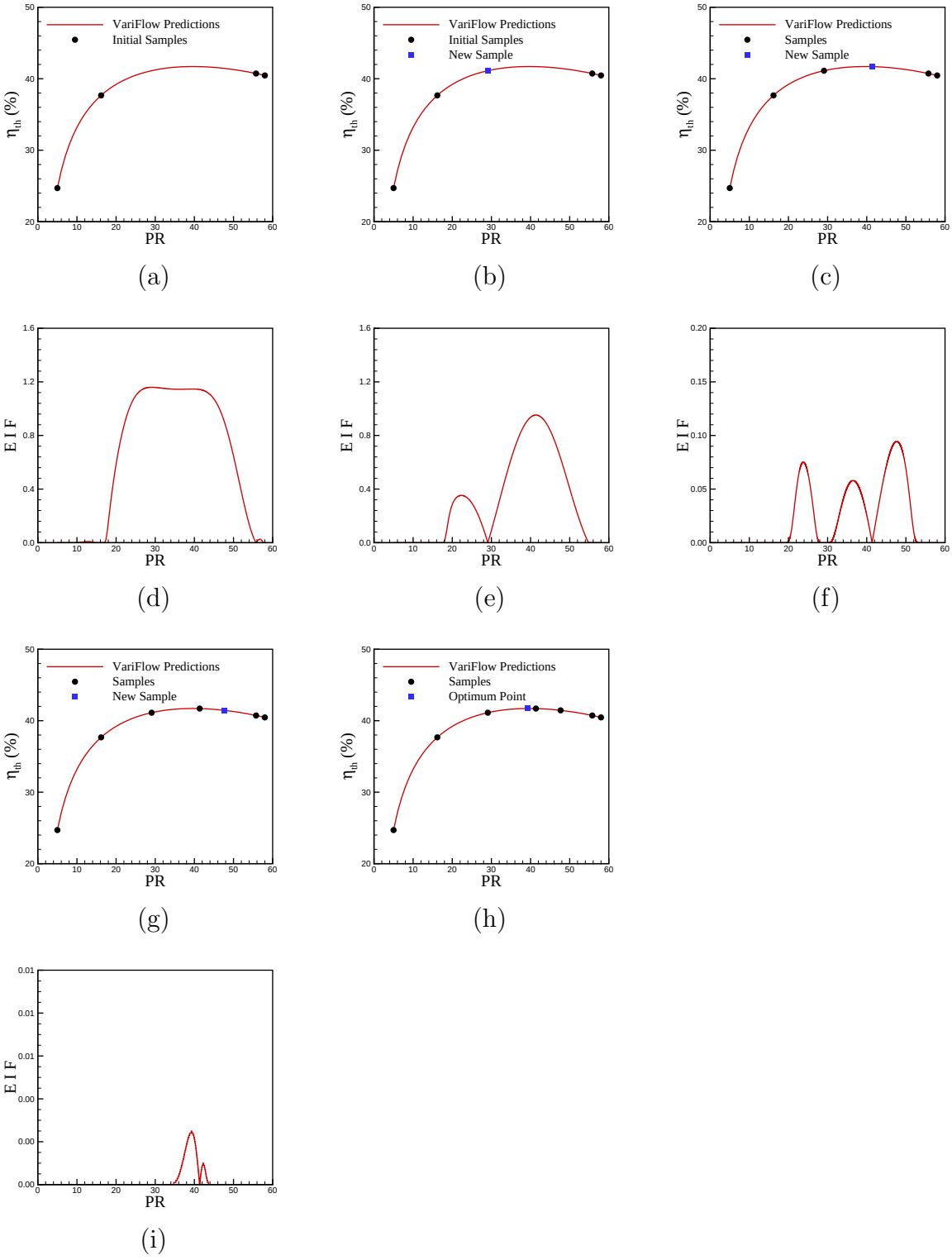

Figure 6.2: EIF optimization of gas turbine efficiency with respect to compressor pressure ratio.

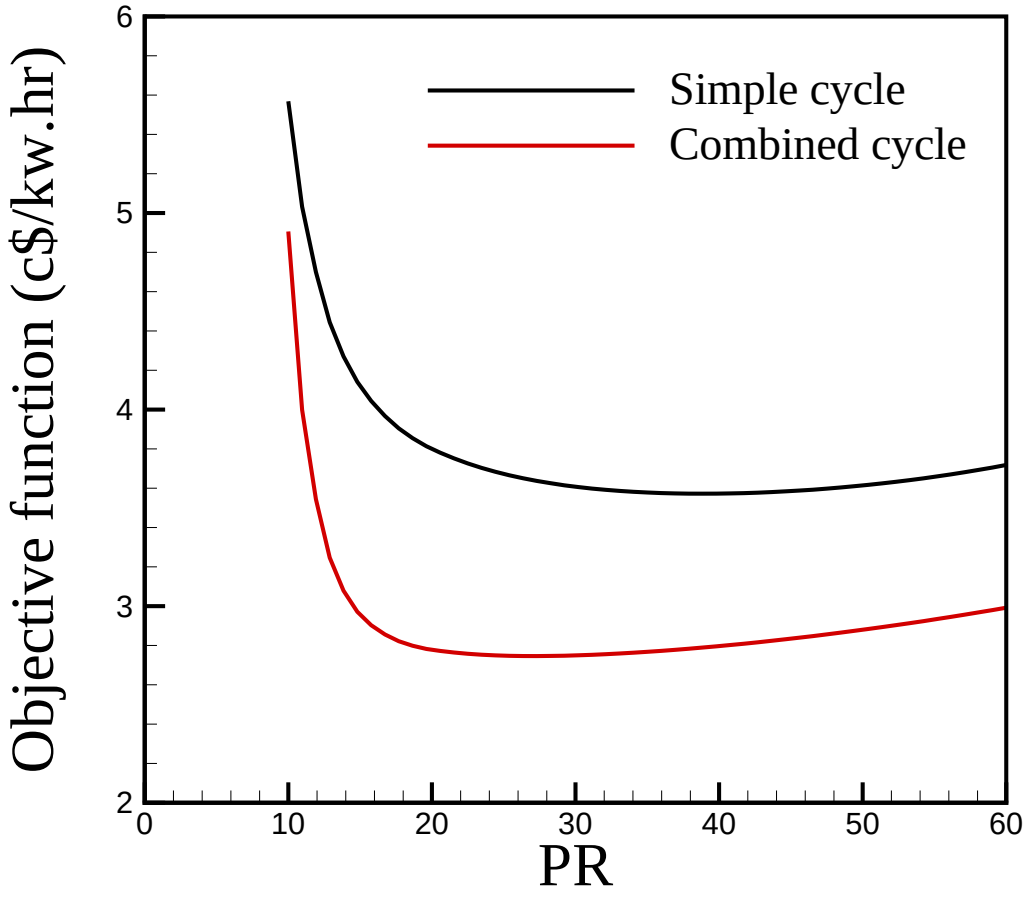

Figure 6.3: Simple and combined cycle cost of producing electricity. TET = 1400°K.

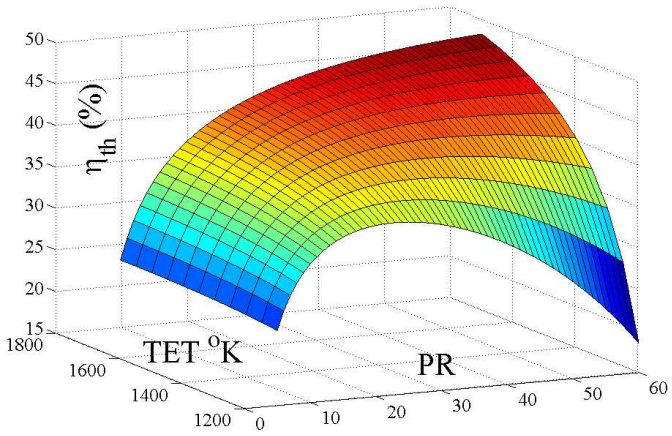

(a) Simple cycle

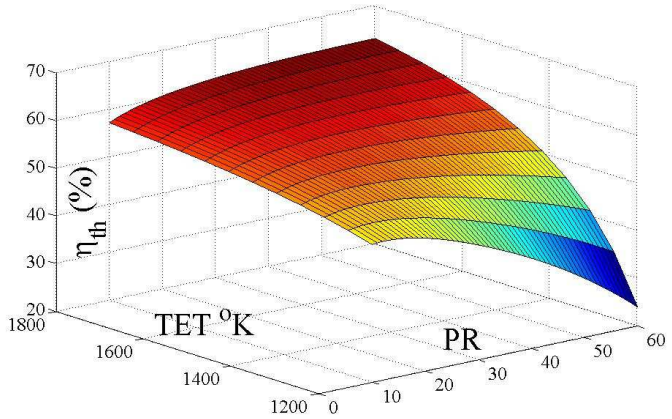

(b) Combined cycle

Figure 6.4: Simple and combined cycle thermal efficiency surface graphs.

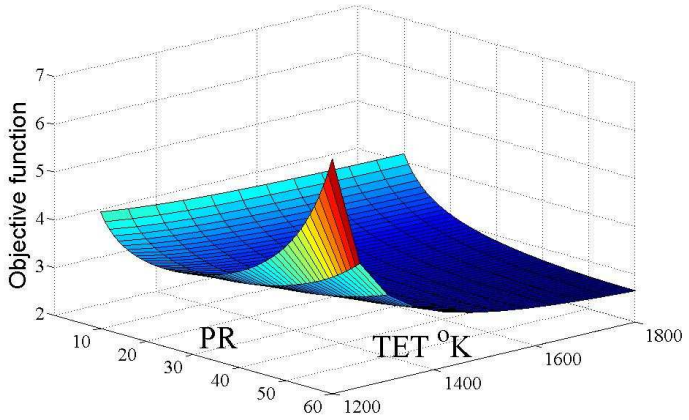

(a) Simple cycle

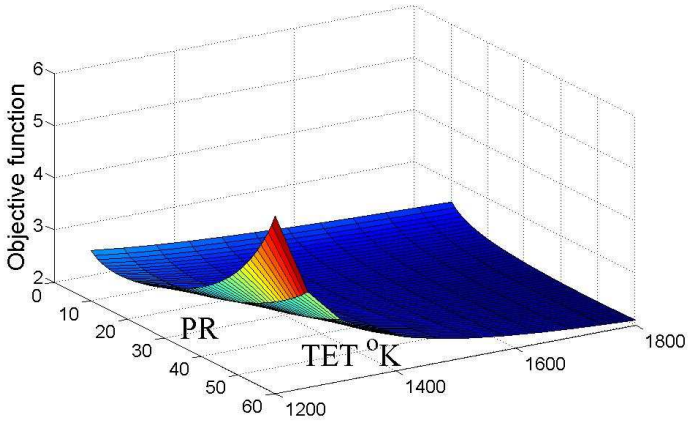

(b) Combined cycle

Figure 6.5: Simple and combined cycle cost of producing electricity surface graphs.

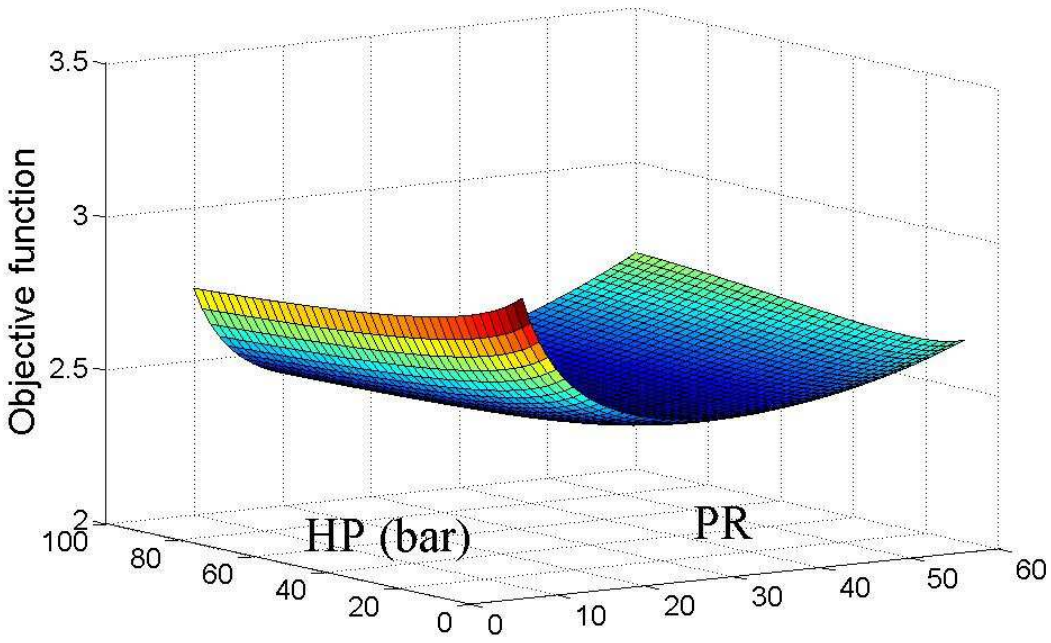

Figure 6.6: Combined cycle cost of producing electricity with compressor pressure ratio and high pressure HRSG. TET = 1400^{o}K.

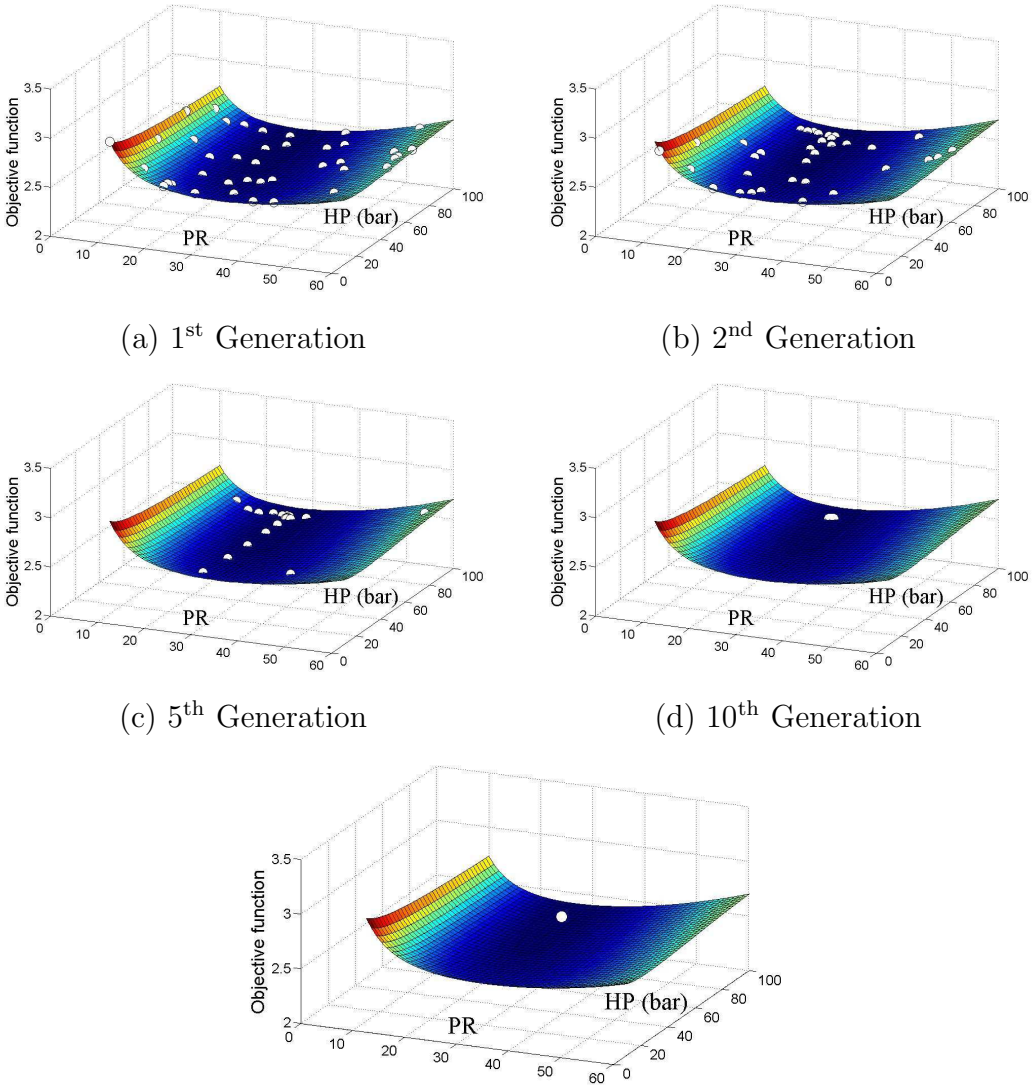

(a) 1st Generation

(b) 2nd Generation

(c) 5th Generation

(d) 10th Generation

(e) Optimal Point

Figure 6.7: Genetic algorithm optimization of profit function.

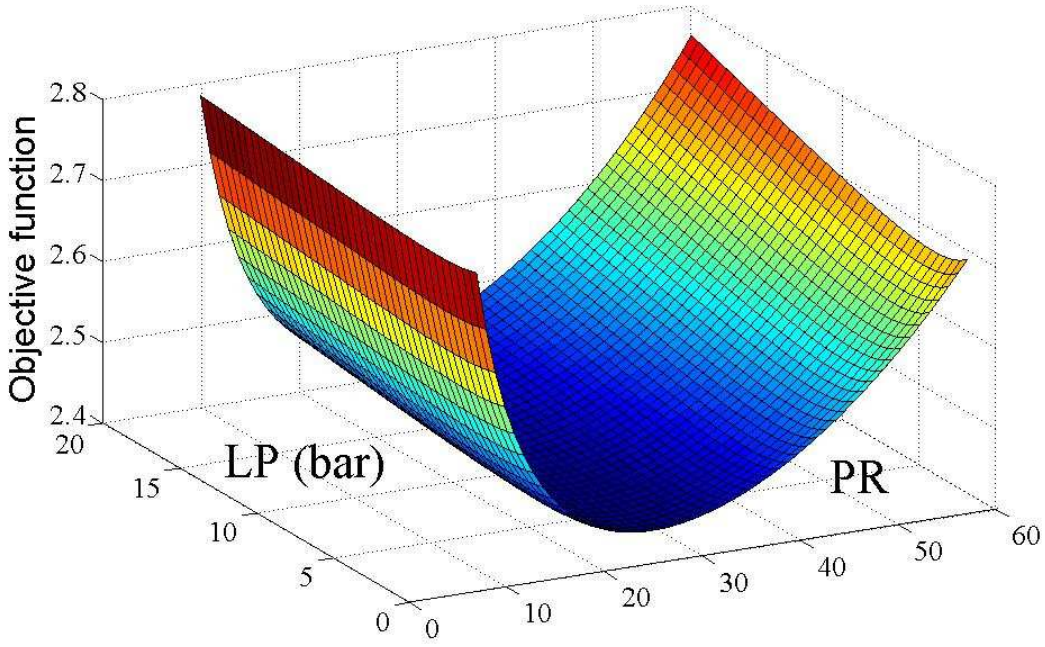

Figure 6.8: Combined cycle cost of producing electricity with compressor pressure ratio and low pressure HRSG. TET = 1400^{o}K.

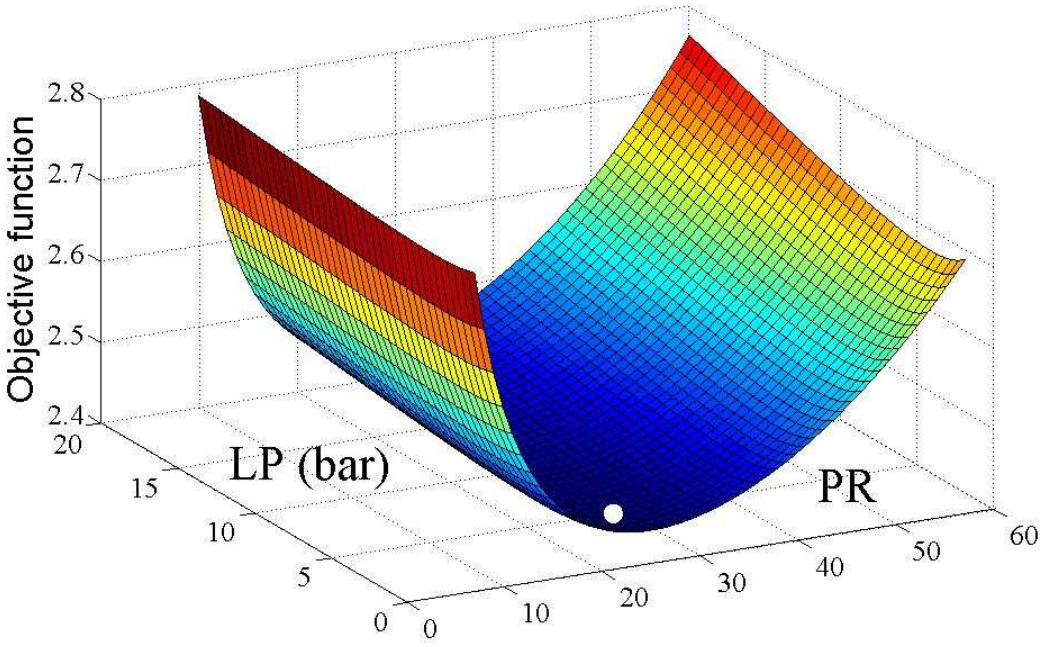

Figure 6.9: Optimal point based on EIF optimization.

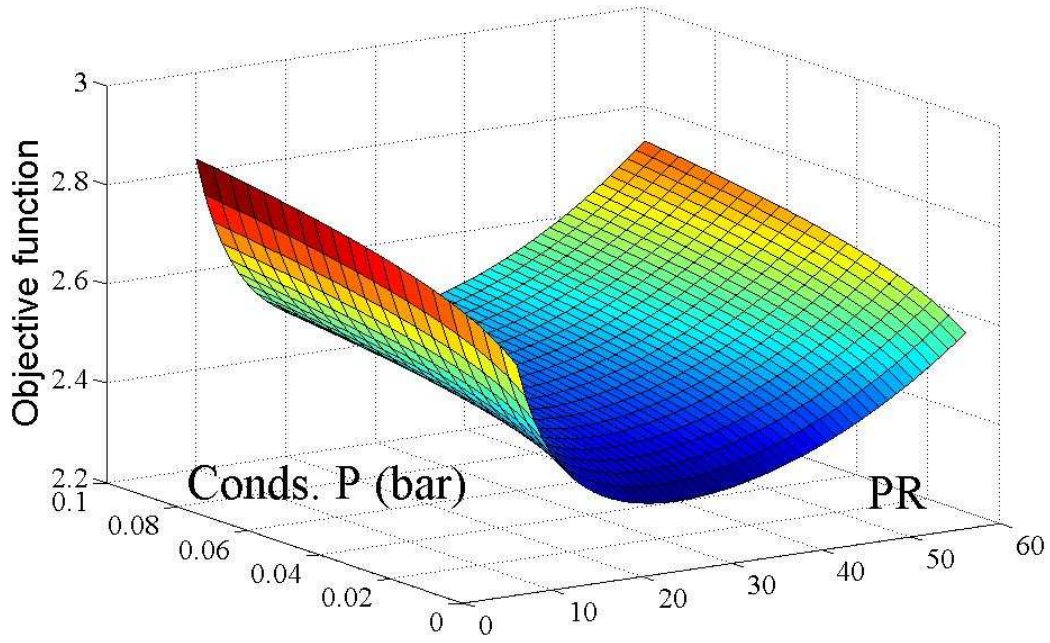

Figure 6.10: Combined cycle cost of producing electricity with compressor pressure ratio and condenser pressure HRSG. TET = 1400^{o}K.

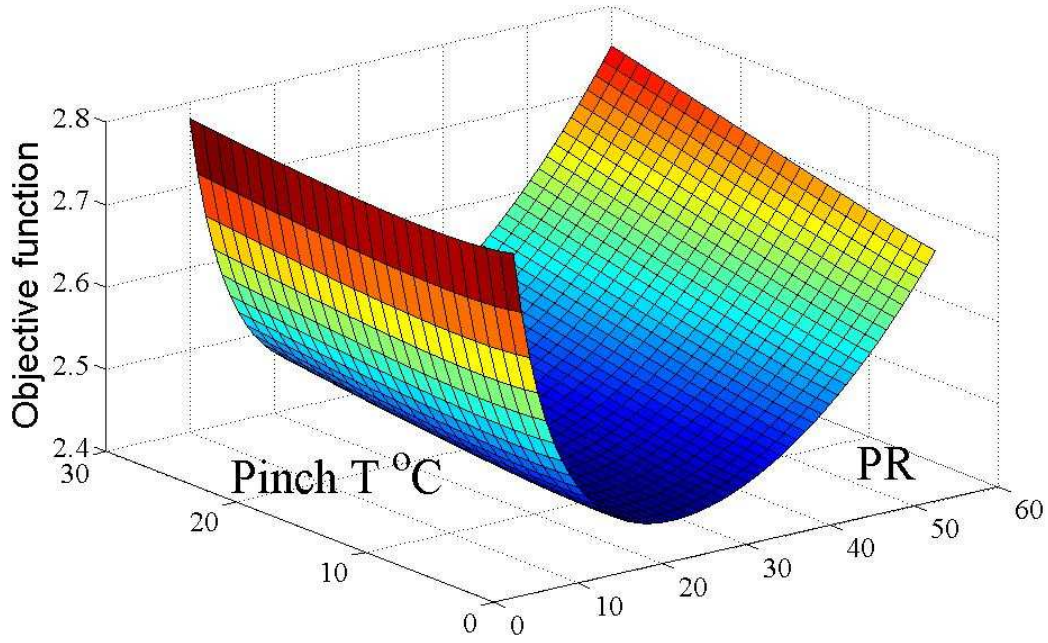

Figure 6.11: Combined cycle cost of producing electricity with compressor pressure ratio and pinch temperature. TET = 1400^{o}K.

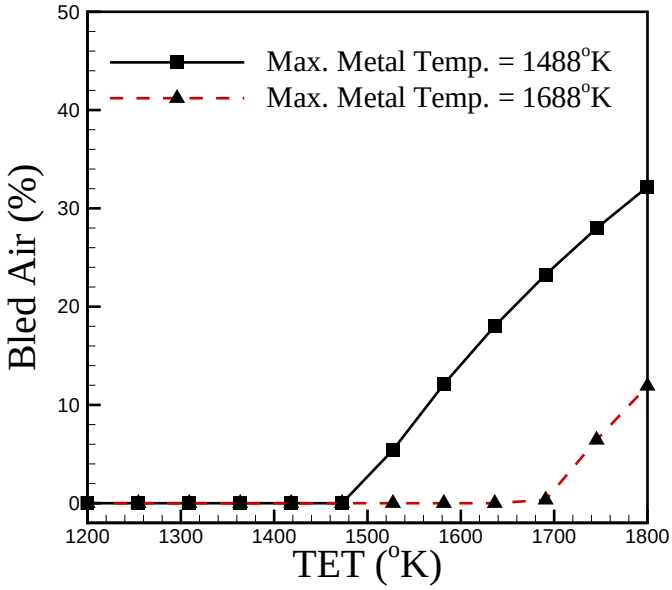

Figure 6.12: Required Compressor Bleeding Air versus TET.

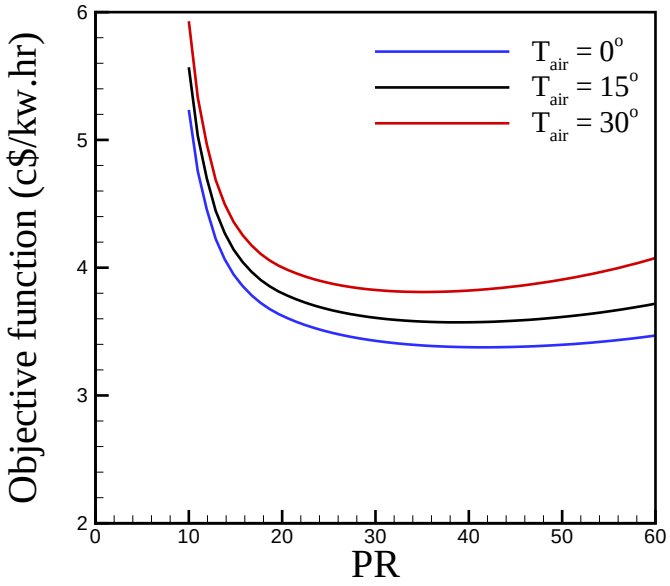

Figure 6.13: Gas turbine cost function for different ambient temperatures.

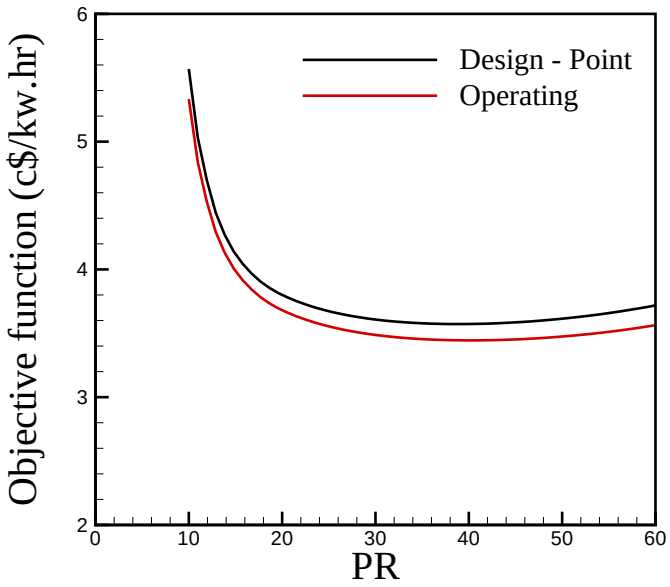

Figure 6.14: Gas turbine cost function for variation in ambient temperatures during plant life time.

Chapter 7

CONCLUSIONS AND FUTURE RESEARCH

The present study is a part of on-going research into development of TERA (Technoeconomical Environmental Risk Analysis) methodology at Cranfield University for the evaluation of advanced engine concepts in order to meet challenging environmental goals. This thesis in particular has developed a framework for thermoeconomic optimization of simple and combined gas-turbine cycles. The objective function to be minimized is the unit cost of producing electricity defined as the total cost per killowatt-hour. The total cost consists of initial cost, annual costs of operating/maintenance, fuel consumption, and annual emissions taxes due to the amount of pollution produced by the power plant. A number of approaches were described to formulate these costs related from design parameters. The optimization framework along with these models were demonstrated successfully for different types of optimization problems.

The main objective of this thesis was to develop a framework for optimal design of simple and combined gas-turbine power plants. The accurate performance prediction of simple and combined gas-turbine cycles is one of the most important tasks in achieving this objective. The study case is a single-shaft engine inspired by the

Alstom GT13-E2 gas turbine with 184.5 MW output power. The performance prediction study began with creating design-point and operating performance models of this engine in the VariFlow code. The design-point model consists of blocks that correspond to engine components (compressor, combustor, turbine, etc.), where the performance parameters in each block can be determined from given data and using the aero-thermodynamic equations. Unfortunately, not all the engine performance parameters are available (such as component efficiencies). What was suggested is to use the so-called engine's performance adaptation that allows us to match the engine's model with the performance data obtained from experiment. The outcome of adaptation method was an engine model which was inspired by real engine with small differences between predicted and observed data.

With the fixed engine geometry from the design-point, the engine must operate effectively over a range of ambient temperature changes. The prediction results showed that an increase in the ambient temperature would reduce the air density and hence the inlet mass flow rate and output power. The higher the ambient temperature, more heat is exhausted to the atmosphere as well, therefore, thermal efficiency decreases with a rise in the ambient temperature. Next, the design-point diagrams of the engine were created for the changes in compressor pressure ratio and turbine entry temperature. The results showed that for a given TET value, there is a corresponding compressor pressure ratio value that maximizes the gas turbine efficiency, such that, the optimum pressure ratio increases with increasing turbine entry temperature. The effects of extracting air from compressor for turbine cooling on the engine's performance were also investigated. The cooling air usually is extracted from the exit stage of high-pressure compressor and carried by ducts to the guide vanes and rotor of hight-pressure turbine. The performance prediction results showed that both thermal efficiency and specific power decrease with a rise in the amount of bled air

from the compressor of engine. The required amount of bled air depends on the allowable metal temperature and turbine inlet such that more amount of air needs to be extracted for cooling if the turbine inlet temperature increases. The amount of cooling air also increases for a metal with smaller allowable temperature as well.

The combined cycle performance prediction results showed that combined cycles has much higher overall efficiency than simple gas turbine. The finding showed the best HRSG type selection to combine the 184.5MW gas turbine with steam turbine is a dual-pressure HRSG. The results also showed that the optimum pressure of combined cycle is much smaller than simple gas-turbine cycle. Again, the optimum pressure ratio increases with increasing turbine entry temperature for both cycles.

Another key task of the optimization framework development is capital cost modeling. The capital cost includes initial investment, operating and maintenance, and interest rate. The cost is annualized using operating hours per year. Some equations were provided in order to estimate the initial investment of compressor, combustor, and turbine. However, it was shown that by using these equations, the cost predictions do not match with available engine prices. The problem of this modeling is that it does not take into account the correlation functions existing between actual engine parameters such as pressure ratio, mass flow, and TET. Using these correlations, the cost predictions match well with available data. In order to estimate the effects of cost coefficient changes into capital cost, a sensitivity analysis was performed. The sensitivity analysis results showed that capital cost predictions are very sensitive to the coefficients related to component efficiencies and turbine entry temperature.

The optimization framework was tested for thermoeconomic optimization of single and combined gas-turbine cycles at design point and off design conditions. Different methods were considered for the optimization. The results showed the benefits of each method. Optimizers based on golden section search are simple to implement and very helpful for single-variable type optimization problems. Genetic algorithm

and simulated annealing have a longer runtime than golden section search, but they are well fitted for multi-variable type of optimization. The results showed that an optimization method based on expected improvement function has smallest runtime amongst used methods. This optimizer also ensures that a global maxima or minima is found.

In the single-variable optimization problem, the compressor pressure ratio was assumed as decision variable. The optimization results confirm that used methods can produce accurate and efficient results for thermodynamic and thermoeconomic optimization. The results showed that the optimum pressure ratio values for maximum efficiency is different for the simple and combined gas-turbine cycles. The combined cycle efficiency is maximum at a lower compressor pressure ratio values. The optimization methods were also tested for multi-variable type optimization problems. The solution of constrained optimization was also described to limit turbine metal temperature and moisture content at the exit stage of steam turbine. Finally, the optimization under operating conditions were shown. The results showed that for engines operating at cold temperatures, a larger compressor pressure ratio is required to minimize the unit cost of producing electricity than an engine operating at standard ambient temperature. This framework can easily be extended to include different scenarios and constraints for optimization as well.

There is still much work needs to be done for future. This includes the thermal and exergy analysis of studied power plants and compare the results with thermoeconomic optimization. Different scenarios of emissions taxes can be defined and tested by the framework. Probabilistic sensitivity analysis using Monte Carlo simulation, perturbation method, and interval method could be used to study the effects of uncertainty in the assumption on the results. The cost model can be updated for emission reduction methods such as water injection. Finally, the developed framework can be tested for the low carbon cycles designed in the TERA program.

Bibliography

[1] Markandya, A. and Halsnaes, K., *Climate Change and Sustainable Development: Prospects For Developing Countries*, Earthscan publications Ltd., London, UK, 2002.

[2] Hester, R. E. and Harrison, R. M., *Environmental Impact of Power Generation*, Royal Society of Chemistry, Cambridge, UK, 1999.

[3] Barbera, P., *Advanced Low Carbon Power Systems: Evaluation of an Integrated Gasification Combined Cycle*, Msc thesis, School of Engineerinhg, Cranfield University, September 2008.

[4] Ruggieri, G., *Advanced Low Carbon Power Systems: Evaluation of Autho Thermal Reformer Combined Cycle*, Msc thesis, School of Engineerinhg, Cranfield University, September 2008.

[5] Di Lorenzo, G., "Low Carbon Energy Technologies: a TERA approach," Project progress review report 1, Cranfield University, Cranfield, December 2007, confidential.

[6] Nagaraj, B. P. and Venkatesh, D., *Basic Thermodynamics*, New Age International Publishers, New Delhi, India, 2005.

[7] Kiameh, P., *Power Generation Handbook*, 2nd edition, The McGraw-Hill Companies, 2012.

[8] Bejan, A., Tsatsaronis, G., and Moran, M., *Thermal Design & Optimization*, John Wiley & Sons, Hoboken, New Jersey, USA, 1996.

[9] Klapp, J., Cervantes-Cota, J., Federico, J., and Alcala, C., *Towards a Clearer Planet: Energy for the Future*, Springer Berlin Heidelberg New York, 2007.

[10] Bakshi, B. R., Gutowski, T., and Sekulic, D., *Thermodynamics and the Destruction of Resources*, Cambridge University Press, New York, 2011.

[11] Hoffmann, S., Bartlett, M., Finkenrath, M., Evulet, A., and Ursin, T. P., "Performance and Cost Analysis of Advanced Gas Turbine Cycles With Precombustion CO_2 Capture," ASME GT2008-51027, ASME Turbo Expo 2008: Power for Land, Sea, and Air, June 913, 2008, Berlin, Germany.

[12] Frangopoulos, C., "Introduction to environomics," *Symposium on Thermodynamics and Energy Systems, ASME Winter Annual Meeting, Atlanta, Ga. December 1-6, New York*, Vol. 191, 1991, pp. 49–54.

[13] Pelster, S., Favrat, D., and von Spakovsky, M. R., "The Thermoeconomic and Environomic Modeling and Optimization of the Synthesis, Design and Operation of Combined Cycles With Advanced Options," *Journal of Engineering for Gas Turbine and Power*, Vol. 123, No. 1, October 2001, pp. 717–726.

[14] Olsommer, B., Favrat, D., and von Spakovsky, M. R., "An Approach for the Time-Dependent Thermoeconomic Modeling and Optimization of Energy System Synthesis, Design and Operation Part II: Reliability and Availability," *Int J. Applied Thermodynamics*, Vol. 2, No. 4, 1999, pp. 177–186.

[15] Islas, J., "Getting Round the Lock-In In Electricity Generating Systems: The Example of the Gas Turbine," *Research Policy*, Vol. 26, 1997, pp. 49–66.

[16] Kuliasha, M. A., Zucker, A., and Ballew, K. J., *Technologies for a Greenhouse-Constrained Society*, Lewis Publications, Chelsea, Michigan, USA, 1992.

[17] Chambers, A., *Power Primer: A Nontechnical Guide from Generation to End Use*, PennWell Publishing Company, Tulsa, Oklahoma, USA, 1999.

[18] Raja, A. K., Srivastava, A. P., and Dwivedi, M., *Power Plant Engineering*, New Age International Publications, Delhi, 2006.

[19] Schobeiri, M., *Turbomachinery Flow Physics and Dynamic Performance*, Springer-Verlag, Berlin, Germany, 2005.

[20] Manninen, J. and Zhu, X. X., "Optimal Gas Turbine Integration to the Process Industries," *Industrial & Engineering Chemistry Research*, Vol. 38, No. 11, 1999, pp. 4317–4329.

[21] Martha De Souza, G. M., *Thermal Power Plant Performance Analysis*, Springer-Verlag, London, 2012.

[22] Achuthan, M., *Engineering Thermodynamics*, PHI Learning Private Limited, Second Edition, New Delhi, India, 2009.

[23] Breeze, P., *Power Generation Technologies*, Elsevier, Oxford, UK, 2005.

[24] Kreith, F. and Yogi Goswam, D., *The CRC Handbook Of Mechanical Engineering*, 2nd Edition, CRC Press, Danvers, MA, USA, 2005.

[25] Kehlhofer, R., Rukes, B., Hannemann, F., and Stirnimann, F., *Combined-Cycle Gas & Steam Turbine Power Plants*, PenWell Corporation, Third Edition, Tulsa, Oklahoma, USA, 2009.

[26] Horlock, J. H., *Advanced Gas Turbine Cycles*, Elsevier Science Ltd, Oxford, 2003.

[27] von Spakovsky, M. R. and Frangopoulos, C. A., "The Environomic Analysis And Optimization of A Gas Turbine Cycle With Cogeneration," *Thermodynamics and the Design, Analysis and Improvement of Energy Systems*, Vol. 33, No. 1, 1994, pp. 15–26.

[28] Boyce, M. P., *Handbook for Cogeneration and Combined Cycle Power Plants*, The American Society of Mechanical Engineers, New York, USA, 2002.

[29] Rovira, A., Sanchez, C., Munoz, M., Valdes, M., and Duran, M. D., "Thermoeconomic Optimisation of Heat Recovery Steam Generators of Combined Cycle Gas Turbine Power Plants Considering Off-Design Operation," *Energy Coversion and Management*, Vol. 52, 2011, pp. 1840–1849.

[30] Tsatsaronis, G., "Thermoeconomic Analysis and Optimization of Energy Systems," *Eneregy Combustion Science*, Vol. 19, No. 1, June 1993, pp. 227–257.

[31] Agazzani, A., Massardo, A. F., and Frangopoulos, C. A., "Environmental Influence on the Thermoeconomic Optimization of a Combined Plant with No_x Abatment," *Journal of Engineering for Gas Turbine and Power*, Vol. 120, No. 1, July 1998, pp. 557–565.

[32] Massardo, A. F. and Scialo, M., "Thermoeconomic Analysis of Gas Turbine Based Cycles," *ASME*, Vol. 122, No. 1, October 2000, pp. 664–671.

[33] El-Sayed, Y. M. and Tribus, M., "Strategic Use of Thermoeconomics for System Improvement," *Proceedings Efficiency and Costing: Second law analysis of Processes*, edited by R. A., A.C.S series, 1983, pp. 215–239, No. 235.

[34] Snow, D. A., *Plant Engineer's Reference Book*, Reed Educational and Professional Publishing, Second Edition, Oxford, UK, 2002.

[35] Hester, R. E. and Harrison, R. M., *Transport and the Environment: Issues in Enviromental Science and Technology*, The Royal Society of Chemistry, Cambridge, UK, 2004.

[36] Clark, J. S. and De Corso, S. M., *Stationary Gas Turbine Alternative Fuels*, American Society for Testing and Materials, Baltimore, USA., 1983.

[37] Knopf, F. C., *Modeling, Analysis and Optimization of Process and Energy Systems*, John Wiley & Sons, Hoboken, New Jersey, USA., 2012.

[38] Khartchenko, N. V., *Advanced Energy Systems*, Taylor & Francis, Washington, DC, USA., 1998.

[39] Hordeski, M. F., *New Technologies for Energy Efficiency*, The Fairmont Press, Lilburn, GA, USA, 2003.

[40] Lefebvre, A. H., "Fuel Effects on Gas Turbine Combustion-Liner Temperature, Pattern Factor and Pollutant Emissions," *AIAA Journal of Aircraft*, Vol. 21, No. 11, October 1984, pp. 887–898.

[41] Rizk, N. K. and Moniga, H. C., "Semianalytical Correlations for NOx CO and UHC Emissions," *Journal of Engineering for Gas Turbine and Power*, Vol. 115, No. 1, October 1993, pp. 612–619.

[42] Valdes, M., Duran, M. D., and Rovira, A., "Thermoeconomic Optimization of Combined Cycle Gas Turbine Power Plants Using Genetic Algorithms," *Journal of Applied Thermal Engineering*, Vol. 23, No. 1, July 2003, pp. 2169–2182.

[43] Attala, L., Facchini, B., and Ferrara, G., "Thermoeconomic Optimization Method as Design Tool in Gas-Steam Combined Plant Realization," *Journal of Energy Conversion and Managment*, Vol. 42, No. 1, July 2001, pp. 2163–2172.

[44] Franco, A. and Russo, A., "Combined Cycle Plant Efficieny Increase Based on the Optimization of Heat Recovery Steam Generator Operating Parameteres," *International Journal of Thermal Sciences*, Vol. 41, No. 1, July 2002, pp. 843–859.

[45] Harder, D., "Economics of refurbishing/rebuilding rocket test stands," *Space 2003*, edited by A. I. of Aeronautics and Astronautics, Long Beach, CA, United Sates, Sep. 23-25 2003.

[46] Sanghi, V., Lakshmanan, B. K., and Sundararajan, V., "Survey of Advancements in Jet-Engine Thermodynamic Simulation," *Journal of Propulsion and Power*, Vol. 16, No. 5, 2000, pp. 797–807.

[47] Saravanamuttoo, H. I. H., Rogers, C. F. C., and Cohen, H., *Gas Turbine Theory*, Harlow: Prentice Hall, 2001.

[48] Oates, G. C., *Aircraft Propulsion System Technology and Design*, AIAA Education Series, Washingto, DC, USA, 1989.

[49] Mattingly, J. D., *Elements of Gas Turbine Propulsion*, McGraw-Hill, New York, USA, 1996.

[50] Buecker, B., *Basics of Boiler & HRSG Design*, PennWell Corporation, Tulsa, Oklaham, USA., 2002.

[51] Touloukian, Y. S. and Tadash, M., *The TPRC Data Series, Thermo-Physical Properties of Matter*, Vol. 6, IFI/Plenunm, New York, USA., 1970.

[52] Antoniou, A. and Lu, W.-S., *Practical Optimization*, Springer, 2007.

[53] Baldick, R., *Applied Optimization*, Cambridge University Press, 2006.

[54] Miller, R. E., *Optimization*, Wiley-IEEE, 2000.

[55] Abadie, J., *Generalized reduced gradient and global Newton methods*, Springer Berlin / Heidelberg, 1986.

[56] Rao, S. S., *Optimization: Theory and Applications*, John Wiley & Sons, NewYork, 1984.

[57] Goldberg, D. E., *Genetic Algorithms in Search, Optimization and Machine Learning*, Addison-Wesley Longman Publishing Co., Inc, Boston, 1989.

[58] Kirkpatrick, S., Gelatt, C. D., and Vecchi, M. P., "Optimization By Simulated Annealing," *Science*, Vol. 220, No. 4598, October 1983, pp. 671–680.

[59] Onwubolu, G. C. and Babu, B. V., *New Optimization Techniques in Engineering*, Springer-Verlag, Berlin, Germany, 2004.

[60] Sakawa, M., *Genetic Algorithms and Fuzzy Multiobjective Optimization*, Kluwer Academic Publications, Norwell, MI, USA, 2002.

[61] Jones, D. R., S. M. and Welch, W. J., "Efficient Global Optimization of Expensive Black-Box Functions," *Kluwer Academic publications*, Vol. 13, No. 1, October 1998, pp. 455–492.

[62] Sacks, J., Welch, W. J., Mitchell, T. J., and Wynn, H. P., "Design and Analysis of Computer Experiments," *Statistical Science*, Vol. 4, No. 4, 1989, pp. 409–435.

[63] Huang, D., Allen, T. A., Notz, A. I., and Miller, R. A., "Sequential kriging optimization using multiple-fidelity evaluations," *Struct Multidisc Optim*, Vol. 32, No. 1, October 2006, pp. 369–382.

[64] Jeanne, E., *High Efficiency Cycles Using Water For Low CO2 Power-Generation Systems*, Master's thesis, School of Engineering, Cranfield University, September 2006.

[65] Schutte, J. S., *Simultaneous Multi-Design Point Approach to Gas Turbine On-Design Cycle Analyis for Aircraft Engine*, Ph.D. thesis, Aerospace Engineering, Georgia Institute of Technology, April 2009.

[66] Lin, T., *An Adaptive Modeling and Simulation Environment for Combined-Cycle Data Reconciliation and Degradation Estimation*, Ph.D. thesis, Georgia Institue of Technology, 2008.

[67] Li, Y. G., Pilidis, P., and Newby, M. A., "An Adaptation Approach for Gas Turbine Design-Point Performance Simulation," *Journal of Engineering for Gas Turbine and Power*, Vol. 128, 2006, pp. 789–795.

[68] Wriggers, P., *Nonlinear Finite Element Methods*, Springer-Verlag, Berlin, 2008.

[69] Zhang, N. and Cai, R., "Analytical Solutions and Typical Characteristics of Part-Load Performances of Single Shaft Gas Turbine and Its Cogeneration," *Energy Conversation and Managments*, Vol. 43, No. 9, 2002, pp. 1323–1337.

[70] Logan, E.and Roy, R., *Handbook of Turbomachinery*, Marcel Dekker, New York, USA, 2003.

[71] Soares, C., *Gas Turbines: A Handbook of Air, Land, and Sea Applications*, Elsevier Science, Burlington, MA, USA, 2008.

[72] Floudas, C. A. and Pardalos, P. M., *Encyclopedia of Optimization, Volume 1*, 2nd Edition, Springer, 2009.

[73] Valdes, M., Rovira, A., and Duran, M. D., "On Existence of Trends Applicable to Thermoecnomic Optimisation of Combined Cycle Gas Turbine Power Plants," *Journal of the Energy Institute*, Vol. 79, No. 2, 2006, pp. 110–115.

[74] Dixon, S. L., *Fluid Mechanics and Thermodynamics of Turbomachinery*, Fourth Edition, Elsevier Science, Burlington, MA, USA, 1998.

[75] Han, J. C., Dutta, S., and Ekkad, S. V., *Gas Turbine Heat Transfer and Cooling Technology*, Taylor & Francis, New York, USA, 2000.

[76] Xiaotao, Z., Hideaki, S., Weidou, N., and Zheng, L., "Economics and Performance Forecast of Gas Turbine Combined Cycle," *Tsinghua Science and Technology*, Vol. 10, No. 5, 2005, pp. 633–636.

[77] Lozano, M. A. and Valero, A., "Thermoeconomic Analysis of Gas Turbine Cogeneration Systems," *Theory of the Exergetic Cost*, Vol. 18, 1993, pp. 939–960.

[78] Silveira, J. L. and Tuna, C. E., "Themoeconomical Analysis Method for Optimization of Combined Heat and Power Systems, Part 1," *Progress in Energy and Combustion Science*, Vol. 29, 2003, pp. 479–485.

[79] Frangopoulos, C. A. and Caralis, Y. C., "A Method for Taking Into Account Enviromental Impacts in the Economic Evaluation of Energy Systems," *Energy Conversation and Managments*, Vol. 38, No. 15-17, 1997, pp. 1751–1763.

[80] Duffie, J. A. and Beckman, W. A., *Solar Engineering of Thermal Processes*, John Wiley & Sons, New York, USA., 1980.

[81] Thissen, W. A. H. and Herder, P. M., *State of the Art in Research and Application*, Kluwer Academic Publishers, Norwell, Massachusettsm, USA, 2003.

[82] Flack, R. D., *Fundamentals of Jet Propulsion with Applications*, Cambridge University Press, New York, USA, 2005.

[83] Bejan, A. and Mamut, E., *Thermodynamic Optimization of Complex Energy System*, Kluwer Academic Publishers, Norwell, Massachusettsm, USA, 1999.

[84] Kensett, R. G., *Changing Scene of Health Care and Technology: Proceedings of the 11th Conference Center, London, 4-8 June*, Taylor & Francis, New York, USA, 1990.

[85] In, J. S. and Lee, S. Y., "Optimization of Heat Recovery Steam Generator Through Exergy Analysis for Combined Cycle Gas Turbine Power Plants," *International Journal of Energy Research*, Vol. 32, 2008, pp. 859–869.

[86] Nag, P. K., *Power Plant Engineering*, Tata McGraw Hill Education, Third Edition, New Delhi, India, 2008.

[87] deSouza, G. F. M., *Thermal Power Plant Performance Analysis*, Springer-Verlag, London, UK, 2012.

[88] Harris, J., *An Introduction to Fuzzy Logic Applications*, Kluwer Academic Publishers, Dordrecht, Netherlands, 2000.

[89] Rathakrishnan, E., *Fundamentals of Engineering Thermodynamics*, PHI Learning Private, New Delhi, India, 2005.

[90] Venkanna, B. K. and Swati, B. V., *Applied Thermodynamics*, PHI Learning Private, New Delhi, India, 2011.

[91] Wu, C., *Thermodynamics And Heat Powered Cycles: A Cognitive Engineering Approach*, Nova Science Publishers, New York, USA, 2007.

[92] Capehart, B. L., *Encyclopedia of Energy Engineering and Technology*, Taylor & Francis Group, Boca Raton, Florida, USA, 2007.

[93] Heselton, K. E., *Boiler Operator's Handbook*, The Fairmont Press, Liburn, Georgia, USA, 2005.

[94] Ghazi, M., Ahmadi, P., Sotoodeh, A. F., and Taherkhani, A., "Modeling and Thermo-Economic Optimization of Heat Recovery Heat Exchangers Using a Multimodal Genetic Algorithm," *Energy Conversion and Management*, Vol. 58, 2012, pp. 149–156.

[95] Nourouzi, E. and Amidpour, M., "Optimal Thermodynamic and Economic Volume of a Heat Recovery Steam Generator By Constructal Design," *International Communications in Heat and Mass Transfer*, Vol. 39, 2012, pp. 12861292.

[96] Bassily, A. M., "Modeling, Numerical Optimization, and Irreversibility Reduction of a Dual-Pressure Reheat Combined-Cycle," *Journal of Applied Energy*, Vol. 81, 2005, pp. 127–151.

[97] Franco, A., "Analysis of Small Size Combined Cycle Plants Based on the Use of Supercritical HRSG," *Applied Thermal Engineering*, Vol. 31, 2011, pp. 785–794.

[98] Singh, S. M., *Electric Power Generation Transmission And Distribution*, PHI Learning Private, New Delhi, India, 2008.

[99] Sanjay, S. O., "Investigation of Effect of Variation of Cycle Parameters on Themodynamics Performance of Gas-Steam Combined Cycle," *Energy*, Vol. 36, 2011, pp. 157–167.

[100] Petchers, N., *Combined Heating, Cooling and Power Handbook: Technologies and Applications : an Integrated Approach to Energy Resource Optimization*, The Fairmont Press, Lilburn, GA, USA, 2003.

[101] Colpier, U. C. and Cornland, D., "The Economics of the Combined Cycle Gas Turbine- An Experience Curve Analysis," *Energy Policy*, Vol. 30, 2002, pp. 309–316.

[102] Flynn, D., *Thermal Power Plant Simulation and Control*, The Institution of Electrical Engineers, Herts, UK, 2003.

[103] Pasha, A. and Jolly, S., "Combined Cycle Heat Recovery Steam Generators Optimum Capabilities and Selection Criteria," *Heat Recovery System & CHP*, Vol. 15, No. 2, 1995, pp. 147–154.

[104] Mohagheghi, M. and Shayegan, J., "Thermodynamic Optimization of Design Variables and Heat Exchangers Layout in HRSGs for CCGT, Using Genetic Algorithm," *Applied Thermal Engineering*, Vol. 29, 2009, pp. 290–299.

[105] Giordano, F. R., Fox, W. P., Horton, S. B., and Weir, M. D., *A First Course in Mathematical Modeling*, Fourth Edition, Books/Cole, Belmont, CA, USA, 2009.

[106] Glover, D. M., Jenkins, W. J., and Doney, S. C., *Modeling Methods for Marine Science*, Cambridge University Press, Cambridge, UK, 2011.

[107] Doherty, D., Freeman, M. A., and Kumar, R., "Optimization with MATLAB and the Genetic Algorithm and Direct Search Toolbox," Tech. rep., The MathWorks Inc., 2004.

Appendix A

Economic Parameter Values(von Spakovsky and Frangopoulos, 1994)

Parameter	Value		
c_{11}	39.5 \$/(kg/s)	c_{12}	0.9
c_{21}	25.6 \$/(kg/s)	c_{22}	0.995
c_{23}	0.018 $/^0K$	c_{24}	26.4
c_{31}	266.3 \$/(kg/s)	c_{32}	0.92
c_{33}	0.036 $/^0K$	c_{34}	54.4
c_{41}	2290 \$/$m^{1.2}$	c_{51}	3650 \$/$(kW/K)^{0.8}$
c_{52}	11,820 \$/(kg/s)	c_{53}	658 \$/$(kg/s)^{1.2}$
c_{fuel}	4E-6 \$/kj	c_{w}	0.47 \$/ m^3
c_{NO_x}	7.5 \$/kg NOx	c_{CO}	1.014 \$/kgCO

Appendix B

The 184.5 MW power single-shaft engine model in VariFlow

```
1           !Working Air, 2 CO2

2           !Fuel:1 Kerosene,2 Natural gas

1           !Fuel in off-design, equal to the previous one

3000        !Rotational speed

556.831     !Mass Flow

101325      !Ambient Pressure

288.15      !Ambient temperature

0.0         !Pressure loss Intake
```

```
0.45        !Mach number at compressor entry

0.881       !compressor efficiency (polytropic)

16.9        !Compressor PR

3.000       !Compressor Map Number

0.0000      !Cooling Bleed Fraction

0.00        !Overboard bleed fraction

0.1         !Medium Mach number in combustor

0.102       !Total Pressure loss in combustor

1394.10     !Turbine Entry Temperature

0.90        !Turbine efficiency(polytropic)

0.22        !Mach number at nozzle exit

360         !Mean turbine Blade speed

65          !Flow Angle At Exit of Turbine NGV
```

```
2           !Number of Turbine Stages


-3          !-3 for design point and stop,-1 for off-design
```